SCIENCE • TECHNOLOGY • RESEARCH HIGHLIGHTS • VISIONS •

Dissertation
92

Modelling the super-equilibria in thermal biomass conversion

Applications and limitations of the constrained free energy method

Petteri Kangas

VTT

VTT SCIENCE 92

Modelling the super-equilibria in thermal biomass conversion

Applications and limitations of the constrained free energy method

Petteri Kangas

Process Chemistry and Environmental Engineering
VTT Technical Research Centre of Finland Ltd

Laboratory of Inorganic Chemistry
Faculty of Science and Engineering
Åbo Akademi University

Thesis for the degree of Doctor of Technology to be presented with the permission of the Faculty of Science and Engineering at Åbo Akademi University for public examination and criticism in auditorium Salin, Axelia, Biskopsgatan 8, Åbo on Thursday, 28th of May, 2015 at 12 o'clock noon.

ISBN 978-951-38-8297-6 (Soft back ed.)
ISBN 978-951-38-8298-3 (URL: http://www.vtt.fi/publications/index.jsp)

VTT Science 92

ISSN-L 2242-119X
ISSN 2242-119X (Print)
ISSN 2242-1203 (Online)

JULKAISIJA – UTGIVARE – PUBLISHER

Teknologian tutkimuskeskus VTT Oy
PL 1000 (Tekniikantie 4 A, Espoo)
02044 VTT
Puh. 020 722 111, faksi 020 722 7001

Teknologiska forskningscentralen VTT Ab
PB 1000 (Teknikvägen 4 A, Esbo)
FI-02044 VTT
Tfn +358 20 722 111, telefax +358 20 722 7001

VTT Technical Research Centre of Finland Ltd
P.O. Box 1000 (Tekniikantie 4 A, Espoo)
FI-02044 VTT, Finland
Tel. +358 20 722 111, fax +358 20 722 7001

Grano Oy, Kuopio 2015

Preface

A large part of this study was conducted during the years 2012–2014, in a project focusing on the thermodynamics of high temperature processes. During the project, I realised that several chemistry problems related to combustion and thermal processing have common features which it might be possible to model by applying the novel constrained free energy method. This study summarises the applications and limitations of the CFE method in the thermal conversion of biomass, i.e. combustion, gasification, pyrolysis, torrefaction, NO emissions and alkali metal chemistry in flue gases.

The study was conducted under the supervision of Professors Pertti Koukkari and Mikko Hupa. Their support, guidance and enthusiasm are highly appreciated. I would also like to acknowledge the work of the co-authors of the publications, Dr. Daniel Lindberg, Dr. Anders Brink, Mr. Risto Pajarre, Ms. Marja Nappa and Mr. Ilkka Hannula.

I am grateful for the financial support I received from Tekes – the Finnish Funding Agency for Innovation, the Academy of Finland, VTT Technical Research Centre of Finland, Åbo Akademi University and the Fortum Foundation.

Finally, I would like to thank my family for their support during my rather long journey towards becoming a scientist.

May 2015, Lohja, Finland

Petteri Kangas

Academic dissertation

Supervisors	Professor Mikko Hupa Laboratory of Inorganic Chemistry Faculty of Science and Engineering Åbo Akademi University, Finland
	Research Professor Pertti Koukkari Process Chemistry and Environmental Engineering VTT Technical Research Centre of Finland, Finland
Reviewers	Professor Franz Winter Institute of Chemical Engineering Vienna University of Technology, Austria
	Professor Rainer Backman Department of Applied Physics and Electronics Umeå University, Sweden
Opponent	Professor Franz Winter Institute of Chemical Engineering Vienna University of Technology, Austria

List of publications

This thesis is based on the following original publications, which are referred to in the text as [I–V]. The publications are reproduced with the kind permission of the publishers.

I Kangas, P., Koukkari, P. & Hupa, M. 2014. Modeling biomass conversion during char gasification, pyrolysis and torrefaction by applying constrained local thermodynamic equilibrium. Energy & Fuels 28 (10), 6361–6370. doi: 10.1021/ef501343d

II Kangas, P., Hannula, I., Koukkari, P. & Hupa, M. 2014. Modelling super-equilibrium in biomass gasification with the constrained Gibbs energy method. Fuel 129, 86–94. doi:10.1016/j.fuel.2014.03.034

III Kangas, P., Koukkari, P., Lindberg, D. & Hupa, M. 2013. Modelling black liquor combustion with the constrained Gibbs energy method. The Journal of Science and Technology for Forest Products and Processes 3 (3), 6–15.

IV Kangas, P., Koukkari, P., Brink, A. & Hupa, M., 2015. Feasibility of constrained free energy method for modeling the NO formation in combustion. Chemical Engineering & Technology, in press. doi: 10.1002/ceat.201400633

V Kangas, P., Pajarre, R., Nappa, M. & Koukkari, P., 2012. Multi-phase thermodynamic modelling of pulp suspensions: Review of the methodology. Nordic Pulp & Paper Research Journal 27 (3), 604–612. doi:10.3183/NPPRJ-2012-27-03-p604-612

Author's contributions

The author was responsible for the original research idea presented in this dissertation, of applying the constrained free energy (CFE) method to thermal biomass conversion.

Publication [I]: The work was planned and the results were interpreted by the author. The applied models and validation data were obtained from the literature. The publication was written by the author under the supervision of Professors Pertti Koukkari and Mikko Hupa.

Publication [II]: The work was planned and the results were interpreted by the author. Mr. Ilkka Hannula provided the experimental models used for defining the immaterial constraints in biomass gasification. Applied validation data were obtained from the literature. The publication was written by the author under the supervision of Professors Pertti Koukkari and Mikko Hupa.

Publication [III]: The work was planned and the results were interpreted by the author. Applied thermodynamic data were obtained from Dr. Daniel Lindberg. The data were extended with the CFE features by the author. The publication was written by the author under the supervision of Professors Pertti Koukkari and Mikko Hupa.

Publication [IV]: The work was planned and the results were interpreted by the author. Reference data and applied models were obtained from the detailed kinetic model provided by Dr. Anders Brink. The publication was written by the author under the supervision of Professors Pertti Koukkari and Mikko Hupa.

Publication [V]: The work was planned and the results were interpreted by the author. The original CFE model of pulp suspension chemistry was developed by Mr. Risto Pajarre. This model was utilised by the author for the development of CFE-based surrogate models. Validation data were provided by Professor Pertti Koukkari and Ms. Marja Nappa. The publication was written by the author under the supervision of Professor Pertti Koukkari. Publication [V] also summarised the main results of the author's licentiate thesis in 2009.

Related publications by the author

1. Kangas, P., Brink, A., Koukkari, P. & Hupa, M. 2014. Applications of constrained Gibbs' free energy method for modelling the super-equilibria in thermal biomass conversion. Presentation at the 21st International Congress of Chemical and Process Engineering CHISA 2014. Prague, Czech Republic.

2. Kangas, P., Koukkari, P., Lindberg, D. & Hupa, M. 2013. Modelling black liquor combustion with the constrained Gibbs energy method. Presentation at the 8th International Black Liquor Colloquium. Belo Horizonte, Brazil.

3. Kangas, P., Koukkari, P. & Hannula, I. 2013. Modelling Super-Equilibrium in Biomass Gasification with the Constrained Gibbs Energy Method. Presentation at the AIChE 2013 Annual meeting, San Francisco, CA, US.

4. Kangas, P., Pajarre, R., Penttilä, K. & Koukkari, P. 2013. Use of immaterial constraints in Gibbs energy minimization for parametric phase diagrams and process modeling. Poster at the CALPHAD XLII. San Sebastian, Spain.

5. Kangas, P., Kaijaluoto, S. & Koukkari, P. 2010. Simulation of the Release of Non-condensable Gases in Sea Water Evaporation. Poster at the AIChE 2010 annual meeting. Salt Lake City, US.

6. Kangas, P. 2009. Multi-phase chemistry in process simulation. Presentation at the Papermaking Research Symposium. Kuopio, Finland.

7. Kangas, P. 2009. Multi-Phase Chemistry in Process Simulation. Licentiate thesis, Helsinki University of Technology.

8. Kangas, P. & Ylén, J.-P. 2005. Modelling reaction kinetics in dynamic process simulator. Presentation at the 10th Mediterranean Congress of Chemical Engineering. Barcelona, Spain.

Contents

List of symbols and abbreviations

Symbols

a	Stoichiometric coefficient in reaction matrix
A	Frequency factor
A	Affinity
b	Total amount of a component in a system
B	Temperature exponent
C	Constant
C	Heat capacity
E	Activation energy
f	Function
G	Gibbs' free energy
H	Enthalpy
k	Rate constant
j	Constituent in reaction matrix
L	Lagrange function
M	Molar mass
n	Molar amount of matter
N	Stoichiometric matrix
p	Pressure
r	Reaction rate
R	Gas constant
R	Number of constrained reactions

S	Entropy
t	Time
T	Temperature

Greek symbols

μ	Chemical potential
v	Stoichiometric coefficient
ξ	Extent of reaction
π	Lagrange's multiplier
Π	Lagrange's multiplier vector
Ψ	Mass balance vector

Super- and subscripts

°	Standard state
b	Constituent involved in reaction
c	Combustion
f	Forward reaction
f	Formation
k	Constituent; Species
K	Number of constituents
l	Component; Element
L	Number of components
p	Pressure
prod	Combustion products
r	Reverse reaction
r	Reaction
x	Immaterial constituent
X	Number of immaterial constituents
y	Immaterial component
Y	Number of immaterial components

Abbreviations

CFE	Constrained free energy
CFD	Computational fluid dynamics
DKM	Detailed kinetic model
EQ	Equilibrium
RCCE	Rate-controlled constrained-equilibrium
Super-EQ	Super-Equilibrium

1. Introduction

Biomass is today an important energy source. It is a renewable material which can, to some extent, replace the use of fossil fuels and thereby, alongside other solar-based energy sources, smoothen the path to the future. Combustible renewables and waste currently cover ~ 10% of the world's total energy usage [1].

In Finland in particular, biomass based on wood forms an even more important energy source than the above facts suggest. The energy content of bio-based fuels use per year covered from 20% to 24% of total energy consumption in Finland during 2000–2013 [2,3], see Figure 1. The steady growth in biomass' share of total energy use is due to the increased usage of forest processed chips. While these forest residues accounted for an almost negligible share in 2000, they covered 4% of total energy consumption by 2013. However, the largest fraction of biofuels is accounted for by black liquor from kraft pulp mills. In addition, bark is a major energy source. Local usage of firewood in homes, cottages and farms is typical in Finland, and can be considered as an important de-centralised bio-based energy source.

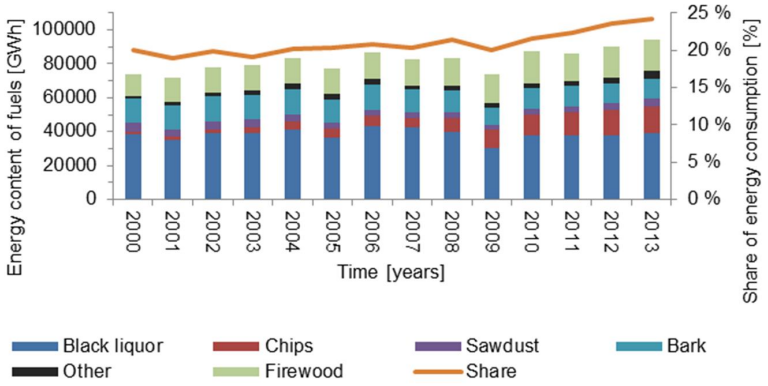

Figure 1. Usage of biomass for energy production in Finland during the years 2000–2013 [2,3].

1.1 Thermal biomass conversion

Today, practically all biomass is converted into energy through combustion, whether the raw material in question is forest processed chips, bark, sawdust, black liquor, firewood or some other bio-based raw-material. Facilities may vary in size, from large-scale combined heat and power plants to small-scale heat boilers for producing local heat and to single fireplaces in domestic houses, but the combustion mechanism remains the same.

During combustion, the biomass passes through the following steps [4–6], as illustrated in Figure 2. First biomass is dried and moisture is evaporated from the wood (100–150°C). Drying is followed by torrefaction, where the oxygen content of the biomass falls while the most volatile material is fractionated from the wood (150–300°C). The next step is pyrolysis of the biomass, whereby the biomass is fully de-volatilised until only solid char remains (300–600°C). Gasification of the char represents the final step whereby hydrogen and carbon monoxide are produced (> 600°C). Finally, all volatile species are oxidised and mainly water and carbon dioxide are produced. During oxidation, emissions, e.g. in the form of nitrogen oxides (NO_x) emissions, are formed. When the flue gas is cooled down in heat exchangers and a chimney, some of the volatile alkali metals may react and condensate, mainly forming fly ash and possibly sticky condensates, which cause corrosion on the metal surfaces of the boiler [7].

The composition of various biomass sources can vary significantly. Cellulose, hemicellulose and the lignin content of woody biomass differ between wood species. The ash content of certain wood species can total no more than parts per thousand, while the inorganic content of black liquor can account for up to 40–50% of the total flow. The temperature and species illustrated in Figure 2 are examples of this.

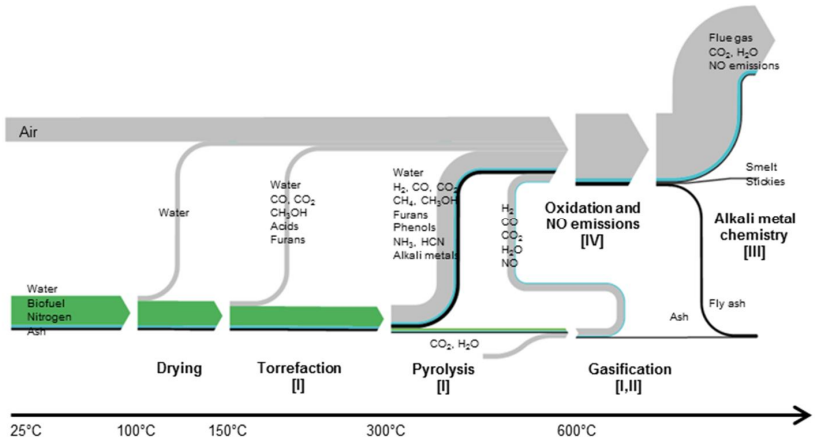

Figure 2. Thermal conversion of biomass while temperature is rising [4–6].

During the last decade, major research and development efforts have been directed at refining biomass into bio-fuels and bio-chemicals. The two main routes for such conversion are the thermo-chemical and biochemical ones. Thermo-chemical conversion has been based on the above-mentioned steps. Examples of the proposed processes include: (i) Use of torrefaction to improve the energy density of biomass and remove excess oxygen. Torrefied biomass could be used for replacing coal in boilers. (ii) Pyrolysis, a technology used for creating liquid bio-oils. These oils could replace heavy fossil oils used in heating applications. (iii) Gasification of biomass is applied in the production of bio-based synthesis gas. This gas could be further utilised in gas-turbines for efficient electricity production, in kilns, or for producing bio-fuels and bio-chemicals. (iv) Hydro-thermal treatment, where steam and heat are applied to biomass to produce intermediate chemicals for further processing. On the other hand, biochemical routes can be used for (v) processing sugars into chemicals or bio-fuels, such as ethanol. Bio-chemical routes utilise enzymes to break down large molecules into smaller ones and microbes for the fermentation and production of final products. In some cases, thermo-chemical and biochemical routes emerge, e.g. through the fermentation of thermo-chemically produced synthesis gas.

This work focuses on the thermo-chemical route, and the related super-equilibria observed during the related processes.

1.2 Super-equilibria

Super-equilibrium is a state within a chemical system in which an excess amount of species occurs during a particular phase compared to the equilibrium state. The term has previously been used to describe the excess amount of free radicals in the flame [8]; here, it is extended to describe all states in which an excess amount of a particular species or phase exists. In addition, super-equilibrium is a local equilibrium state with higher free energy within the system. The chemical system is constrained in some way: chemical kinetics, mass and heat transfer or mixing may constrain the system from reaching a global equilibrium. In this work, I also assume that the super-equilibrium system is only partly constrained, and is characterised by additional degrees of freedom. For example, the mass transfer between the gaseous and solid phase may be constrained, but the local equilibria in the gaseous and solid phases are present.

The opposite of super-equilibrium is sub-equilibrium, whereby there is a shortage of a particular species in a certain phase. In practice, super-equilibrium and sub-equilibrium exist concurrently. There is a surplus of some species and a shortage of others compared to the global equilibrium state. In general, the terms non-equilibrium or para-equilibrium are used for these local equilibrium states. However, in this work, excess amounts of species are observed in certain phases, which justifies the use of the term ‘super-equilibrium’.

Examples of super-equilibria are shown in Figure 3. An excess amount of solid biomass is present during pyrolysis [I]. During biomass gasification, an excess

amount of methane is present [II]. In the case of a kraft pulp mill recovery boiler, there is excess sulfur and sodium in the flue gas [III]. Radical over-shoot, i.e. a super-equilibrium of free radicals, causes NO emission formation at the very beginning of combustion, resulting in elevated emission levels [IV].

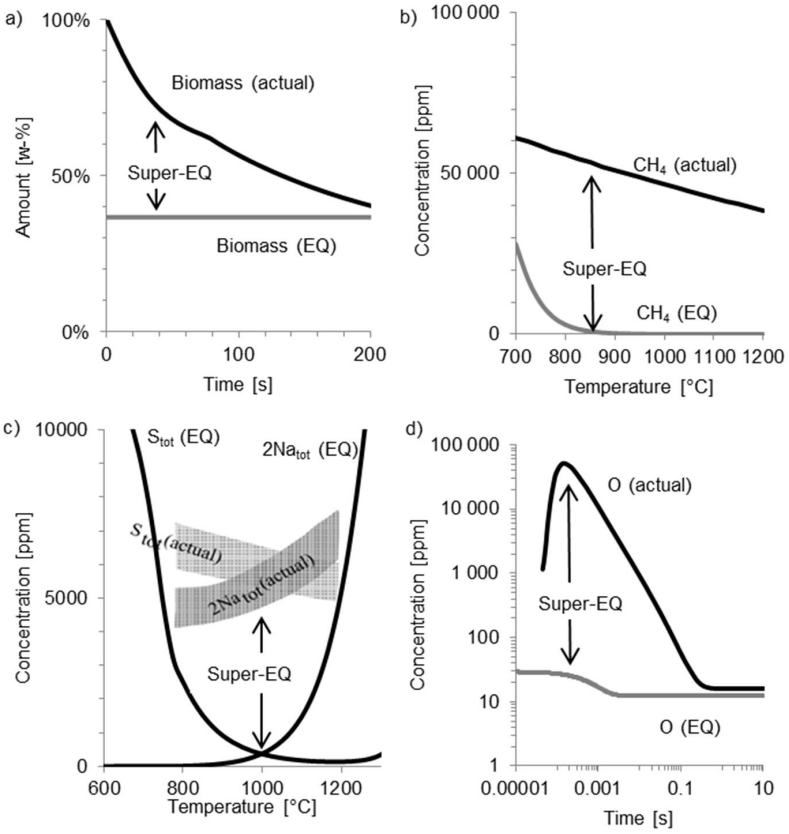

Figure 3. Super-equilibria observed during thermal biomass conversion. a) Biomass conversion during pyrolysis [I]. b) Gasification of biomass, where an excess amount of methane is present [II]. c) Kraft pulp mill recovery boiler, where excess sulfur and sodium are present in the flue gas [III]. d) NO emission formation due to the oxygen radical over-shoot at the very beginning of combustion [IV].

1.3 Constrained free energy method

Nature drives processes and systems towards thermodynamic equilibrium over time, based on the second law of thermodynamics. Simultaneously, the entropy of a closed system increases. This process is rapid at the elevated temperatures present in the processes related to thermal biomass conversion. However, the pure global thermodynamic equilibrium is seldom reached in practice, as shown in Figure 3.

Similar phenomena have been observed previously in other processes. Due to this finding, a rigorous method has been developed for constraining the thermodynamic system [9–12]. Constrained free energy, CFE, method allow the extension of the thermodynamic system with additional immaterial constraints. These constraints can be defined based on the extent of the reaction [13,14], the surface area [15,16] and volume [17,18] and electrochemical potential [17,18]. Successful applications have been reported in inorganic chemistry [13,14], paper making [18,19], metallic alloys [20] and bio-chemistry [21,22].

CFE is a method which describes the dynamic phenomena simultaneously with the equilibrium calculation, while resolving the local constrained equilibrium state of the process. Chemical reactions, the enthalpic effect of reactions and state variables are calculated concurrently.

1.4 Aim of the study

Thermodynamic equilibrium calculation has been a widely used method to describe the thermal processes of biomass conversion. In reality, these processes do not reach the equilibrium state, but super-equilibria states are present as seen in Figure 3. Previously, these dynamic features of thermal biomass conversion processes have been modelled using detailed kinetic models, or by decoupling the kinetic features from equilibrium calculations. This thesis evaluates the feasibility of a novel approached, based on the constrained free energy, CFE, method, for describing observed super-equilibria in thermal biomass conversion.

The hypotheses of the study are:

- The constrained free energy, CFE, method is a feasible practice for describing the observed dynamic phenomena of thermal biomass conversion.
- The method could be applicable in processes such as torrefaction, pyrolysis, and the gasification of biomass, thermal and fuel NO emission formation, and pyrolysis and the combustion of black liquor with dissolved wood.
- The thermodynamic system may be constrained based on different kinds of models: constant values, empirical models, global kinetic models and models based on elementary kinetic reactions could be implemented as part of the CFE method.

2. Background

This study evaluates several processes whereby the thermal conversion of biomass is conducted and super-equilibria are observed. Publication [I] applies this approach to low temperature processes, such as biomass pyrolysis and gasification. Carbon conversion and char gasification are presented in Publication [I]. Publication [II] evaluates the observed super-equilibrium of methane, tar and ammonia in the syngas of a biomass gasifier, discussing char formation during this process. Publication [III] presents the super-equilibria of alkali metals, sulfur and chlorine observed in the flue gases of a kraft pulp mill recovery boiler. Publication [IV] discusses NO emissions and the related super-equilibria of free radicals during combustion. Finally, in publication [V], the basics of the CFE method are represented. The main features of these processes and the related super-equilibria, as well as a review of earlier modelling efforts, are given here. In addition, there is an introduction to other applications in which the CFE method has already been applied.

2.1 Biomass torrefaction, biomass pyrolysis and char gasification

Biomass, i.e. wood in this study, accounts for a significant portion of energy usage as seen in Figure 1. Woody biomass is composed of the following main components: (i) cellulose (40–50 w-%), (ii) hemicellulose (25–35 w-%), and (iii) lignin (20–35 w-%) and (iv) extractives. A significant amount of (v) ash is present, which may have an effect on the ash chemistry of boilers. Some (vi) nitrogen, which is volatilised during combustion and causes fuel-based nitrogen oxide emissions, also exists in biomass. In addition, the moisture-level of biomass can be as high as 50%, requiring a large amount of water to be removed before or after the mass reaches the boiler.

The structure of the main wood components differs, entailing that the composition of volatile species is heavily influenced by the original biomass [4,23]. This is especially true in low temperature applications such as the torrefaction and pyrolysis of biomass. Cellulose is composed of linear glucose chains. The volatile components of cellulose include levoglucosans. Hemicelluloses are a mixture of polysaccharides. Polymer chains are branched and are shorter than cellulose chains.

Lignin can be defined as an irregular array of phenylpropane units. Phenolic groups in volatile species originate from the lignin in biomass.

During thermal conversion, biomass passes through the following stages [4,24]: (i) First, the biomass is dried when the temperature is below 150°C. (ii) Torrefaction occurs in a temperature window of 150–300°C. (iii) Pyrolysis of biomass is conducted at a temperature of 300–600°C. (iv) Finally, char is gasified with an additional gasification agent (CO_2 or H_2O) when the temperature is above 600°C. The temperature ranges of different wood fractions vary: hemicellulose decomposes first, after which cellulose and lignin are considered the most difficult materials to decompose. Naturally, the wood species in question has an influence on the decomposition speed and temperature [25].

Torrefaction can be applied as a process itself, in order to reduce the oxygen content of biomass, while increasing its energy density. A proposed application for torrefied biomass involves the replacement of solid fuels, such as coal and biomass, in the boiler. In the production of liquid biofuels, pyrolysis is an alternative. In such a case, a condensable part of the volatile light hydrocarbons is utilised as biofuel. Then, the most promising end use would involve replacing heavy heating oil with bio-oil in power plants.

Carbon conversion and composition of volatile species

The decomposition and volatilisation of biomass during the torrefaction and pyrolysis phases are slow phenomena. A super-equilibrium state of solid biomass is apparently present in these processes, as seen in Figure 3a. This super-equilibria during torrefaction [26], pyrolysis [4] and also char gasification [27] is often observed by measuring the biomass conversion during these processes.

As previously mentioned, the composition of the gaseous phase originates in the biomass. During torrefaction, oxygen-containing species such as water, carbon monoxide and dioxide, acids (formic, acetic and lactic), methanol, hydroxyacetone and furfural are formed [28]. During pyrolysis, hydrogen, carbon monoxide, carbon dioxide, acids (acetic), furans (furfural, HMF), anhydrosugars (levoglucosan), phenols and methanol [4,5] are observed. The amount of these species exceeds the equilibrium values, which leads to the further observation of super-equilibrium states.

Previous modelling efforts

Global reaction kinetics is most commonly used for modelling biomass torrefaction [26,28,29] , biomass pyrolysis [30–32] and char gasification [33–36]. In such cases, frequent use is made of models based on Arrhenius kinetics. Such models allow the empirical definition of temperature and time-dependent parameters for these processes. Volatilisation and char formation are described through intermediate states, as presented in [l]. More information on other models of torrefaction

[26,37], pyrolysis [38] and char gasification [39,40] is widely available in the literature on the subject.

Since a majority of torrefaction and pyrolysis models, and char gasification models, were based on the kinetic approach, this may form a good test case for evaluating the feasibility of the constrained free energy, CFE, method. The aim of the Publication [I] was to evaluate these processes and the super-equilibria of solid biomass, as well as the composition in each case during the gaseous phase.

2.2 Biomass gasification

Gasification has been suggested as a promising technology for improving the energy efficiency of biomass combustion, or even upgrading biomass into biofuels or bio-chemicals. This process is based on a thermo-chemical route whereby a synthesis gas (mixture of CO, CO_2, H_2, H_2O and other light hydrocarbons) is produced from biomass in a reductive environment. Such a synthesis gas can be further upgraded to form a different end product, or can be combusted in gas turbines and kilns.

Three types of gasification processes have been developed [40]: (i) Fixed bed gasifiers are applicable in smaller processes. (ii) Fluidised bed gasifiers represent the most promising technology for biomass gasification. (iii) Entrained flow gasifiers can be very large and produce syngas with fewer tars, but the size reduction of biomass and corrosivity of molten ash from biomass are drawbacks. Two heating options for gasifiers are available: In direct heating, part of the biomass is oxidised and heat is generated simultaneously. In this case air and oxygen can be used as gasification media. In in-direct heating, an external heat source is applied and thus higher heating value of synthesis gas is obtained. [40]

During gasification, the biomass undergoes rapid drying, torrefaction, pyrolysis and char gasification steps [39] similarly to the processes that occur during combustion, as seen in Figure 2. However, as there is always a limited amount of oxygen present, the final combustion stage is at least partly neglected. During the biomass gasification, the role of the torrefaction and pyrolysis phases is emphasised, whereas during coal gasification the final char gasification is the key step in the production of synthetic gas [40,41].

Methane, tar, char and ammonia formation during gasification

The generation of light hydrocarbons (mainly methane), tar, char and ammonia is observed during fluidised bed gasification [39–42]. The source of these species is the biomass itself. During torrefaction and pyrolysis, volatile compounds are released. The structure and composition of these gaseous compounds originate in the biomass structure [23]. Due to the gas phase reactions, e.g. oxidation and water-gas-shift reaction, smaller molecules of the synthesis gas are produced. When the temperature is raised or a more oxidative media is supplied, the amount

of methane, tar, char and ammonia falls [41,42]. Publication [II] discusses these topics further.

Previous attempts to model biomass gasification

Thermodynamic equilibrium is often assumed as a basis for modelling the gasification process [43–45]. However, this is a simplified approach which does not allow the accurate prediction of the presence of light hydrocarbons, ammonia and tars in the synthesis gas or the char formation. When thermodynamic equilibrium is assumed, these super-equilibria states are totally neglected.

Quasi-temperature models are viewed as one possible solution for improving the accuracy of thermodynamic models. Here, a lower temperature is applied to the calculation of thermodynamic equilibrium, as the formation of methane, char and tar increases at lower temperatures. In this way, the right composition of synthesis gas can be obtained. However, the temperature difference must be defined experimentally, on a case-by-case basis, and the actual process temperature can be 250–500°C [46,47] higher than that used for modelling. Even when the chemical reactions could be modelled using this quasi-temperature approach, the enthalpic effects are neglected.

Modified thermodynamic models take a dual approach to modelling the gasification process [34,41,42,48]. Part of the incoming biomass is separated from the main flow and converted to char, tar, ammonia and light hydrocarbons based on experimental models. The rest of the raw material is modelled based on the thermodynamic equilibrium assumption. Later, these two streams are mixed in order to create the correct composition of the final synthesis gas.

Recent reviews of biomass gasification models [39,40] indicate that other efforts have been made to model biomass gasification: kinetic models which describe the proposed reaction mechanisms; fluidisation models which describe the phenomena observed in the fluidised bed; and a limited number of CFD models of biomass gasification. These models can provide comprehensive details of particular problems, but often include a very high number of unknown parameters, which require definition.

Here again, the need for a unified solution relating to the super-equilibrium state and enthalpic effect in biomass gasification was apparent. Thus Publication [II] evaluates the feasibility of a solution based on the CFE method. Somewhat similar ideas have been presented by others: the amount of reactive char can be limited when calculating the thermodynamic equilibrium [47,49], and methane formation during gasification can be fixed [49].

2.3 Black liquor combustion

Black liquor is a very plentiful source of bioenergy, as shown in Figure 1. This energy originates from the dissolved wood in black liquor, where roughly half of the processed biomass [50] is dissolved during the delignification process in the

fibre line of a kraft pulp mill. In addition, large quantities of sodium and sulfur are present in the black liquor, as sodium hydroxide and sodium sulfide are used as the main cooking chemicals. The potassium and chlorine levels are lower but have a significant effect on the chemistry of the recovery boiler. The dry content of black liquor is high, since multi-step evaporation is used for removing excess water before the process reaches the recovery boiler. The composition of black liquor varies from mill to mill, based on the wood species, the properties of cooking chemicals, the type of process applied and water connections.

Black liquor is combusted in a recovery boiler, which has two functions: the first of these involves converting dissolved wood into energy. This heat is used for running and generating electricity for the pulp mill, as well as producing electricity for sale. The second function involves salvaging the used cooking chemicals as sodium carbonate and sodium sulfide. Special process conditions are required in order to achieve this dual target: the lower part of the recovery boiler furnace is operated under reductive conditions, in order to ensure the conversion of sodium sulfate into sodium sulfide. The upper part of the furnace is operated under oxidative conditions, in order to ensure the full combustion of organic substances contained in black liquor.

Enrichment of alkali metals and sulfur into flue gas

Black liquor is sprayed into the boiler for combustion. The droplets are dried, devolatilised and pyrolysed during the in-flight, and the remaining char is gasified and burned in the bed in a similar way to that shown for biomass in Figure 2. It has been observed that, during these steps, large quantities of alkali metals are reduced [51] and volatilised, chlorine is directly vaporised [51] and sulfur is released as organosulfur gases [52]. Thus, these species are enriching for the flue gases of the recovery boiler and a super-equilibrium is again achieved, see Figure 3.

In [III] some observations of previous studies [53–57] are summarised. The amount of vaporised sulfur in the incoming quantity can be up to ~ 50%, and up to ~ 20% respectively in the case of vaporised sodium. It is also known that potassium and chlorine tend to enrich into flue gases to an even greater extent. A comparison shows that the enrichment value is up to 2.5 for potassium and up to 6.0 for chlorine, respectively [III].

Previous attempts to model a recovery boiler

Several modelling approaches have been used for describing the observed super-equilibria in a recovery boiler and the related issues of stickies and possible corrosion. A major study involved the development of a thermodynamic database applicable to the alkali metal salts observed in the recovery boiler. In [III] the thermodynamic system for Na-K-S-Cl-C-O-H described in [58–60] have been utilised. Recently, the database was further upgraded with the addition of bromides [61].

The thermodynamic approach has been widely used for describing the upper furnace and flue gas channel and, in particular, the formation of stickies and corrosive salts [62,63] on top of heat exchangers as 'boiler advisor' tools. The most recent development incorporates the experimentally-based database of detrimental corrosive conditions in the flue gas channel and allows the boiler designer to choose the proper materials for those conditions [7]. A lower surface and the enrichment of species into flue gas are considered as boundary conditions in such models: experimental values, kinetic models [64], thermodynamic equilibrium [53] or a combination of these [56] are applied to defining the volatilisation of alkali metals, sulfur and chorine.

Thermodynamic equilibrium models are also used as part of the large-scale process simulation. The lower furnace is again modelled using kinetic models. The upper furnace and flue gas channel are described on the basis of several thermodynamic equilibrium reactors in series [65,66].

Computational fluid dynamics (CFD) models are used for boiler design and troubleshooting. Here, separate models for gas phase combustion, droplet modelling and char bed burning are combined [67] with mixing models implemented in CFD tools. The latest developments in terms of recovery boiler CFD models incorporate a changing bed shape [64] and flue gas particle formation [68].

Separate models for black liquor spraying and droplet formation [69], and fly ash particle formation, have been reported [55,70]. Detailed descriptions of various models are given in reviews [51,64,71].

In general, all of the above examples involve decoupling the formation of super-equilibrium from thermodynamic equilibrium calculations. It therefore again seemed that the CFE method could be used as a unified method of modelling these super-equilibrium conditions. This method could be a practical approach when modelling the chemistry and heat generation of a recovery boiler. The feasibility of CFE in modelling the super-equilibria in recovery boilers was evaluated in [III].

2.4 Nitrogen oxide emissions

Nitrogen oxide emissions (NO_X = NO + NO_2) during the combustion of biomass and black liquor formed another interesting case. It has been estimated that biomass combustion is causing 20% of anthropogenic NO_X emissions in the world [72]. These emissions are causing acidic rain, while tropospheric ozone is having a detrimental effect. Control of nitrogen oxide emissions is therefore essential.

In general, during combustion four different sources of NO_X emissions have been recognised [73]: (i) Thermal NO_X formation through the oxidation of atmospheric nitrogen at high temperatures. (ii) Prompt NO_X, which is formed in a fuel-rich zone if hydrocarbons are reacting with atmospheric nitrogen. (iii) The N_2O route, and (iv) Fuel NO_X whereby nitrogen is volatilised from wood and further oxidised to form NO emissions. Because the amount of NO_2 is considered low compared to NO, only term NO emissions are used in this study.

Over-shoot of free radicals and freezing of NO emissions

During the very first steps of combustion, there is a rapid increase in the amount of free radicals. During this over-shoot of radicals, the super-equilibria of for example O, H and OH radicals are formed. These super-equilibria initiate combustion but also facilitate the rapid development of NO emission.

After combustion is finalised and the flue gases have cooled down, the achieved level of NO emission remains, even if the final temperature is low. Again, super-equilibrium is formed for these frozen NO emissions.

Previous attempts at modelling NO emissions

Detailed kinetic models, DKM, are often applied when the accurate prediction of combustion phenomena and NO emissions is required. These models concurrently compute radical build-up, the combustion of hydrocarbons and NO formation. Major research efforts have led to the assessment of detailed reaction mechanisms and reaction parameters. Examples of DKM include Gri-Mech 3.0 mechanism [74] and the ÅA mechanism [75]. These models explain the combustion of light hydrocarbons and the related emissions, and may include hundreds of elementary reactions. Due to the complexity of the models, they are usually applied to cases involving simplified reactor setups, such as a series of ideal reactors or as plug-flow reactors.

In order to reduce the complexity of the models, a separate set of reduced models has been developed. Here, the most critical element in the whole reaction mechanism is applied. A third option is so-called global models, which can describe the oxidation of hydrocarbons [76] and formation of NO emissions [77–79]. The model structure of these global models is often Arrhenius type equations, although the parameters are either defined experimentally or model based. A typical use of reduced and global models is computational fluid dynamics, CFD. In such cases, mixing and combustion are calculated first, with NO emissions often determined as a post-processing step. More details on the modelling of NO emissions are given in the review papers [73,80,81].

DKM used for NO emissions is considered the best validated kinetic mechanism available. It has therefore seemed tempting to evaluate the feasibility of the CFE method in modelling NO emissions and to compare the results to those of DKMs. Previous studies [82,83] have applied a somewhat similar technique – rate-controlled constrained-equilibrium, RCCE – to the modelling of NO emissions in internal combustion engines. This has made the use of the CFE method in modelling NO emissions seem plausible in biomass combustion too. Publication [IV] discusses this topic.

2.5 Constrained thermodynamic equilibrium

The constrained thermodynamic equilibrium of a chemical system is achieved when something is limiting the system from proceeding further towards the global equilibrium. Such a constraint can be defined based on (i) the extent of the various reactions, (ii) electrochemical potential, (iii) surface area, and (iv) volume.

The first attempts to constrain the calculation of thermodynamic equilibrium based on reaction rates were conducted for the freezing of CO and NO emissions during internal combustion in the gas phase [82,83]. This method was later named RCCE, Rate-controlled constrained-equilibrium, and studies were focused on the combustion of light hydrocarbons in internal combustion engines [84]. The constraints applied to the RCCE method were based on the extent of the reactions, which were often deduced from detailed kinetic models. Typical constraints with respect to these included the number of moles or the quantity of radicals in the system [84].

The CFE method was developed [13,85] somewhat in parallel, to allow for the calculation of multiphase systems constrained by other physical factors too. The first applications of this kind primarily lay in high-temperature inorganic chemistry, such as the production of titanium oxide. New application areas, such as aqueous suspension chemistry in paper making [18] and the production of metal alloys [20], emerged later. Simultaneously, new types of constraints were found and defined, such as electrochemical potential [18], surface area [15,16] and volume [17,18]. In addition, based on this method immaterial constituents were introduced alongside the immaterial constraints of components [9]. The method was named the constrained free energy method, abbreviated to CFE. RCCE, with its 'extent of reaction' based constraints, can be considered a sub-set of the more generic CFE method.

A detailed description of the CFE method is given in the literature [11,12,86]. In addition, some examples of CFE method are summarised in [10]. A short review follows of the various constraints and application areas. The published applications are summarised in Table 1.

Extent of reaction

The reaction rate or chosen extent of reaction is one of the most widely used constraints with respect to the CFE method. In general, all RCCE applications and the majority of CFE applications are based on the 'extent of reaction' type of constraint. Publications [I– IV] also use this approach when defining super-equilibria.

A large number of published applications are related to combustion: constraining 'aromaticity' in benzene flames [87], internal combustion of hydrogen [84,88], methane [84,89,90], methanol [90], formaldehyde [90] and ethanol [89] have been reported on. In addition, the freezing of NO and CO emissions in internal combustion engines have been studied [82,83].

The extent of reaction approach is also used for predicting the dissolution and precipitation of calcium carbonate and the release of carbon dioxide from paper making water suspension [18,19]. This application is discussed in more detail in [V]. Anatase-rutile transformation has also been reported in the production of titanium oxide [13,14] and the mercury-chlorine system [86]. In addition, the para-equilbria involved in steelmaking, where [20] the mass transport between different solidifying phases is constrained, can be considered an example of the 'extent of reaction' type of constraint. Finally, the analyses of biochemical reaction pathways [21,22] illustrates a wholly new application area for the CFE method.

The width of the applied constraints vary greatly: minimal models such as the production of titanium oxide [13,14] or the dissolution and precipitation of calcium carbonate include only one or two constraints and a similar number of kinetic reactions which are used for defining the constraints. On the other hand, the most extensive models of ethanol combustion [89] or biochemical pathways [21,22] can include dozens of constraints and even hundreds of reactions (see Table 1). In general, in CFE models the aim is to minimise the number of required constraints by defining the slowest and most critical reactions. These reactions are constrained and local thermodynamic equilibrium is otherwise considered.

Electrochemical potential

Constraints based on the electrochemical potential between the two aqueous phases formed in pulp suspensions have been reported [17,18] as one application area of CFE. Here, an aqueous suspension with anions and cations is present. Wood pulp has some immobile anions during the fibre phase. Due to this charge, the distribution of anions and cations varies between the fibrous and bulk aqueous phases. By defining this constraint based on the electrochemical potential difference, it was possible to model e.g. accurate calcium chemistry during paper making processes [91].

Volume and surface area

Volume as a constraint was also applied to paper making applications [17,18]. The amount of water inside the pulp fibres was considered constant and a constant volume was therefore defined as a constraint. This had effects on the ionic strength of the two aqueous phases.

Surface area is used as a constraint when the surface tension of liquid mixtures and e.g. metal alloys is modelled [15,16]. When both surface area and volume are used as constraints, the thermochemical properties of nano-particles greatly affected by the surface energy can be modelled [12,92].

Applied tools

A large share of CFE models are implemented in the ChemSheet program [93]. This tool allows the easy extension of multiphase thermodynamic systems with immaterial constraints applicable to the CFE-technique. However, other tools can also be used: para-equilibriums are calculated with Fact-Sage [20] and various NASA equilibrium codes are used in RCCE applications [88]. In some cases, where the number of constraints and reactions is very large, it may be necessary to use a separate differential equation solver suitable for stiff numerical systems [88].

In Publications [I–V], ChemSheet is applied as a tool for the calculation of super-equilibria using the CFE method.

Table 1. Applications of constrained thermodynamic equilibrium.

Constraint	Application area	Details	C/R[a]	Reference
Extent of reaction	Combustion	Benzene combustion	1-2/-	[87]
.	Inorganic chemistry	Anatase-rutile transformation	1/1	[13,14]
	Inorganic chemistry	combustion of $TiCl_4$	1/1	[94,95]
	Inorganic chemistry	Mercury-chlorine system	3/3	[86]
	Biochemistry	Reaction pathways	up to 17/17	[21,22]
	Papermaking	Calcium chemistry	2/2	[18,19,91,96],[V]
	Metallic alloys	Para-equilibriums in steel making	(NP-1)x(M-1)[b]	[20]
	Internal combustion	NO freezing	2/14	[82,83]
	Internal combustion	CO freezing	2/9	[82,84]
	Internal combustion	Hydrogen combustion	3/14 & 6/15 16/42 & 12/20 &	[84,88]
	Internal combustion	Methane combustion	16/352	[84,89,90]
	Internal combustion	Methanol combustion	10/16	[90]
	Internal combustion	Formaldehyde	9/12	[90]
	Internal combustion	Ethanol combustion	16/232	[89]
	Biomass combustion	Black liquor combustion	4/4	[I]
	Biomass combustion	Biomass gasification	5/5	[II]
	Biomass combustion	Char gasification	1/2	[III]
	Biomass combustion	Biomass pyrolysis	2/3	[III]
	Biomass combustion	Biomass torrefaction	3/3	[III]
	Combustion	Thermal-NO	1/1 - 5/11	[IV]
	Combustion	Fuel-NO	5/7	[IV]
Electrochemical potential	Papermaking	Aqueous ion exchange	2/-	[17,18] and [V]
Surface area	Metal alloys	Surface tension	1 & L + (N-1)[c]	[15,16]
	Metal alloys	Nano-particles	1/-	[12,92]
Volume	Papermaking	Fibre - Water -phases	1/-	[17,18]

[a] C is the number of applied constraints and R is the number of applied reaction. [b] NP is number of phases and M is number of metallic species. [c] 1 for monolayers. For multilayers L is number of layers and N number of chemical species.

3. Methodology

The presented study is computational in nature, with the applicability of the CFE methodology being evaluated against different model structures in the cohesive application areas. The numerical values of the defined constraints are obtained from the literature for all Publications [I–IV]. The results are evaluated against the literature results for [I–III] and against an alternative model for [IV]. The presented method is applied in 0-D or 1-D models representing ideal mixing reactors or laminar plug-flow reactors. Publication [V] summarises the applied CFE methodology, which is also presented here in brief.

3.1 Calculation of thermodynamic equilibrium

The thermodynamic equilibrium of a closed chemical system is achieved when the entropy of the system is maximised or its free energy minimised. Gibbs' free energy of the system can be defined as Equation 1.

$$G = H - TS = \sum_{k=1}^{K} n_k \mu_k \tag{1}$$

Here, G is Gibbs' free energy, H is the enthalpy of the system, T is the temperature, S is the entropy of the system, k refers to each constituent in the multi-phase system, K is the number of constituents in the multi-phase system, n is the molar amount of each constituent and μ is the chemical potential of each constituent.

When this function is minimised, the Lagrange method for undetermined multipliers is often used [97,98], see Equation 2. The minimum of Gibbs' free energy is found when the partial derivatives of Lagrange function L are zero, see Equations 3 and 4. The chemical potentials of constituent are defined by Equation 3 and the mass balance of system is defined by Equation 4.

$$L = G - \pi\Psi = \sum_{k=1}^{K} n_k \mu_k - \sum_{l=1}^{L} \pi_l \left(\sum_{k=1}^{K} \nu_{kl} n_k - b_l \right) \tag{2}$$

$$\left(\frac{\partial L}{\partial n_k}\right)_{n_{n\neq k}} = \mu_k - \sum_{l=1}^{L} \pi_l \nu_{kl} = 0 \tag{3}$$

$$\left(\frac{\partial L}{\partial \pi_l}\right)_{\pi_{n\neq l}} = \sum_{k=1}^{K} \nu_{kl} n_k - b_l = 0 \tag{4}$$

Here π is the Lagrange multiplier vector. Ψ is the mass balance of the different components of each constituent, written in terms of the amount of matter (mol). L is the number of components in the system. π_l is the Lagrange multiplier of component l, b_l is the total amount of component l in the system, and ν_{kl} is the stoichiometric coefficient of component l in constituent k.

More details for solving the minimum of Gibbs' free energy are available in the literature. Generic presentations of the topic are given in [11,97–100]. The linearisation of Equations 3 is described in [97]. A representation in matrix form is given in [100] and [V].

3.2 Inclusion of immaterial constraints

The local thermodynamic equilibrium is solved by the inclusion of additional immaterial constraints in the chemical system. In this study, the CFE technique is used for estimating the super-equilibria based on the extents of the reactions used as constraints. The affinity of a chemical reaction A is defined as a negative partial derivative of Gibbs free energy G with respect to extent of reaction ξ, see Equation 5. Thus, the change in Gibbs energy with respect to chemical system ΔG, due to the constrained reactions, can be expressed as Equation 6.

$$A = -\left(\frac{\partial G}{\partial \xi}\right)_{T,p} \tag{5}$$

$$\Delta G = -\sum_{r=1}^{R} A_r \xi_r \tag{6}$$

Here, T is temperature and p is pressure, and r refers to each constraining reaction. R is the number of constrained reactions. A typical chemical system is composed of K amount of constituents, which are formed from L amount of components, which are typically elements. When additional immaterial constraints are included in the chemical system, the stoichiometric matrix is extended as shown in Equation 7. In the extended matrix, there is X number of immaterial constituents and Y number of immaterial components.

The immaterial component y is incorporated in the actual constituents, with a value of ν_{ky}. Each immaterial constituent ν_{xy} is connected to the corresponding immaterial components y with a positive value, if this particular reaction is increas-

ing the amount of immaterial component. Likewise, a negative value applies if the amount is decreasing due to the reaction. The values of immaterial constituents can be set based, for example, on the reaction stoichiometry. Practical examples of extended matrices are given in [I–V].

$$\mathrm{N} = \begin{bmatrix} \nu_{1,1} & \cdot & \nu_{1,L} & \nu_{1,L+1} & \cdot & \nu_{1,L+Y} \\ \cdot & \cdot & \cdot & \cdot & \cdot & \cdot \\ \nu_{K,1} & \cdot & \nu_{K,L} & \cdot & \cdot & \cdot \\ \nu_{K+1,1} & \cdot & \cdot & \nu_{K+1,L+1} & \cdot & \cdot \\ \cdot & \cdot & \cdot & \cdot & \cdot & \cdot \\ \nu_{K+X,1} & \cdot & \cdot & \cdot & \cdot & \nu_{K+X,L+Y} \end{bmatrix} \tag{7}$$

3.3 Defining constraints

Extent of reaction can be defined based on the (i) constant value as applied in Publication [I,II], (ii) experimental models as in [I,II], (iii) global kinetic models reported in [III–V], or (iv) models based on elementary kinetic reactions as in [IV]. Definitions for different cases are given in Equations 8a, 8b and 8c.

$$\xi_x = C_x \qquad \text{(constant value)} \tag{8a}$$

$$\xi_x = f_x(T) \qquad \text{(temperature dependent model)} \tag{8b}$$

$$\xi_x = \int_0^t r_x dt \qquad \text{(global and elementary kinetic reactions)} \tag{8c}$$

Here, ξ_x refers to extent of reaction *x*. *C* is a constant value, while *f* stands for function. *T* is temperature, *t* refers to time and *r* is the reaction rate. The extent of the reaction is given as the reaction rate integrated from the beginning to the current time step, since the constraint is dependent on time.

The reaction rate can be given as a net reaction rate or by defining independent reaction rates of forward and reverse reactions, Equation 9. In the former case, only one immaterial constituent is implemented in the extended reaction matrix *N*, Equation 7. In the latter case, two separate immaterial constituents are needed for defining both the forward and reverse reactions.

$$r_x = r_{xf} - r_{xr} \tag{9}$$

Here, the subscript *f* refers to forward reaction and *r* to reverse reaction. Global kinetic models and models based on elementary kinetic reactions are often given

as Arrhenius types of model. Equation 10 defines the reaction rate based on the rate constant and concentrations. Equation 11 gives the definition of the rate constant, which is dependent on the temperature and different Arrhenius type of constants.

$$r_x = k_x \prod_b [j]^{a_b} \tag{10}$$

$$k = AT^B \exp^{(-E/RT)} \tag{11}$$

Here k is the rate constant. j is the constituent in the reaction matrix, a is the stoichiometric coefficient of the constituent, and b refers to all constituents involved in the reaction. A is frequency factor, B is temperature exponent, E is activation energy, R is gas constant and T is temperature. Additional details on implementing extents of reaction as part of the CFE method are available in the literature [11,13,96] and [I–V].

3.4 Affinities of constrained reactions

Constraints based on the extent of reaction were defined as an extension of the calculation of Gibbs' free energy of system in Equation 6. The affinities of each chemical reaction are defined according to Equations 12a, 12b and 12c. If a particular reaction is in equilibrium, the affinity is 0. A positive value for the affinity indicates that the reaction is not finalised, something is constraining the reaction and a super-equilibrium state is thereby formed.

$$A_r = -\Delta_r G = \sum_k a_k \mu_k \tag{12a}$$

$$A_r = \sum_k a_k \mu_k = 0 \quad \text{(for all equilibrium reactions)} \tag{12b}$$

$$A_r = \sum_k a_k \mu_k = \sum_k a_k \sum_{l=1}^{L+X} \nu_{kl} \pi_l \neq 0 \quad \text{(for all constrained super-equilibrium reactions)} \tag{12c}$$

Here A is affinity of reaction. Δ_r refers to the change due to each reaction. G is again Gibbs' free energy, and a_k is used for the stoichiometric coefficient in the reaction matrix for species k in a given reaction. Here, and in Equation 6, v refers to the coefficient of the stoichiometric matrix. (In many cases, reversed notation is used for a and v. Typically, a is used for the stoichiometric matrix and v for the reaction matrix. However, here this given notation is used for the sake of consistency with the notation used in Publications [I–V]).

More details on applying affinities in CFE calculations are given in the literature, [11,96] and [I].

3.5 Thermodynamic data and applied tools

Thermodynamic data are obtained from (i) HSC [101] for Publication [I,II], (ii) from FactSage [58] [III], and (iii) from the DKM/ÅA mechanism [75] [IV]. ChemSheet [93] was used as a modelling tool in all Publications [I–V].

Estimation of H, S and C_p for biomass

The ultimate analysis of fuel was employed as the input composition of biomass in Publications [II,III]. Volatile species were used for input composition in [IV]. However, in [I] the standard enthalpy, entropy and heat capacity of biomass were determined based on different pseudo-biomass fractions.

Thornton's rule [102] was applied to estimating the standard enthalpy of formation. This rule is based on an assumption of oxycalorific equivalence of 450 kJ/mol O_2 required for the complete combustion of biomass as presented in Equation 13. A similar method is proposed for the standard entropy of formation [102]. This method is based on the experimental measurement of the standard entropy of formation of different biomass compounds, see Equation 14. Although the set of measurements reported is rather small, it has been noted [102] that the method provides a reasonably good estimation for larger bio-molecules. Finally, the heat capacity is estimated based on the average of different wood species reported in the literature [103], see Equation 15. The feasibility of this estimation method is evaluated in Publication [I].

$$\Delta_f H_k = \Sigma \Delta_f H_{prod} - 450.0 n_{O_2,c} \tag{13}$$

$$\Delta_f S_k = -0.813 \Sigma S^o_{k,atoms} \tag{14}$$

$$C_{p,k} = (5.304T - 299) M_k \tag{15}$$

Here, $\Delta_f H_k$ is the estimated standard enthalpy of formation and $\Delta_f S_k$ the estimated standard entropy, respectively. k refers to species k. $\Sigma\Delta_f H_{prod}$ is the sum of the standard enthalpies of combustion products (CO_2 and H_2O) in full combustion. $n_{O2,c}$ refers to the number of oxygen atoms needed for the full combustion of reactants. $\Sigma S°_{k,atoms}$ is the sum of the standard entropies of the individual atoms. $C_{p,k}$ refers to the heat capacity of species k . M_k is the molar mass.

3.6 Applied constraints

Constraints were defined based on the models reported in the literature. Constant values were used as constraints for the black liquor gasification reported in Publication [III] and for the biomass gasification [41] reported in [II]. Also, the extent of reaction defined based on the experimental models was applied in the same Publications [II–III]. Global kinetic models were applied to the biomass torrefaction

[29], biomass pyrolysis [38], char gasification [34] discussed in [I] as well as the thermal NO emission [75] applied in [IV]. (Publication [V] also applies global kinetic models for the dissolving and precipitation of calcium carbonate in aqueous solution.) Models based on elementary kinetic reactions were used for modelling thermal NO formation [75] in [IV]. The simplified reaction schemes applied in Publications [I–IV] are illustrated in Figure 4.

3.7 Validation of results

Validation data for the models were obtained from the literature. Biomass torrefaction, pyrolysis and char gasification models in [I] were compared to the results of pure kinetic models [29,34,38]. The biomass gasification model in [II] was validated against the literature data [41,104,105]. The results for the combustion of black liquor were compared to global thermodynamic equilibrium in [III]. Reference data for NO emissions were obtained from DKM, whereas the ÅA mechanism [75] was applied in [IV].

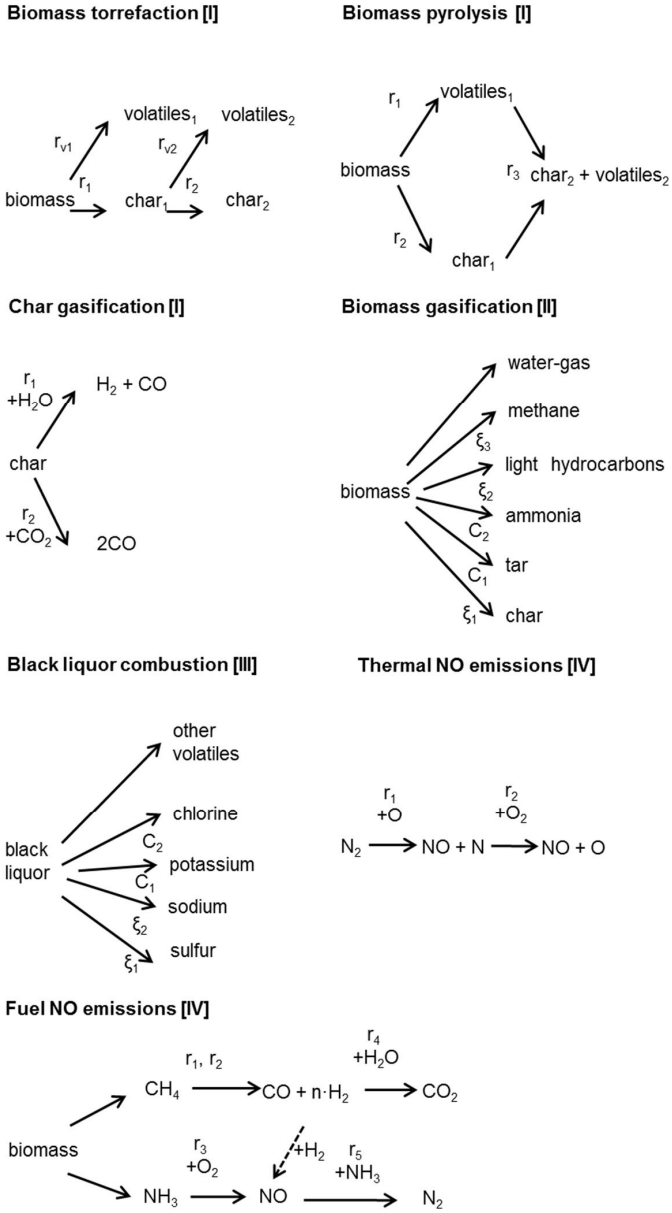

Figure 4. Applied models for defining the extent of reaction. *r* refers to the reaction rate [I,IV], *ξ* to the extent of reaction [II,III] and *C* to the constant value [II, III].

4. Results and discussion

The key results of Publications [I–V] are presented in this section and are related to the original hypotheses of the study. The applicability of the CFE method to the various super-equilibria conditions illustrated in Figure 3, as well as the usability of different kinds of model structures, is reported and discussed in this chapter.

4.1 Super-equilibrium of solid biomass

The constrained conversion of solid material to volatile species is a common feature of all processes related to the thermal conversion of biomass. An example of this is illustrated in Figure 3a. Several kinetic models have therefore been developed and published to describe this conversion in various processes such as torrefaction, pyrolysis and gasification. The aim of Publication [I] was to apply the CFE method to this problem and discern whether the method is feasible for modelling the super-equilibrium of solid material observed in these processes.

The applied reaction schemes are illustrated in Figure 4 and discussed in greater detail in [I]. Here, a short description is given. When torrefaction and pyrolysis processes were considered, the reaction schemes included three different kinds of solid material: (i) the original biomass, (ii) the intermediate product, and (iii) the torrefied product or char. Two fractions of volatile species are also separated, one from the original biomass and the second from the intermediate product. However, the scheme for char gasification is simpler. Here, solid char is volatilised as H_2 or CO after reacting with the gasification agent, steam or CO_2.

Solid fraction in char gasification was modelled 'traditionally' as coal and the corresponding thermodynamic properties were applied. A single, immaterial constraint was used for limiting the volatilisation of char. Two different kinetic models were applied, one for steam gasification and the other for carbon dioxide gasification. The value of the immaterial component was set according to the molar mass of coal. This allows constraints to be defined based on mass conversion rather than molar conversion. More details are given in [I].

A pseudo-component approach, described in Equations 13–15, was used for the torrefaction and pyrolysis processes. Ultimate biomass analysis was used for defining the average composition of these pseudo-biomass fractions (for example, $CH_{1.52}O_{0.72}$ for biomass). Based on Equations 13–15, the thermodynamic proper-

ties of these fractions can be estimated as follows (for example M = 25.04 g mol^{-1}, H_f = -123.55 kJ mol^{-1}, S_f = 145.08 J mol^{-1} K^{-1} and C_p = 32.6 J mol^{-1} K^{-1} for the biomass). For torrefaction and pyrolysis, two immaterial constraints were used: first, to describe the original biomass and intermediate biomass and, second, to represent the final product. Here again, the values of the immaterial components for these pseudo-biomass fractions were defined based on the molar mass, allowing the use of mass-based kinetic reactions. More examples are given in [I].

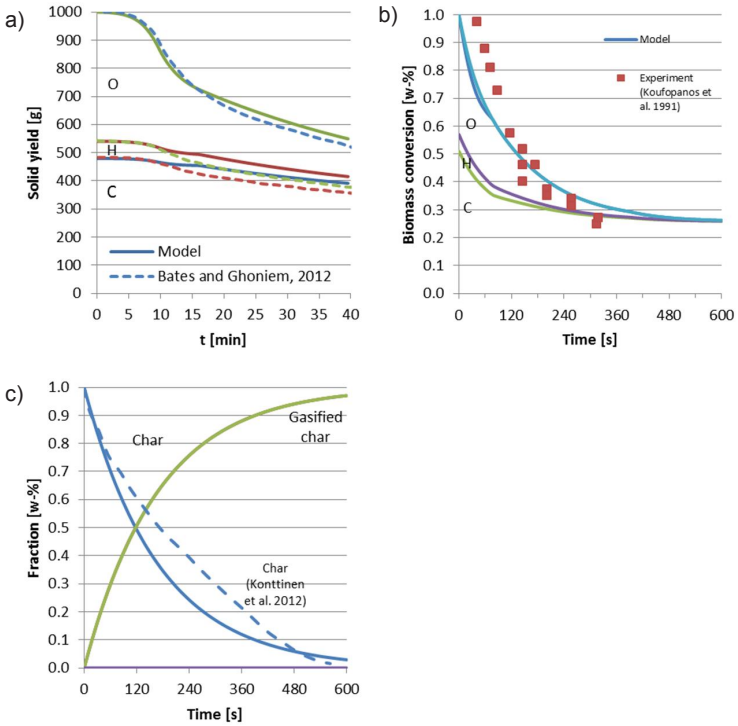

Figure 5. Biomass conversion [I] during: (a) biomass torrefaction T_0 = 200°C, ΔT = 10°C/min, T_{max}=300°C, (b) biomass pyrolysis at 350°C and (c) char gasification at 850°C. Validation data for a) [28], for b) [32] and for c) [34]. Solid lines indicate the results. Dashed lines and markers refer to the validation data.

Figure 5a illustrates the elementary composition of solid biomass fraction during the torrefaction process. The proposed model follows the reference data and thereby illustrates that the proposed pseudo-biomass fractions combined with CFE method are a plausible way of describing biomass conversion and changes in the elementary composition of solid biomass. Biomass conversion during pyrolysis is illustrated in Figure 5b and char conversion in Figure 5c. Both cases further con-

firm that the results of implementing constraints based on the CFE method in the calculation of thermodynamic equilibrium provide a feasible way of describing the super-equilibria of solid biomass in thermal biomass conversion.

4.2 Super-equilibria in the gaseous phase

Next, the study evaluated the gas phase composition in thermal biomass conversion processes. Because the CFE method was a feasible method of describing the composition of the solid fraction of biomass, the elementary composition in the gaseous phase should be described simultaneously. Publication [I] evaluates the applicability of the CFE method to describing the gaseous phase in biomass torrefaction, biomass pyrolysis and char gasification processes.

In [I] it was assumed that local thermodynamic equilibrium formed in the gaseous phase and no other additional immaterial constraints were applied at that point. According to [28], only a limited number of gaseous species were applied to the torrefaction of biomass and, according to [41], to the pyrolysis of biomass and char gasification.

When a low-temperature pyrolytic process (200–300°C), such as torrefaction, is considered, the proposed model fails to predict the super-equilibrium during the gaseous phase, as seen in Figure 6a. In reality, components such as acetic acid, methanol and furfural are formed but the model merely predicts the formation of water, acetol and carbon dioxide. As previously stated, the volatilised species originate in the structure and molecules of wood. Those volatile species do not react further, as the gas phase kinetics is very slow in low temperature processes.

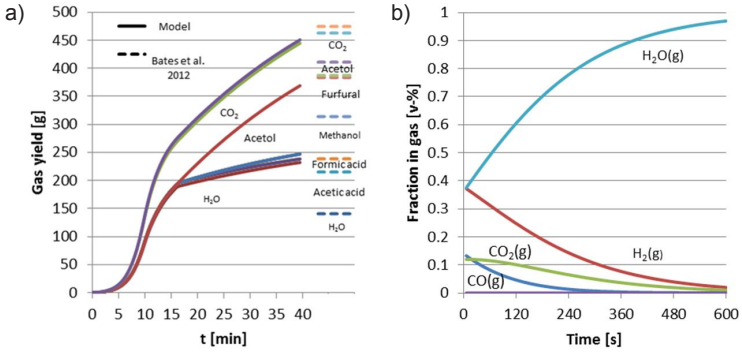

Figure 6. Composition of gaseous phase [I] during a) biomass torrefaction. T_0 = 200°C, ΔT = 10°C/min, T_{max}=300°C, and b) continuous steam gasification of birch char at 850°C. Solid lines refers to the results and dashed lines respectively to validation data from [28] where cumulative formation of compounds is presented.

When observing a higher temperature (850°C) process, such as char gasification, the local thermodynamic equilibrium constitutes a better assumption with respect to the gaseous phase. An example is given in Figure 6b. We can thereby infer that low temperature processes (<600°C) do not reach local equilibrium and the CFE method is not applicable in these conditions, because a fully kinetically constrained system is needed.

As the results in Publication [I] seemed reasonable for modelling the gas phase composition in high temperature processes, a more comprehensive study of biomass gasification was conducted in [II]. Although the local thermodynamic equilibrium in the gaseous phase is a moderate assumption, super-equilibrium states are clearly present. Figure 3b illustrates the super-equilibrium of methane in synthesis gas based on biomass gasification. In addition, the formation of other light hydrocarbons, tar and ammonia is observed and the biomass is partly converted into char.

In Publication [II], the applicability of the CFE method to modelling the fluidised bed gasifier was evaluated. In this, the ultimate analysis of biomass was used as an input feed for the model. A similar gas phase composition was used as previously in the char gasification case. Experimental models defining the constraints were obtained from the literature [41].

The other aim of Publication [II] was to study different CFE model structures and test various immaterial constraints. The base case was thermodynamic equilibrium, see Figure 7a. Five possible model structures were evaluated. Figure 7b illustrates a super-equilibrium model in which carbon conversion and the amount of light hydrocarbons (as total), tar and ammonia were constrained. Figure 7c represents the results of a model based on which an additional constraint was implemented for methane. Figure 7d shows the results of a model in which all individual light hydrocarbons where constrained separately, and only the local equilibrium of water-gas (H, CO, CO_2, H_2O) was assumed [II].

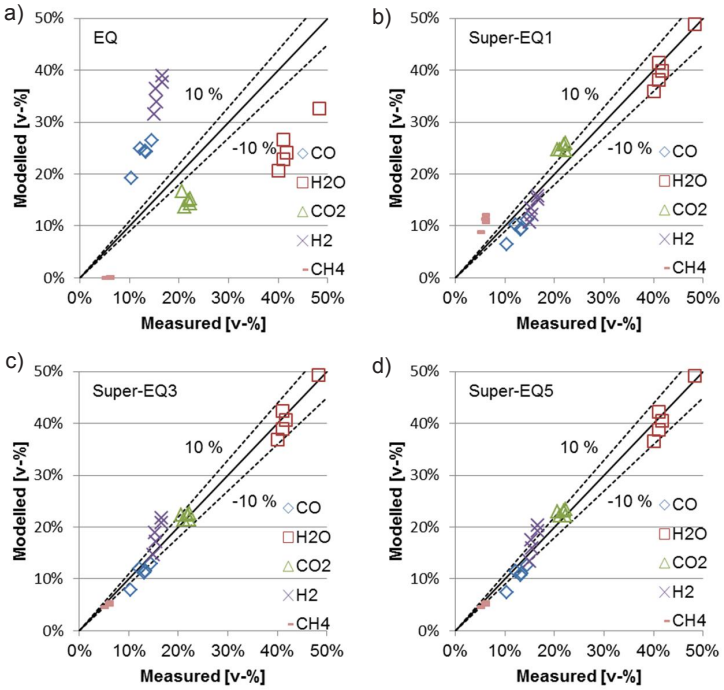

Figure 7. Biomass gasification and major synthesis gas species (CO, H_2O, CO_2, H_2 and CH_4) [II]. Four different models structures presented: a) Thermodynamic equilibrium without constraints. b) Carbon conversion, tar and ammonia formation and the total amount of light hydrocarbons are constrained. c) An additional constraint for methane is defined. d) The amount of every hydrocarbon is constrained and only water-gas is considered as local equilibrium. Validation data is obtained from [41].

These results indicate that, with limited constraints, it is possible to achieve results that are as good as in the case of a fully constrained system. By defining a separate constraint for methane, the prediction of the composition of synthesis gas is improved. Thus, the observed super-equilibrium seen in Figure 3b can be predicted. The biomass gasification model was also validated against two other independent datasets derived from the literature [104,105], with satisfactory results. Figure 8a shows the validation results for a fluidised bed gasifier and Figure 8b shows those for an air-blown circulating bed gasifier. First, this indicates that the applied experimental model is also valid for other cases and, secondly, that it is possible to generate generic models by implementing the CFE method. Naturally, be redefining the experimental models used for defining constraints, the proposed model structure could be applied on an even wider basis.

Based on the results in [II], it can be stated that, in the case of particularly high temperature processes, super-equilibria can be described using the CFE method, as the majority of the species are in a local thermodynamic equilibrium.

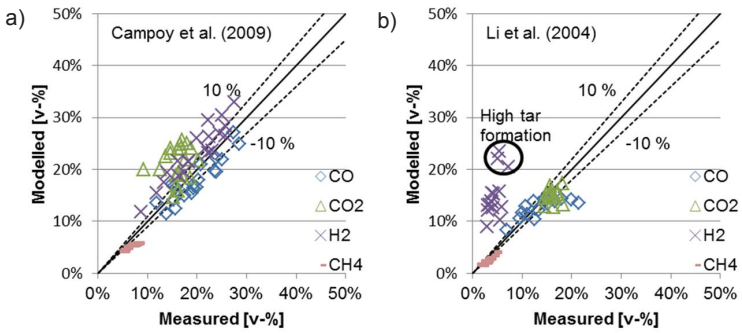

Figure 8. Validation of the biomass gasification model [II] in a) an air/steam-blown fluidised bed gasifier and in b) an air-blown circulating bed gasifier. Major syngas components (CO, CO_2, H_2 and CH_4) in dry gas are presented. Validation data of is obtained from [104,105].

4.3 Super-equilibria of volatile inorganic species

As stated above, the composition and related super-equilibrium states of organic species in the gaseous phase could be successfully modelled using the CFE method in a high temperature gasification process. Concurrently, the feasibility of the CFE method was evaluated for modelling the super-equilibria of volatile inorganic species. The results of this part of the study were presented in detail in [III].

The recovery boiler of a kraft pulp mill was chosen as a test case for two reasons: firstly, the black liquor covers the largest share of all biofuels in Finland as shown in Figure 1, and secondly, because the black liquor contains a large amount of inorganic cooking chemicals (alkali metals and sulfates), the super-equilibrium of these volatile species is evident as observed in Figure 3c. Thus, the steam parameters are also limited to lower values in recovery boilers compared to other biomass power plants.

A comprehensive thermodynamic database of Na-K-S-Cl-C-O-H [59,60] was applied in [III]. The same database is widely used for evaluating the ash chemistry of biofuel power plants, for example in [7]. In this case, the industrial measurements summarised in Publication [III] were used for defining constraints in the volatility of sodium, potassium, chlorine and sulfur. The corresponding four immaterial constraints were defined for these species. All volatile species containing sodium, potassium, chlorine and sulfur were connected to a particular immaterial component with the respective stoichiometric value.

Figure 9a illustrates the thermodynamic equilibrium levels of S and Na in the fume, as also shown in Figure 3c. The volatility of sodium and sulfur is very low at normal operating temperatures between 900–1,100°C. The super-equilibrium of sodium and sulfur is illustrated in Figure 9b, in which a CFE-based model is applied.

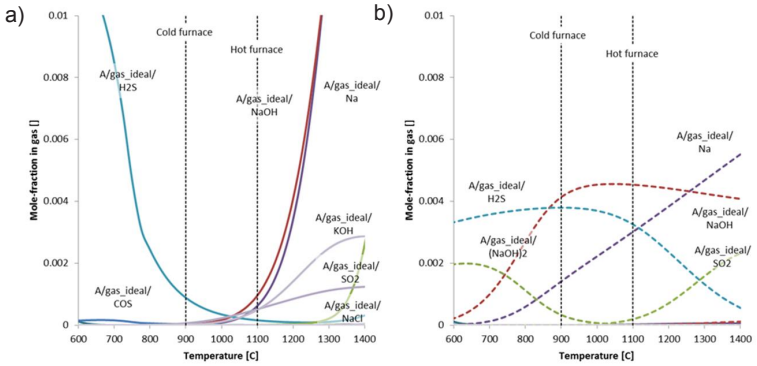

Figure 9. Sodium and sulfur concentrations of major constituents in the fume of a kraft recovery boiler [III]. a) Equilibrium concentrations applied. b) Super-equilibrium concentrations applied. Solid lines indicate here equilibrium concentrations and dashed lines super-equilibrium concentrations respectively. $\lambda_{furnace}$ = 0.7. Volatility of sodium = 10% and sulfur = 30% at 1,000°C. The enrichment factor for potassium is 1.4 and for chlorine 2.5.

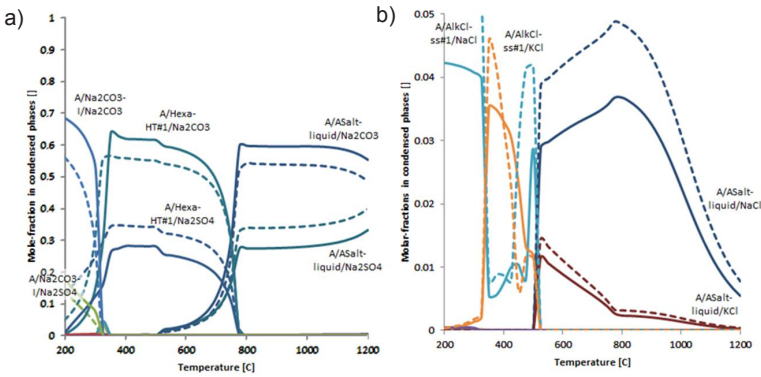

Figure 10. Condensed phases from the fume of a kraft recovery boiler [III]. Major constituents a) with potassium and b) with chlorine are shown. The solid lines refer to equilibrium concentrations and dashed lines to super-equilibrium concentrations. $T_{furnace}$ = 1,100 C. $\lambda_{furnace}$ = 0.7. Volatility of sodium = 10%, and sulfur = 30% at 1,000°C. The enrichment factor is 1.4 for potassium and 2.5 for chlorine.

The volatile species of sodium, potassium, chlorine and sulfur have a clear influence on the ash chemistry in the flue gas channel and on top of heat exchangers. Figure 10 illustrates the difference by comparing a more accurate CFE-based super-equilibrium model to a thermodynamic equilibrium model. In [III], it is shown that the sticky temperature can decline by 40–50°C for temperature T_{15} and 10°C for T_{70} when the super-equilibrium model is applied, This has an apparent effect on the functionality of the recovery boiler, as a sticky temperature is indicative of an area in which there is a greater risk of alkali metal condensates and the related corrosivity issues.

Publication [III] presents a unified method based on which the super-equilibrium in the lower furnace, the related chemical reactions and heat production can be resolved simultaneously using the CFE method, and confirms the applicability of the CFE method for this purpose.

4.4 Super-equilibrium of radicals related to NO emissions

Finally, the applicability of the CFE method to the modelling of NO emissions was studied in [IV]. Promising results in modelling the super-equilibrium of organic species in gasification [II] and inorganic species in recovery boiler processes [III] provided a solid background for further studies.

NO emissions have been modelled using comprehensive detailed kinetic models, i.e. DKMs, [74,75] in which the formation and destruction of several dozen species are controlled based on hundreds of elementary reactions. It seemed tempting to test whether a simplified CFE method could be used for modelling the same problems. In addition, some early results were published for NO freezing in internal combustion engines [82], based on a somewhat similar approach to the CFE method.

In [IV], several NO emission cases were evaluated with increasing complexity: (i) the heating of pure air, (ii) the combustion of carbon monoxide in dry and moist air, and (iii) the combustion of methane and ammonia (as biomass with nitrogen). DKM [75] were used for the calculation of reference and validation. In the case of the CFE model, the same thermodynamic data were applied as for the reference DKM. Elementary and global kinetic models were used to define the necessary constraints.

Thermal NO emissions during the heating of pure air were successfully modelled using the CFE method, as illustrated in Figure 11a. In this case, two immaterial constraints were applied and reaction kinetics was defined based on the Zeldovich mechanism. Figure 11b illustrates NO formation during the combustion of CO with pure air. Here, additional constraints were defined on the degradation of CO as well as the O-radical overshoot.

When rapid high-temperature combustion and the formation of thermal NO emissions are taken into consideration, the CFE method seems applicable to modelling these processes.

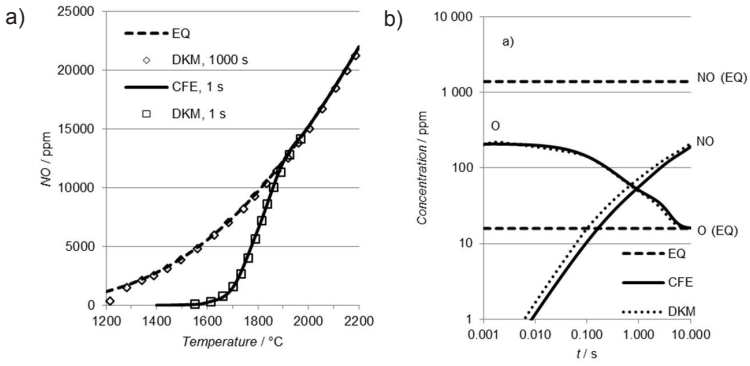

Figure 11. a) Formation of thermal NO emissions while heating pure air. b) Combustion of CO with dry air. Temperature 1,500°C, λ=1.2, and dry air (21 v-% O2 and 79 v-% N2). [IV] Here EQ refers to the equilibrium concentrations, CFE to the super-equilibrium concentrations and DKM to the validation results from the detailed kinetic model.

When more complex Fuel NO emissions were considered, global reaction kinetic models were best used alongside the CFE method. Separate models were used for the oxidation of methane into carbon monoxide and further into carbon dioxide, as well as for the oxidation of ammonia into NO emissions [76,79]. A total of five immaterial constraints were defined, based on seven kinetic reactions.

Figure 12a illustrates the oxidation of methane. It can be observed that the speed of oxidation is faster when the CFE model is compared to the results of DKM. This is mainly due to the fact that simplified global kinetic models applied to the CFE method do not predict the radical build-up and over-shoot correctly. The same off-timing is visible in the case of NO emissions, as illustrated in Figure 12b. However, the final NO emission level is predicted correctly and there is no difference between the CFE model and DKM.

In [IV], it was stated that the CFE method can be applied to modelling fuel NO emissions if global kinetic models are used.

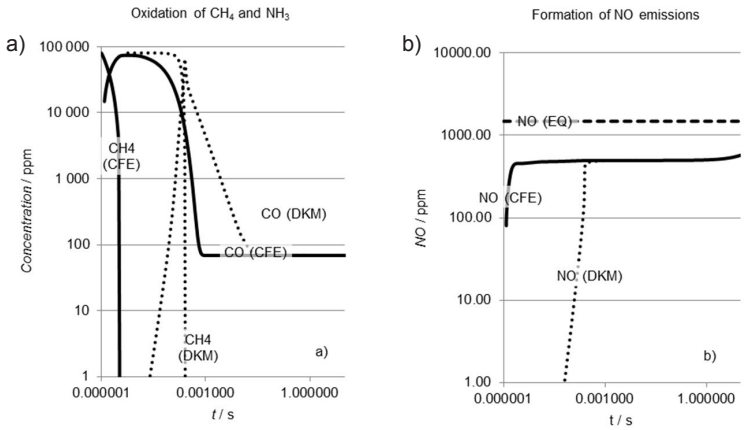

Figure 12. Fuel NO emissions [IV]. Biomass is modelled as methane, and nitrogen in biomass as ammonia. a) Combustion of hydrocarbons. b) NO emissions. The temperature is 1,500°C and λ=1.2. Here EQ refers to the equilibrium concentrations, CFE to the super-equilibrium concentrations and DKM to the validation data obtained from the detailed kinetic model.

4.5 Applicability of different model types as constraints

The second aim of this study was to evaluate which kinds of models could be used for defining the immaterial constraints of the CFE procedure. Four different types of approaches were used in the Publications: (i) constant values [II,III], (ii) experimental models [I,II], (iii) global kinetic models [III–V], and (iv) models based on elementary kinetic reactions [IV].

Publication [III] utilises constant values for defining the constraints. Here, the enrichment of potassium and chlorine were defined based on the fixed enrichment factors. In [II], the amount of tar and ammonia were described based on the constant values. Measured constant values seem to present a practical approach to many industrial cases, where data are available and more insight into the thermochemistry of the process is requested. Based on the positive results in [II,III], it is proposed that constant values be used for defining immaterial constraints in the CFE method, including for other types of high-temperature thermal biomass conversion.

Experimental temperature-dependent models were used in the same way as for defining the constraints in [II]. For example, the amount of char and methane declined as the temperature rose. Additionally, in [III] temperature-dependent models were used to describe the volatility of sodium and sulfur. In general, immaterial constraints can be conveniently defined based on experimental models, in which different parameters besides the reaction temperature are used.

Global kinetic models are often specified based on experimental data. In such cases, the time and temperature dependence are taken in account. During the torrefaction and pyrolysis of the biomass, two-step degradation of biomass was assumed in [I]. Simultaneously, part of the material was volatilised. Char gasification with steam and carbon dioxide were described as single-step reactions in [I]. In [IV], the fuel NO emissions and oxidation of methane were modelled using global kinetic models. (In addition the Publication [V] utilises global kinetic models in other domains for modelling the dissolving and precipitation of calcium carbonate in water suspension and the release of carbon dioxide.) The results in [III–V] confirm that global kinetic models with moderate immaterial constraints and related reactions can be utilised as part of the CFE method for constraining the system.

Models based on elementary kinetic reactions were used as constraints in [IV]. When small amount of reactions were considered, such as thermal NO emissions with the Zeldovich mechanism or carbon monoxide combustion with pure air, the CFE method appeared plausible.

However, when a more complex kinetic scheme was considered, such as the combustion of carbon monoxide with moist air, the calculations did not converge, as can be seen in Figure 13a. Here, the quantities of O, H and OH radicals were constrained individually and the formation and destruction of radicals were controlled based on several competing elementary reactions with different reaction rates.

Several methods for improving the stability of CFE method using elementary reactions were tested in [IV]: (i) decreasing the time-step, (ii) applying a better numerical method (4^{th} order Runge-Kutta instead of Euler method), (iii) lumping free radicals under a single constraint as seen in Figure 13b, and (iv) applying a steady-state assumption for radicals as seen in Figure 13c.

Figure 13b illustrates that, while combining O, H and OH radicals under a single constraint predicts the shape of the radical over-shoot somewhat correctly, the level of radicals remains inaccurate. Figure 13c demonstrates that, by defining the steady-state assumption for O radicals, the over-shoot can be modelled well but prediction fails near the equilibrium value.

Based on the results of [IV], it is proposed that models based on elementary kinetic reactions can be combined with the CFE method when the magnitude of the model is greatly reduced. In some cases, such as thermal NO emissions, this can be straightforwardly accomplished. If a large number of competing elementary reactions are needed to achieve a precise model, numerical instability issues occur. Such cases could be modelled to some extent using simplified global kinetic models for Fuel NO emissions as above shown, but certain aspects of the model will be lost, such as radical build-up, radical over-shoot and ignition delay. When such aspects are the focus of interest, DKMs seem a better alternative.

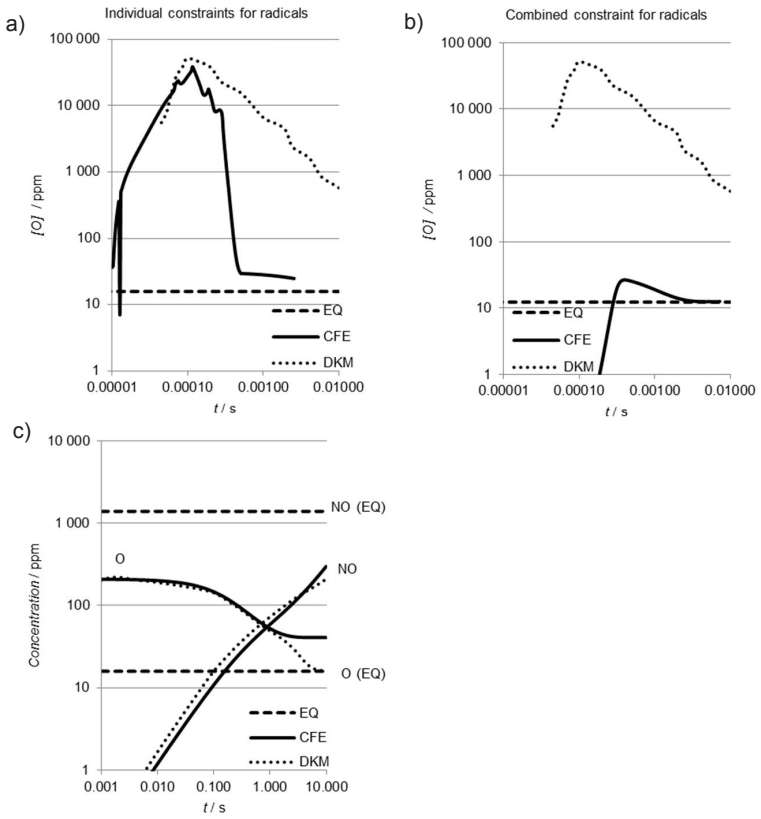

Figure 13. Modelling of radical build-up and over-shoot during combustion [IV]. Super-equilibrium model is defined as: a) Individual constraints on O, H and OH radicals. b) Combined constraint on the amount of O, H, and OH radicals. c) Steady-state assumption for O radicals. Here EQ refers the equilibrium concentrations, CFE to respective super-equilibrium concentrations and DKM to the validation data obtained from the detailed kinetic model.

5. Conclusions

This study evaluates the feasibility of the constrained free energy, CFE, method for modelling super-equilibria in thermal biomass conversion. The new application areas for the generic method applied in this study are biomass torrefaction, biomass pyrolysis, char gasification, biomass gasification, black liquor combustion and the related inorganic chemistry, and finally the NO emissions generated by combustion processes. Several types of models were used as constraints in defining the super-equilibrium conditions: constant values, experimental models, global kinetic models and models based on elementary kinetic reactions. A summary of the applications and applied constraints, as well as a feasibility evaluation, are shown in Table 2.

5.1 Applications

It was shown that, in high temperature processes (T>600°C), the CFE method is appropriate for the modelling of super-equilibria in thermal biomass conversion processes such as char gasification [I], biomass gasification [II], combustion of black liquor [III] and NO emission formation [IV]. In addition, the super-equilibrium of solid biomass conversion was successfully defined based on the CFE method in low temperature processes, such as biomass torrefaction and pyrolysis [I]. In general, it is stated that in high temperature processes where a clear local thermodynamic equilibrium is present and this super-equilibrium is constrained by a limited number of constraints, CFE is a pertinent means of modelling the processes.

Super-equilibria within the thermodynamic system are successfully constrained on the basis of various models, such as the constant values [I,II], experimental models [I,II] and global kinetic models [III–V]. In addition, a model based on the small number of elementary kinetic reactions was implanted in the CFE method. Experimental models and global kinetic models often combine several case-specific factors such as reactions, mass- and energy transfer, which are mixed into single rate equations which describe the super-equilibrium composition. These kinds of generic constraints can be easily implemented in CFE models.

Table 2. Applications and type of applied constraints.

Applications	**Types of constraints**			
	Constant values	Experimental Models	Global kinetic models	Models based on elementary kinetic reactions
Torrefaction			+ Applicable for char conversion [I] - Not feasible for predicting gaseous phase [I]	
Pyrolysis			+ Applicable for char conversion [I] - Not feasible for predicting gaseous phase [I]	
Gasification	+ Applicable to predicting, tar, and ammonia [II]	+ Applicable to predicting methane and char [II]	+ Applicable for char gasification [I]	
Recovery boiler	+ Applicable to the enrichment of alkali metals, sulfur and chlorine [III]			
NO emissions			+ Applicable for Fuel NO emissions [IV]	± Plausible for Thermal NO emissions [IV] - Not feasible for Fuel NO emissions [IV]

+ implies advantages in applying CFE method; - implies drawbacks in applying CFE method; ± indicates possibilities of using CFE method

5.2 Limitations

Super-equilibria in the gaseous phase in low temperature processes such as biomass torrefaction and pyrolysis could not be predicted [I]. This was due to the fact that the composition of volatile species is influenced by the chemical composition of wood itself. In low temperature processes, gas phase reactions are very slow and no local equilibrium can be assumed during the gaseous phase. Thus, a fully

constraint kinetic model is needed in order to predict gas phase super-equilibria in low temperature processes.

In high temperature processes, another limitation of the CFE method was found when comparing the results with those of kinetic calculations: super-equilibria of free radicals and the related radical build-up, over-shoot and thus ignition delay were not in agreement with the results received using DKM techniques. Numerical issues emerged when a large set of competing reactions in a stiff chemical system were implemented using the model. The number of constraints and reactions required was too large. If such topics are of interest, it would be more convenient to use detailed kinetic models for prediction.

5.3 Future research ideas

This study introduced several new applications of the CFE method in the area of thermal biomass conversion. A possible use of these models is large-scale process simulation. In many cases, simplified approaches, such as pure thermodynamic equilibrium or global kinetic models, are assumed. The CFE method could combine these two approaches and concurrently give an estimate of super-equilibria, chemical reactions and the related reaction enthalpies. Thus, in standard flow-sheet simulators researchers are encouraged to implement the CFE method as a new reactor type.

Automatic extension of the chemical system in simulators based on the implemented constraints would be a very efficient way of developing CFE models. Currently, the extension must be implanted manually into data files based on the constraints. This is prone to error and, in all cases, rather laborious. In addition, it restricts the usability of the CFE method to a limited number of simulation programs, in which databases can be extended. This also excludes all proprietary tools and databases beyond the scope of the CFE method.

Using the CFE method to model internal combustion processes would extend the work done for the current study. Simultaneously, the CFE and RCCE methods could be combined. Since a large number of elementary reactions in stiff chemical systems can be successfully modelled using the RCCE method, the related research should also resolve some of the unresolved problems that emerged in this study. An investigation of the combustion of new biofuels and the related new bio-based components in fuel mixtures would be of particular interest.

Sulfur oxide (SO_x) emissions from power plants and engines could be studied using the CFE method. An approach similar to that taken with respect to nitrogen oxide emissions is proposed here for sulfur oxide emission modelling. In addition, the CFE technique can be used for modelling the scrubbing of flue gas based on aqueous multi-phase models.

Implementing the CFE method as part of large CFD models is another topic requiring evaluation. Thus, a more precise model of chemical reactions could also be used in large models. However, it is assumed that this would be a highly com-

putational, intensive task. As part of the CFD models, parallel CFE solvers would probably also be needed.

Surrogate or meta-models as constraints in the CFE method form another line of future study. Based on a large dataset or detailed kinetic models, a surrogate model could be defined and later used for constraining critical reactions and defining the local super-equilibria states of chemical systems. Thus, a surrogate model based on complicated phenomena in industrial processes could be implemented for the rigorous calculation of thermodynamic equilibrium.

5.4 Finally

The CFE method is an applicable practice in modelling super-equilibria in high temperature processes. The distinct benefit of this method lies in the calculation of chemical reactions, enthalpic effects and state properties at the same time as the super-equilibrium is solved. The CFE method is a good alternative in many modelling cases, where a global thermodynamic equilibrium or reduced kinetic models are traditionally used for describing the thermal conversion of biomass.

References

[1] IPPC 2014. Climate Change 2014: Mitigation of Climate Change. http://www.ipcc.ch/report/ar5/wg3/

[2] Statistics Finland 2013. Official statistic of Finland (SVT): Supply and demand of energy. http://www.tilastokeskus.fi/til/ehk/index.html

[3] METLA 2013. Usage of wood. http://www.metla.fi/metinfo/tilasto/puunkaytto/

[4] Yang, H., Yan, R., Chen, H., Lee, D.H. & Zheng, C. 2007. Characteristics of hemicellulose, cellulose and lignin pyrolysis. Fuel 86(12-13), 1781–1788. doi:10.1016/j.fuel.2006.12.013

[5] De Wild, P.J., Uil, H. Den, Reith, J.H., Kiel, J.H. a. & Heeres, H.J. 2009. Biomass valorisation by staged degasification. J. Anal. Appl. Pyrolysis 85(1-2), 124–133. doi:10.1016/j.jaap.2008.08.008

[6] Bergman, P.C.A., Boersma, A.R.R., Zwart, W.R. & Kiel, J.H.A. 2005. Torrefaction for biomass co-firing in existing coal-fired power stations, Energy research Centre of the Netherlands.

[7] Enestam, S. 2011. Corrosivity of hot flue gases in the fluidized bed combustion of recovered waste wood, Dissertation, Åbo Akademi.

[8] Drake, M.C., Correa, S.M., Pitz, R.W., Shyy, W. & Fenimore, C.P. 1987. Superequilibrium and thermal nitric oxide formation in turbulent diffusion flames. Combust. Flame 69(3), 347–365. doi:10.1016/0010-2180(87)90126-X

[9] Koukkari, P. & Pajarre, R. 2006. Calculation of constrained equilibria by Gibbs energy minimization. Calphad 30(1), 18–26. doi:10.1016/j.calphad.2005.11.007

[10] Koukkari, P. 2009. Advanced Gibbs Energy Methods for Functional Materials and Processes – ChemSheet 1999–2009, Espoo, Finland. http://www.vtt.fi/inf/pdf/tiedotteet/2009/T2506.pdf

[11] Koukkari, P. 2014. Introduction to constrained Gibbs energy methods in process and materials, Espoo, Finland. http://www.vtt.fi/inf/pdf/technology/2014/T160.pdf

[12] Pajarre, R. 2015. Constrained and extended free energy minimization for modelling of processes and materials (un-published).

[13] Koukkari, P. 1993. A physico-chemical method to calculate time-dependent reaction mixtures. Comput. Chem. Eng. 17(12), 1157–1165. doi:10.1016/0098-1354(93)80096-6

[14] Koukkari, P., Pajarre, R. & Hack, K. 2008. Setting kinetic controls for complex equilibrium calculations, in: SGTE Caseb., doi:10.1533/9781845693954.3.359

[15] Pajarre, R., Koukkari, P., Tanaka, T. & Lee, J. 2006. Computing surface tensions of binary and ternary alloy systems with the Gibbsian method. Calphad 30(2), 196–200. doi:10.1016/j.calphad.2005.08.003

[16] Pajarre, R., Koukkari, P. & Tanaka, T. 2013. Surface tension of a liquid metal–oxygen system using a multilayer free energy model. Int. J. Mater. Res. 104(8), 736–747. doi:10.3139/146.110921

[17] Koukkari, P., Pajarre, R. & Pakarinen, H. 2002. Modeling of the Ion Exchange in Pulp Suspensions by Gibbs Energy Minimization. J. Solution Chem. 31(8), 627–638. doi:10.1023/A:1020201909118

[18] Pajarre, R., Koukkari, P. & Räsänen, E. 2006. Inclusion of the Donnan effect in Gibbs energy minimization. J. Mol. Liq. 125(1), 58–61. doi:10.1016/j.molliq.2005.11.016

[19] Koukkari, P., Pajarre, R., Pakarinen, H. & Salminen, J. 2001. Practical Multiphase Models for Aqueous Process Solutions. Ind. Eng. Chem. Res. 40(22), 5014–5020. doi:10.1021/ie010236r

[20] Pelton, A.D., Koukkari, P., Pajarre, R. & Eriksson, G. 2014. Para-equilibrium phase diagrams. J. Chem. Thermodyn. 72, 16–22. doi:10.1016/j.jct.2013.12.023

[21] Blomberg, P. & Koukkari, P. 2009. The combination of transformed and constrained Gibbs energies. Math. Biosci. 220(2), 81–88. doi:10.1016/j.mbs.2009.04.004

[22] Blomberg, P. & Koukkari, P. 2011. A systematic method to create reaction constraints for stoichiometric matrices. Comput. Chem. Eng. 35(7), 1238–1250. doi:10.1016/j.compchemeng.2010.07.024

[23] Aho, A. 2008. Catalytic pyrolysis of biomass in a fluidized bed reactor, Dissertation, Åbo Akademi University.

[24] Khazraie Shoulaifar, T., DeMartini, N., Willför, S., Pranovich, A., Smeds, A.I., Virtanen, T.A.P., et al. 2014. Impact of Torrefaction on the Chemical Structure of Birch Wood. Energy & Fuels 28(6), 3863–3872. doi:10.1021/ef5004683

[25] Tapasvi, D., Khalil, R., Skreiberg, Ø., Tran, K.-Q. & Grønli, M. 2012. Torrefaction of Norwegian Birch and Spruce: An Experimental Study Using Macro-TGA. Energy & Fuels 26(8), 5232–5240. doi:10.1021/ef300993q

[26] Prins, M.J. 2005. Thermodynamic analysis of biomass gasification and torrefaction, Dissertation, Technische Universiteit Eindhoven.

[27] Di Blasi, C. 2009. Combustion and gasification rates of lignocellulosic chars. Prog. Energy Combust. Sci. 35(2), 121–140. doi:10.1016/j.pecs.2008.08.001

[28] Bates, R.B. & Ghoniem, A.F. 2012. Biomass torrefaction: modeling of volatile and solid product evolution kinetics. Bioresour. Technol. 124, 460–469. doi:10.1016/j.biortech.2012.07.018

[29] Di Blasi, C. & Lanzetta, M. 1997. Intrinsic kinetics of isothermal xylan degradation in inert atmosphere. J. Anal. Appl. Pyrolysis 40-41, 287–303. doi:10.1016/S0165-2370(97)00028-4

[30] Srivastava, V.K. & Jalan, R.K. 1996. Prediction of concentration in the pyrolysis of biomass material—II. Energy Convers. Manag. 37(4), 473–483. doi:10.1016/0196-8904(95)00200-6

[31] Babu, B.V. & Chaurasia, a. S. 2004. Pyrolysis of biomass: improved models for simultaneous kinetics and transport of heat, mass and momentum. Energy Convers. Manag. 45(9-10), 1297–1327. doi:10.1016/j.enconman.2003.09.013

[32] Koufopanos, C.A., Papayannakos, N., Maschio, G. & Lucchesi, A. 1991. Modelling of the pyrolysis of biomass particles. Studies on kinetics, thermal and heat transfer effects. Can. J. Chem. Eng. 69(4), 907–915. doi:10.1002/cjce.5450690413

[33] Barrio, M. 2002. Experimental investigation of small-scale gasification of woody biomass, Dissertation, The Norweigian University of Science and Technology. http://www.diva-portal.org/smash/get/diva2:126378/FULLTEXT01.pdf

[34] Konttinen, J.T., Moilanen, a., DeMartini, N. & Hupa, M. 2012. Carbon conversion predictor for fluidized bed gasification of biomass fuels—from TGA measurements to char gasification particle model. Biomass Convers. Biorefinery 2(3), 265–274. doi:10.1007/s13399-012-0038-2

[35] Zhang, R., Wang, Q.H., Luo, Z.Y., Fang, M.X. & Cen, K.F. 2013. Competition and Inhibition Effects during Coal Char Gasification in the Mixture of H 2 O and CO 2. Energy & Fuels 27(9), 5107–5115. doi:10.1021/ef4007998

[36] Zhang, R., Wang, Q.H., Luo, Z.Y., Fang, M.X. & Cen, K.F. 2014. Coal Char Gasification in the Mixture of H 2 O, CO 2 , H 2 , and CO under Pressured Conditions. Energy & Fuels 28(2), 832–839. doi:10.1021/ef4018527

[37] Van der Stelt, M. 2010. Chemistry and Reaction Kinetics of Biowaste Torrefaction, Dissertation, Eindhoven University of Technology.

[38] Prakash, N. & Karunanithi, T. 2008. Kinetic Modeling in Biomass Pyrolysis – A Review. J. Appl. Sci. Res. 4(12), 1627–1636.

[39] Puig-Arnavat, M., Bruno, J.C. & Coronas, A. 2010. Review and analysis of biomass gasification models. Renew. Sustain. Energy Rev. 14(9), 2841–2851. doi:10.1016/j.rser.2010.07.030

[40] Gómez-Barea, A. & Leckner, B. 2010. Modeling of biomass gasification in fluidized bed. Prog. Energy Combust. Sci. 36(4), 444–509. doi:10.1016/j.pecs.2009.12.002

[41] Hannula, I. & Kurkela, E. 2012. A parametric modelling study for pressurised steam/O2-blown fluidised-bed gasification of wood with catalytic reforming. Biomass and Bioenergy 38, 58–67. doi:10.1016/j.biombioe.2011.02.045

[42] Hannula, I. & Kurkela, E. 2010. A semi-empirical model for pressurised air-blown fluidized-bed gasification of biomass. Bioresour. Technol. 101(12), 4608–15. doi:10.1016/j.biortech.2010.01.072

[43] Kuo, P.-C., Wu, W. & Chen, W.-H. 2014. Gasification performances of raw and torrefied biomass in a downdraft fixed bed gasifier using thermodynamic analysis. Fuel 117, 1231–1241. doi:10.1016/j.fuel.2013.07.125

[44] Hejazi, B., Grace, J.R., Bi, X. & Mahecha-Botero, A. 2014. Steam gasification of biomass coupled with lime-based CO2 capture in a dual fluidized bed reactor: A modeling study. Fuel 117, 1256–1266. doi:10.1016/j.fuel.2013.07.083

[45] Materazzi, M., Lettieri, P., Mazzei, L., Taylor, R. & Chapman, C. 2013. Thermodynamic modelling and evaluation of a two-stage thermal process for waste gasification. Fuel 108, 356–369. doi:10.1016/j.fuel.2013.02.037

[46] Kersten, S., Prins, W., Van der Drift, A. & Van Swaaij, W. 2002. Interpretation of biomass gasification by "'quasi'"-equilibrium models, in: Proc. Twelfth Eur. Conf. Biomass Energy, Ind. Clim. Prot., Amsterdam, Netherlands.

[47] Li, X., Grace, J., Watkinson, A., Lim, C. & Ergüdenler, A. 2001. Equilibrium modeling of gasification: a free energy minimization approach and its application to a circulating fluidized bed coal gasifier. Fuel 80(2), 195–207. doi:10.1016/S0016-2361(00)00074-0

[48] Barba, D., Prisciandaro, M., Salladini, a. & Mazziotti di Celso, G. 2011. The Gibbs Free Energy Gradient Method for RDF gasification modelling. Fuel 90(4), 1402–1407. doi:10.1016/j.fuel.2010.12.022

[49] Mendiburu, A.Z., Carvalho, J. a., Zanzi, R., Coronado, C.R. & Silveira, J.L. 2014. Thermochemical equilibrium modeling of a biomass downdraft gasifier: Constrained and unconstrained non-stoichiometric models. Energy 71, 624–637. doi:10.1016/j.energy.2014.05.010

[50] Kangas, P., Kaijaluoto, S. & Määttänen, M. 2014. Evaluation of future pulp mill concepts - Reference model of a modern Nordic kraft pulp mill. Nord. Pulp Pap. Res. J. 29(4), 620–634. doi:10.3183/NPPRJ-2014-29-04-p620-634

[51] Grace, T.M. 2001. A review of char bed combustion, in: Int. Chem. Recover. Conf., Whistler, BC, Canada.

[52] Sricharoenchaikul, C., Frederick, W.J. & Grace, T.M. 1997. Sulphur Species Transformations During Pyrolysis of Kraft Black Liquor. J. Pulp Pap. Sci. 23(8), J394–J400.

[53] Hupa, M., Backman, R., Skrifvars, B. & Forssén, M. 2001. Liquor-to-Liquor Differences in Combustion and Gasification Processes : Dust Composition and Melting Properties. J. Pulp Pap. Sci. 27(12), 416–422.

[54] Salmenoja, K., Kivilinna, V.-A., Hupa, M. & Backman, R. 2004. Chemical Balance of Non-Process Elements in Five Finnish Pulp Mills, in: Int. Chem. Recover. Conf., Charleston, SC, US.

[55] Mikkanen, P. 2000. Fly ash particle formation in kraft recovery boilers recovery boilers, Dissertation, Helsinki University of Technology. http://www.vtt.fi/inf/pdf/publications/2000/P421.pdf

[56] Janka, K., Wall, J. & Backman, R. 2004. Prediction of dust content and properties in kraft recovery boilers: comparison of theory and experimental results. Pulp Pap. Canada 105(1), 46–50.

[57] Vakkilainen, E.K. 2010. Predicting Ash Properties in Recovery Boilers, in: Int. Chem. Recover. Conf., Williamsburg, VA, US.

[58] Bale, C.W., Chartrand, P., Degterov, S.A., Eriksson, G., Hack, K., Ben Mahfoud, R., et al. 2002. FactSage thermochemical software and databases. Calphad 26(2), 189–228. doi:10.1016/S0364-5916(02)00035-4

[59] Bale, C.W., Bélisle, E., Chartrand, P., Decterov, S. a., Eriksson, G., Hack, K., et al. 2009. FactSage thermochemical software and databases — recent developments. Calphad 33(2), 295–311. doi:10.1016/j.calphad.2008.09.009

[60] Lindberg, D. 2007. Thermochemistry and melting properties of alkali salt mixtures in black liquor conversion processes, Dissertation, Åbo Akademi.

[61] Bankiewicz, D., Vainikka, P., Lindberg, D., Frantsi, a., Silvennoinen, J., Yrjas, P., et al. 2012. High temperature corrosion of boiler waterwalls induced by chlorides and bromides – Part 2: Lab-scale corrosion tests and thermodynamic equilibrium modeling of ash and gaseous species. Fuel 94, 240–250. doi:10.1016/j.fuel.2011.12.023

[62] Pejryd, L. & Hupa, M. 1984. Bed and furnace gas composition in recovery boilers - Advanced equilibrium calculations, in: Tappi Pulping Conf., San Fransisco, CA, US.

[63] Backman, R., Eriksson, G. & Sundström, K. 1996. The Recovery Boiler Advisor. Combination of practical experience and advanced thermodynamic modeling, in: 3rd Colloq. Process Simul., Espoo, Finland.

[64] Engblom, M. 2010. Modeling and Field Observations of Char Bed Processes in Black Liquor Recovery Boilers, Dissertation, Åbo Akademi.

[65] Uloth, V., Richardson, B., Hogikyan, R. & Haynes, J. 1992. Using a recovery boiler computer simulation to evaluate process alternatives for obtaining incremental recovery capacity. Tappi J. 75(11), 137–147.

[66] Cardoso, M. 1998. Análise da unidade de recuperação do licor negro de eucalipto ·no processo “kraft”, avaliando alternativas de processamento, Dissertation, Universidade Estadual de Campinas.

[67] Grace, T., Walsh, A., Jones, A., Sumnicht, D. & Farrington, T. 1989. Three-dimensional mathematical model of the kraft recovery furnace, in: Int. Chem. Recover. Conf., Ottawa, ON, CA.

[68] Leppänen, A., Välimäki, E. & Oksanen, A. 2012. Modeling fine particles and alkali metal compound behavior in a kraft recovery boiler. Tappi J. 11(7), 9–14.

[69] Järvinen, M.P., Kankkunen, A.P., Miikkulainen, P.H. & Heikkilä, V.P. 2011. A One-Dimensional Flow Model of a Flashing Black Liquor Gun: Study of Vapor Generation Sub-Models, in: Swedish-Finnish Flame Days 2011, Piteå, Sweden.

[70] Jokiniemi, J.K., Pyykönen, J., Mikkanen, P. & Kauppinen, E.I. 1996. Modeling fume formation and deposition in kraft recovery boilers. Tappi J. 79(7), 171–181.

[71] Grace, T.M. 1996. A critical review of computer modeling of kraft recovery boilers. Tappi J. 79(7), 182–190.

[72] Jaeglé, L., Steinberger, L., Martin, R. V. & Chance, K. 2005. Global partitioning of NOx sources using satellite observations: Relative roles of fossil fuel combustion, biomass burning and soil emissions. Faraday Discuss. 130, 407–423. doi:10.1039/b502128f

[73] Hill, S.. & Smoot, L.D. 2000. Modeling of nitrogen oxides formation and destruction in combustion systems. Prog. Energy Combust. Sci. 26(4-6), 417–458. doi:10.1016/S0360-1285(00)00011-3

[74] Smith, G.P., Golden, D.M., Frenklach, M., Moriarty, N.W., Eiteneer, B., Goldenberg, M., et al. n.d. GRI-Mech 3.0. http://www.me.berkeley.edu/gri_mech/

[75] Coda Zabetta, E. & Hupa, M. 2008. A detailed kinetic mechanism including methanol and nitrogen pollutants relevant to the gas-phase combustion and pyrolysis of biomass-derived fuels. Combust. Flame 152(1-2), 14–27. doi:10.1016/j.combustflame.2007.06.022

[76] Andersen, J. 2009. Experimental and CFD investigation of gas phase freeboard combustion, Dissertation, Technical University of Denmark Department.

[77] De Soete, G.G. 1975. Overall reaction rates of NO and N2 formation from fuel nitrogen. Symp. Combust. 15(1), 1093–1102. doi:10.1016/S0082-0784(75)80374-2

[78] Mitchell, J.W. & Tarbell, J.M. 1982. A kinetic model of nitric oxide formation during pulverized coal combustion. AIChE J. 28(2), 302–311. doi:10.1002/aic.690280220

[79] Brink, A., Kilpinen, P. & Hupa, M. 2001. A Simplified Kinetic Rate Expression for Describing the Oxidation of Volatile Fuel-N in Biomass Combustion. Energy & Fuels 15(5), 1094–1099. doi:10.1021/ef0002748

[80] Vanderlans, R., Glarborg, P. & Dam-Johansen, K. 1997. Influence of process parameters on nitrogen oxide formation in pulverized coal burners. Prog. Energy Combust. Sci. 23(4), 349–377. doi:10.1016/S0360-1285(97)00012-9

[81] Glarborg, P. 2003. Fuel nitrogen conversion in solid fuel fired systems. Prog. Energy Combust. Sci. 29(2), 89–113. doi:10.1016/S0360-1285(02)00031-X

[82] Keck, J.C. & Gillespie, D. 1971. Rate-controlled partial-equilibrium method for treating reacting gas mixtures. Combust. Flame 17(2), 237–241. doi:10.1016/S0010-2180(71)80166-9

[83] Delichatsios, M. & Keck, J. 1975. Rate-Controlled Constrained-Equilibrium Calculations of CO and NO Freezing in Internal Combustion Engines. ACS Symp. Prepr. 20,

[84] Keck, J.C. 1990. Rate-controlled constrained-equilibrium theory of chemical reactions in complex systems. Prog. Energy Combust. Sci. 16(2), 125–154. doi:10.1016/0360-1285(90)90046-6

[85] Koukkari, P. 1995. A physico-chemical reactor calculation by successive stationary states, Dissertation, Helsinki University of Technology.

[86] Koukkari, P. & Pajarre, R. 2006. Introducing mechanistic kinetics to the Lagrangian Gibbs energy calculation. Comput. Chem. Eng. 30(6-7), 1189–1196. doi:10.1016/j.compchemeng.2006.03.001

[87] Alberty, R.A. 1989. Thermodynamics of the formation of benzene series polycyclic aromatic hydrocarbons in a benzene flame. J. Phys. Chem. 93(8), 3299–3304. doi:10.1021/j100345a081

[88] Hamiroune, D., Bishnu, P., Metghalchi, M. & Keck, J.C. 1998. Rate-controlled constrained-equilibrium method using constraint potentials. Combust. Theory Model. 2(1), 81–94. doi:10.1080/713665370

[89] Nicolas, G.J. 2012. The rate-controlled constrained-equilibrium modeling of C1-C2 / O2 / diluent mixtures, Dissertation, Northeastern University. http://hdl.handle.net/2047/d20002907

[90] Janbozorgi, M., Ugarte, S., Metghalchi, H. & Keck, J.C. 2009. Combustion modeling of mono-carbon fuels using the rate-controlled constrained-equilibrium method. Combust. Flame 156(10), 1871–1885. doi:10.1016/j.combustflame.2009.05.013

[91] Kalliola, A., Pajarre, R., Koukkari, P., Hakala, J. & Kukkamäki, E. 2012. Multi-phase thermodynamic modelling of pulp suspensions: Application to a papermaking process. Nord. Pulp Pap. Res. J. 27(03), 613–620. doi:10.3183/NPPRJ-2012-27-03-p613-620

[92] Lee, J., Lee, J., Tanaka, T., Mori, H. & Penttilä, K. 2005. Phase Diagrams of Nanometer-Sized Particles in Binary Systems. JOM J. Miner. Met. Mater. Soc. 57(3), 56–59. doi:10.1007/s11837-005-0235-6

[93] Koukkari, P., Penttilä, K., Hack, K. & Petersen, S. 2005. CHEMSHEET – An Efficient Worksheet Tool for Thermodynamic Process Simulation, in: Y. Bréchet (Ed.), Microstruct. Mech. Prop. Process., Weinheim.doi:10.1002/3527606157.ch51

[94] Koukkari, P., Pajarre, R. & Hack, K. 2008. Modelling TiO2 production by explicit use of reaction kinetics, in: SGTE Caseb. Thermodyn. Work, doi:10.1533/9781845693954.4.437

[95] Koukkari, P., Pajarre, R. & Hack, K. 2001. Setting Kinetic Controls for Complex Equilibrium Calculations. Zeitschrift Für Met. 92(10), 1151–1157.

[96] Koukkari, P., Pajarre, R. & Blomberg, P. 2011. Reaction rates as virtual constraints in Gibbs energy minimization. Pure Appl. Chem. 83(5), 1063–1074. doi:10.1351/PAC-CON-10-09-09

[97] Eriksson, G. 1971. Thermodynamic studies of high temperature equilibria. III. SOLGAS, a Computer Program for Calculating the Composition and Heat Condition of an Equilibrium Mixture. Acta Chem. Scand. 25(7), 2651–2656.

[98] Smith, W.R. & Missen, R.W. 1991. Chemical reaction equilibrium analysis: theory and algorithms, Malabar, FL, US.

[99] Eriksson, G. & Rosén, E. 1973. Thermodynamic Studies of High Temperature Equilibria. VII. General equations for calculation of equilibria in multiphase systems. Chem. Scr. 4(5), 193–194.

[100] Weber, C.F. 1998. Convergence of the Equilibrium Code SOLGASMIX. J. Comput. Phys. 145(2), 655–670. doi:10.1006/jcph.1998.6046

[101] Roine, A., Lamberg, P., Mansikka-aho, J., Björklund, P., Kentala, J., Talonen, T., et al. 2007. HSC Chemistry 6.12.

[102] Battley, E.H. 1999. An empirical method for estimating the entropy of formation and the absolute entropy of dried microbial biomass for use in studies on the thermodynamics of microbial growth. Thermochim. Acta 326(1-2), 7–15. doi:10.1016/S0040-6031(98)00584-X

[103] Dupont, C., Chiriac, R., Gauthier, G. & Toche, F. 2014. Heat capacity measurements of various biomass types and pyrolysis residues. Fuel 115, 644–651. doi:10.1016/j.fuel.2013.07.086

[104] Campoy, M., Gómez-Barea, A., Vidal, F.B. & Ollero, P. 2009. Air–steam gasification of biomass in a fluidised bed: Process optimisation by enriched air. Fuel Process. Technol. 90(5), 677–685. doi:10.1016/j.fuproc.2008.12.007

[105] Li, X.T., Grace, J.R., Lim, C.J., Watkinson, a. P., Chen, H.P. & Kim, J.R. 2004. Biomass gasification in a circulating fluidized bed. Biomass and Bioenergy 26(2), 171–193. doi:10.1016/S0961-9534(03)00084-9

PUBLICATION I

Modeling biomass conversion during char gasification, pyrolysis and torrefaction by applying constrained local thermodynamic equilibrium

Energy & Fuels 28 (10), 6361–6370.

energy&fuels

Article

pubs.acs.org/EF

Modeling Biomass Conversion during Char Gasification, Pyrolysis, and Torrefaction by Applying Constrained Local Thermodynamic Equilibrium

Petteri Kangas,*[,†] Pertti Koukkari,[†] and Mikko Hupa[‡]

[†]VTT Technical Research Centre of Finland, 02044 Espoo, Finland

[‡]Åbo Akademi University, 20500 Turku, Finland

Supporting Information

ABSTRACT: The char and biomass conversions during gasification, pyrolysis, and torrefaction were studied using the constrained free energy (CFE) method. The Gibbs free energy minimization method is extended by implementing immaterial constraints for describing partial equilibria in the gaseous phase and for kinetically controlling slow reactions associated with the conversion of char and biomass. The connection between immaterial constraints and the affinities of slow chemical reactions are illustrated. The method presented allows for the Arrhenius type of kinetic model to be incorporated into the calculation of local constrained thermodynamic equilibrium. Thus, the kinetically constrained chemical reactions, equilibrium reactions, and reaction enthalpies can be solved simultaneously by applying CFE methodology. A conceivable approach for introducing pseudo-biomass components into the thermochemical system is evaluated. The technique applies to statistical estimates of standard enthalpy and standard entropy based on assumed molecular compositions. When incorporated into a thermodynamic model, the pseudo-components allow for estimating the composition of biomass during the process and the fast volatilization of oxygen- and hydrogen-containing species at the beginning of the processes. The CFE method was successfully used for modeling the char conversion. The high operating temperature of the gasification process justifies the assumption of local equilibrium in the gas phase. The immaterial constraint can be used for controlling the release of carbon to the gas phase as the reaction proceeds. When pyrolysis and torrefaction were studied, the immaterial constraints could be successfully used for describing biomass conversion in solid phases. However, for these processes, the assumption of local equilibrium in the gas phase is not valid, because no equilibrium reactions occur in the low-temperature conditions.

INTRODUCTION

Thermal conversion of biomass is one promising alternative for reducing the usage of fossil carbon resources for energy production. Apart from conventional biomass combustion, a number of emerging technologies have been studied and piloted: (i) gasification of biomass for producing syngas to be used for biofuels and biochemicals, (ii) pyrolysis of biomass for producing bio-oils, e.g., heating applications, and (iii) torrefaction of biomass to improve the energy density of fuel by reducing the oxygen content. Much effort has been invested in understanding the reaction kinetics and biomass conversion rates of these processes.

Woody biomass is mainly composed of three components: cellulose (40−50 wt % wood), hemicellulose (25−35 wt %), and lignin (20−35 wt %). In addition, ash and extractives exist in smaller amounts. Hemicelluloses are a mixture of polysaccharides. They have a lower molecular weight than cellulose and can be branched. On the other hand, cellulose is composed of linear glucose chains, and the degree of polymerization is higher. Lignin can be described as an irregular array of three different kinds of phenylpropane units. The differences in chemical structure of the main wood components also affect the observed phenomena of biomass during torrefaction and pyrolysis.[1] In addition, the gas-phase composition is affected by the composition of biomass in low-temperature applications, such as torrefaction and pyrolysis. For example, phenolic groups are considered to originate from lignin, and levoglucosan is considered to originate from cellulose.[2]

During thermal treatment of biomass with increasing the temperature, these three wood fractions decompose, react with other compounds, and volatilize. The first step is the drying of biomass, which occurs when the temperature of the biomass is below 150 °C. The temperature window for torrefaction is 150−300 °C. The biomass experiences a pyrolysis stage between 300 and 600 °C. If the gasification agent (e.g., O_2, H_2O, or CO_2) is present, the remaining char is gasified when the temperature is above 600 °C. Hemicelluloses are considered to decompose first, when the temperature is between 220 and 315 °C. Celluloses degenerate at a temperature range of 315−400 °C. Lignin is the most difficult compound to be decomposed. Changes in lignin structure appear along a large temperature range from ambient up to 900 °C.[1,3] Different wood species react differently; for example, birch tends to volatilize easier than spruce during torrefaction.[4] Different processing steps are illustrated in Figure 1.

During the torrefaction, species such as water, carbon monoxide and carbon dioxide, acids (formic, acetic, and lactic),

Received: June 16, 2014
Revised: September 11, 2014
Published: September 11, 2014

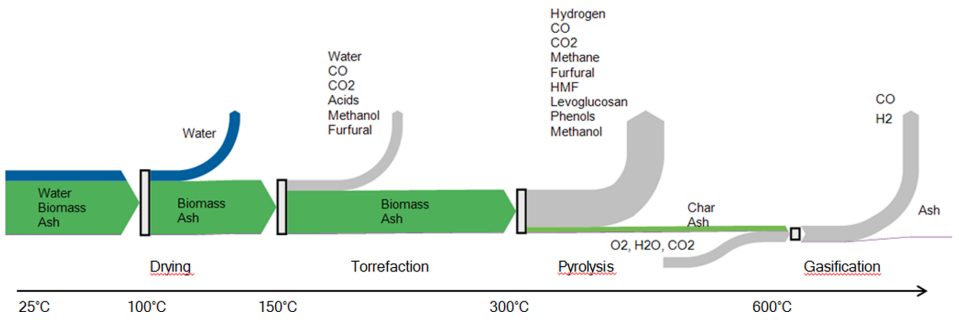

Figure 1. Thermal conversion of biomass. This figure was composed according to refs 1, 6, and 7.

Scheme 1. Proposed Reaction Schemes of Biomass Torrefaction,[17] Biomass Pyrolysis,[14] and Char Gasification[10]

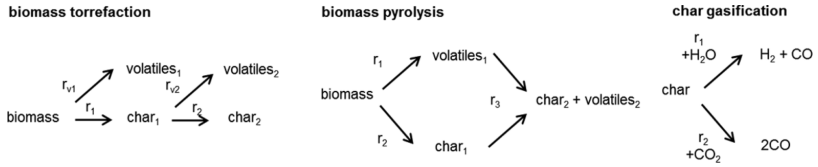

methanol, hydroxyacetone, and furfural are formed.[5] The respective species at the pyrolysis stage are hydrogen, carbon monoxide, carbon dioxide, acids (acetic), furans [furfural and hydroxymethylfurfural (HMF)], anhydrosugars (levoglucosan), phenols, and methanol.[1,6] During the char gasification, steam and carbon dioxide react with char, carbon monoxide (and hydrogen) is produced, and equilibrium in the gas phase is reached. Compounds are shown in Figure 1.

Studies of torrefaction, pyrolysis, and char gasification are frequently conducted with a thermogravimetric analyzer (TGA), where the mass loss of biomass is observed, e.g., Prins for torrefaction,[8] Yang et al. for pyrolysis,[1] and Di Blasi for char gasification.[9] The main focus of several studies has been on optimizing the biomass and char conversion and process conditions accordingly. In addition, results of gas-phase composition during the torrefaction, pyrolysis, and gasification processes have been published. Gas composition is measured with gas chromatography (GC) by[8] Fourier transform infrared (FTIR) spectroscopy[1] or high-performance liquid chromatography (HPLC) for condensed phases.[8]

Thermodynamic equilibrium is seldom reached in these kinetically restricted processes. The rate of mass loss and formation of volatile species as well as char are frequently described using the Arrhenius type of model, where time- and temperature-dependent parameters are fitted to experimental data. Examples of these kinetic models are (i) the char gasification model proposed by Barrio[10] and further developed by Konttinen et al.[11] and Zhang et al.,[12,13] which includes two competing reactions of char carbon with steam and carbon dioxide, respectively, (ii) the pyrolysis model developed by Koufopanos et al.[14] and further developed in refs 15 and 16, comprising intermediate volatile and char, which react further to produce final products, and (iii) the torrefaction model proposed by Di Blasi and Lanzetta[17] and further developed by Prins[8] and Bates and Ghoniem,[5] which includes a two-stage process with intermediate products. Reaction schemes of these models are shown in Scheme 1. These kinetic models will be used in this study for defining the constraints to be applied in the thermochemical model calculation. Reviews of other torrefaction,[8,18] pyrolysis,[19] and gasification[20,21] models are available in the literature.

The aim of this study is to combine the determination of kinetic reaction rates with non-stoichiometric thermodynamic equilibrium. For this purpose, the constrained free energy (CFE) method[22] is used to describe these super-equilibrium states, where, for instance, the presence of char exceeds the amount seen in the global equilibrium state. The CFE methodology is an extension of the Gibbs free energy method, in which additional immaterial constraints are implemented to model for controlling, for example, the progress of dominant reactions. The respective methodology has been introduced for the conservation of "aromaticity" in benzene combustion[23] and for describing the extent of the reaction for internal combustion problems.[24,25] The authors of this paper have applied the methodology to other areas of thermal biomass conversion; biomass gasification and related super-equilibrium conditions of tars, char, ammonia, and light hydrocarbons are described using the CFE method in ref 26. The super-equilibrium of sodium, potassium, chlorine, and sulfur in the fume of a kraft pulp mill recovery boiler is discussed in ref 27. Other reported applications of the CFE method are, for example, partitioning of electrolytes in an aqueous membrane,[28,29] surface energy in a multicomponent system,[30] and reaction pathways.[31] More information on CFE methodology is given in the chapters that follow, as well as in ref 22.

METHODS

Our work addresses the issues of computational methodology related to usage of the CFE method for modeling the phenomena seen in char gasification, pyrolysis, and torrefaction processes. Supporting reaction kinetics and validation data are obtained from the literature, mainly from refs 1, 5, and 11. Thermodynamic data are obtained from HSC.[32] ChemSheet software[33] is applied as a modeling tool, because it provides a convenient approach to extending the thermodynamic system with immaterial constraints.

CFE Method. The thermodynamic equilibrium of a non-stoichiometric chemical system is solved by minimizing the Gibbs energy. The Lagrange method of undetermined multipliers (eq 1)[34,35] is used for finding the minimum when the partial derivatives are defined as zero (eqs 2 and 3)

$$L = G - \pi\Psi = \sum_{k=1}^{K} n_k\mu_k - \sum_{l=1}^{L} \pi_l\left(\sum_{k=1}^{K} \nu_{kl}n_k - b_l\right) \quad (1)$$

$$\left(\frac{\partial L}{\partial n_k}\right)_{n_{n\neq k}} = \mu_k - \sum_{l=1}^{L} \pi_l\nu_{kl} = 0 \quad (2)$$

$$\left(\frac{\partial L}{\partial \pi_l}\right)_{\pi_{n\neq l}} = \sum_{k=1}^{K} \nu_{kl}n_k - b_l = 0 \quad (3)$$

where G is the Gibbs free energy of the system, π is the Lagrange multiplier vector, Ψ is the mass balance of the different components of each constituent written in terms of the amount of matter (mol), n is the molar amount of constituent k, μ is the chemical potential of the constituent k, k refers to each constituent in the multiphase system, L is the number of components in the system, and K the number of constituents. π_l is the Lagrange multiplier of component l, and b_l is the total amount of component l in the system. Equation 2 defines the chemical potential components as a linear combination of the Lagrange multipliers. Equation 3 is used to describe the amounts of components in the chemical system. More information on Gibb's energy minimization can be found in refs 34−36. In practice, computer programs, such as SolGasMix and ChemSheet,[33,35] are used for solving the thermodynamic equilibrium.

Next, the thermodynamic system is extended with additional immaterial constraints; see eq 4. X defines the number of immaterial constraints. Implementation of X amount of additional columns to the chemical system, here from $L + 1$ to $L + X$, it is possible to force certain constituents and phases to form during the minimization.[23,24,37] If additional virtual constituents are implemented in the chemical system (rows $K + 1$ to $K + X$) and those virtual constituents are linked to corresponding virtual components, it is possible to control both the formation and disappearance of actual constituents. These virtual constituents can be defined using the forward and reverse rates of chemical reactions.

$$\mathrm{N} = \begin{bmatrix} \nu_{1,1} & \cdot & \nu_{1,L} & \nu_{1,L+X} \\ \cdot & \cdot & \cdot & \cdot \\ \nu_{K,1} & \cdot & \nu_{K,L} & \cdot \\ \nu_{K+X,1} & \cdot & \cdot & \nu_{K+X,L+X} \end{bmatrix} \quad (4)$$

When kinetic reactions are considered, immaterial constraints can be defined as follows and are illustrated in Table 1. The elementary reaction A + B ↔ C + D has a kinetically controlled reaction rate forward, r_f, and backward, r_r. In this system, the virtual component R* is interconnected to another reaction product (here C) with a positive number of 1. The first virtual constituent r_f is also connected to the same virtual component R* with a positive number of 1. The other virtual constituent r_r is connected to the virtual component R* with a negative number of −1. With implementation of these immaterial constraints, it is possible to enter the reaction rate of the forward reaction to virtual constituent r_f and the reaction rate of the reverse reaction to virtual constituent r_r. This extension allows for calculation of a local thermodynamic equilibrium with one kinetically constrained reaction incorporated into the system.

Table 1. Example of the Stoichiometric Matrix of Elementary Reaction A + B ↔ C + D[a]

	component		
constituent	C1	C2	R*[b]
A	2		
B		1	
C	1		1
D	1	1	
r_f			1
r_r			−1

[a]Additional constraints are used for defining forward and reverse reaction rates. [b]Immaterial constraint (R*).

In general, the dynamics of chemical reactions are caused by reaction kinetics, heat and mass transfer, or a combination of these factors. While the matrix extension directly affects the chemical changes involved, all previous aspects can be encompassed in the CFE method. For example, (i) elementary reaction kinetics in the gaseous phase are incorporated to CFE models;[24,38] (ii) the changes because of the reaction enthalpy when calculating the local thermodynamic equilibrium are linked to the temperature-dependent reaction rates in adiabatic processes (or with an iterative algorithm, which connects the enthalpy of the system to an external heat-transfer model);[39] and (iii) restrictions in the rate of dissolving in aqueous suspension are coupled to the models.[28] Quite often all of these three phenomena are combined in the (iv) overall reaction rate, which can be experimentally defined for certain types of processes and raw materials.[26,27,40] A simplified example of the CFE method for modeling mass-transfer kinetics in a closed system is attached as Supporting Information.

Finally, the equilibrium reactions, such as the water−gas shift reaction, in the gaseous phase can be defined according to eq 5. Kinetically slow reactions, such as char gasification, are defined according to eq 6.

$$\sum_k a_k\mu_k = 0 \qquad \text{(equilibrium reactions)} \quad (5)$$

$$\sum_k a_k\mu_k = \sum_k a_k \sum_{l=1}^{L+X} \nu_{kl}\pi_l \neq 0$$

$$\text{(all constrained super-equilibrium reactions)} \quad (6)$$

Here, a_k is used for the stoichiometric coefficient of species k in a given reaction. The thermodynamic affinity becomes zero by eq 5 for the equilibrium reactions and remains non-zero for kinetically constrained non-equilibrium reactions (eq 6). The affinity of the non-equilibrium reaction is related to the calculated "constraint potentials" of the virtual components.[41] This is illustrated with the super-equilibrium condition in the char gasification in the next chapter.

CALCULATIONS

Three different cases are presented to estimate the applicability of the CFE method for the modeling of thermal biomass conversion and ways to implement kinetic constraints in the thermodynamic equilibrium.

Char Gasification. The first example focuses on the char gasification process. Two parallel reactions are considered: (i) char gasification with carbon dioxide and (ii) char gasification with steam, as shown in Scheme 1. In both cases, carbon in the char is released as carbon monoxide (which can further react in the gaseous phase, for instance, because of the water−gas shift reaction). The following kinetic reactions are used in this study, as previously defined in ref 11. Net reaction rates, r_1 and r_2, shown in eqs 7−9, and the Arrhenius type of equation for rate constant $k_{x,y}$ are defined. The applied pre-exponential factor and activation energies for both reactions are shown in Table 2.

$$r_1 = \frac{\mathrm{d}m_{\mathrm{C-H_2O}}}{\mathrm{d}t} = \frac{k_{1\mathrm{f},1}p_{\mathrm{H_2O}}}{1 + (k_{1\mathrm{f},1}/k_{3,1})p_{\mathrm{H_2O}} + (k_{1\mathrm{b},1}/k_{3,1})p_{\mathrm{H_2}}} \quad (7)$$

dx.doi.org/10.1021/ef501343d | Energy Fuels 2014, 28, 6361−6370

Table 2. Pre-exponential Factors and Activation Energies of the Char Gasification Model

reaction	gasifier	$k_{0,1f}$	E_{1f}	$k_{0,1b}$	E_{1b}	$k_{0,3}$	E_3
r_1	H_2O	6.49×10^7	204.0	95.3	54.32	1.64×10^9	243.0
r_2	CO_2	1.64×10^7	188.0	4.59×10^2	88.27	8.83×10^7	225.0

Table 3. Extended Stoichiometric Matrix Applied to Char Gasification and Pyrolysis Modeling

phase	constituent	C[a,b]	O[a,b]	H[a,b]	Si[a,b]	char*[a,b,c]	biomass*[a,c]
gas phase	$CO^{a,b}$	1	1				
	$H_2{}^{a,b}$			2			
	$CO_2{}^{a,b}$	1	2				
	$N_2{}^{a,b}$						
	$H_2O^{a,b}$		1	2			
	$CH_4{}^{a,b}$	1		4			
biomass[a]	$CH_{1.4}O_{0.63}$	1	0.63	1.4			23.69
intermediate[a]	$CH_{0.5}$	1		0.5			12.51
char[a,b]	C	1				12.01	
ash[a,b]	SiO_2		2		1		
constraint	$r_{char}{}^{a,b}$					$1^a/-1^b$	
	$r_{biomass}{}^{a}$						−1

[a]Applied in the pyrolysis case. [b]Applied in the char gasification case. [c]Immaterial constraint (char* and biomass*).

$$r_2 = \frac{dm_{C-CO_2}}{dt} = \frac{k_{1f,2}p_{CO_2}}{1 + (k_{1f,2}/k_{3,2})p_{CO_2} + (k_{1b,2}/k_{3,2})p_{CO}} \quad (8)$$

$$k_{x,y} = k_{0,x,y}\exp(-E_{x,y}/RT) \quad (9)$$

The simplified thermodynamic system is defined for the char gasification model, including six gaseous constituents (water, hydrogen, carbon monoxide, carbon dioxide, methane, and nitrogen). The char is modeled as carbon, and ash is modeled as silicon dioxide (inert constituent). Thermodynamic data are obtained from HSC.[32] The applied system is shown in Table 3. One immaterial constraint is used here for the irreversible reaction of gasification, namely, $r_{char} = r_1 + r_2$, and this is defined as a negative value because the amount of char is decreasing as a result of the gasification process. Constraints are defined in such a way that the net mass rate can be used as a constraint and the respective amount of char is gasified. The gaseous phase is considered to be in local equilibrium.

Chemical Affinities. Kinetic reactions are limiting the chemical system to reach thermodynamic equilibrium. Instead, a local constrained equilibrium is supposedly present. The affinities of limited reactions are positive, and they can also be solved from the chemical potentials of immaterial constraints.[42] Here, four examples are given related to the char gasification process: (i) water−gas shift reaction (eq 10), (ii) methanation (eq 11), (iii) gasification with water (eq 12), and (iv) gasification with carbon dioxide (eq 13).

$$CO(g) + H_2O \leftrightarrow CO_2(g) + H_2(g)$$
(water−gas shift reaction)

$$A_{WGS} = -\Delta_r G = \mu_{CO(g)} + \mu_{H_2O(g)} - (\mu_{CO_2(g)} + \mu_{H_2(g)}) = \pi_C + \pi_O + 2\pi_H + \pi_O - (\pi_C + 2\pi_O + 2\pi_H) = 0 \quad (10)$$

$$CO(g) + 3H_2(g) \leftrightarrow CH_4(g) + H_2O(g)$$
(methanation)

$$A_{meth} = -\Delta_r G = \mu_{CO(g)} + 3\mu_{H_2(g)} - (\mu_{CH_4(g)} + \mu_{H_2O(g)}) = \pi_C + \pi_O + 6\pi_H - (\pi_C + 4\pi_H + 2\pi_H + \pi_O) = 0 \quad (11)$$

$$C(s) + H_2O(g) \leftrightarrow CO(g) + H_2(g)$$
(char gasification with steam)

$$A_{C-H_2O} = -\Delta_r G = \mu_{C(s)} + \mu_{H_2O(g)} - (\mu_{CO(g)} + \mu_{H_2(g)}) = \pi_C + \pi_{char*} + 2\pi_H + \pi_O - (\pi_C + \pi_O + 2\pi_H) = \pi_{char*} \neq 0 \quad (12)$$

$$C(s) + CO_2(g) \leftrightarrow 2CO(g)$$
(char gasification with carbon dioxide)

$$A_{C-CO_2} = -\Delta_r G = \mu_{C(s)} + \mu_{CO_2(g)} - (2\mu_{CO(g)})\pi_C + \pi_{char*} + \pi_C + 2\pi_O - (2\pi_C + 2\pi_O) = \pi_{char*} \neq 0 \quad (13)$$

Local thermodynamic equilibrium of all reactions in the gaseous phase is present, because no constraints are defined for those reactions. This is a valid assumption for the char gasification process, because the reaction temperature is high enough (850 °C). Thus, the chemical affinities of equilibrium reactions are also zero, and no spontaneous reactions occur (eqs 10 and 11). On the other hand, when we are observing the reactions with char and gaseous species, the immaterial constraint is effective and global equilibrium of the whole chemical system cannot be achieved (eqs 12 and 13). The affinity of char gasification reactions is positive when char tends to move to the gaseous phase. Here, a super-equilibrium is formed, because more char exists in the local equilibrium (when compared to the respective global condition). In some cases, this particular affinity could be negative, indicating that the reverse reaction would occur. In that case, a sub-equilibrium

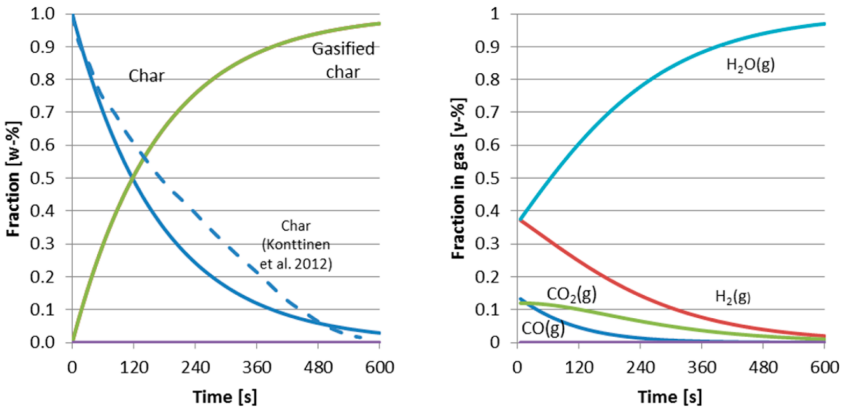

Figure 2. Continuous gasification of birch char. T = 850 °C. Char conversion is on the left and composition of the gaseous phase is on the right. Reference data are from ref 11.

Table 4. Thermodynamic Properties of Solid Pseudo-biomass Compounds Used for Modeling Torrefaction and Pyrolysis, $C_p = C_{p,A} + C_{p,B}T$

compound	formula	molar mass (g/mol)	H_f (kJ mol^{-1})	S_f (J mol^{-1} K^{-1})	C_p at 25 °C (J mol^{-1} K^{-1})	$C_{p,A}$ (J mol^{-1} K^{-1})	$C_{p,B}$ (J mol^{-1} K^{-1})
biomass[a]	$CH_{1.4}O_{0.63}$	23.69	−102.69	132.72	30.9	−7.084	0.127
intermediate[a]	$CH_{0.5}$	12.51	46.16	31.23	16.3	−3.742	0.067
biomass[b]	$CH_{1.52}O_{0.72}$	25.04	−123.55	145.08	32.6	−7.487	0.134
intermediate[b]	$CH_{1.12}O_{0.41}$	19.75	−51.76	98.58	25.7	−5.906	0.105
torrefied[b]	$CH_{0.12}O_{0.02}$	12.44	45.53	12.71	16.2	−3.721	0.066

[a]Applied in the pyrolysis case. [b]Applied in the torrefaction case.

exists and carbon would condensate from the gaseous phase following the Bouduard equilibrium.

Pyrolysis of Biomass. The two-stage process with intermediate volatile and char products as proposed by Koufopanos[14] is shown in Scheme 1. Biomass is reacting to intermediate products and finally to final products. The related kinetic model, net mass production rates, r_x, and rate constants, k_x, are defined according to ref 19 and shown in eqs 14−19

$$r_1 = \frac{dm_{G1}}{dt} = k_1 m_B - k_3 m_{G1} m_{C1} \quad (14)$$

$$r_2 = \frac{dm_{C1}}{dt} = k_2 m_B - k_3 m_{G1} m_{C1} \quad (15)$$

$$r_3 = \frac{dm_{C2}}{dt} = \frac{dm_{G2}}{dt} = k_3 m_{G1} m_{C1} \quad (16)$$

$$k_1 = 9.973 \times 10^{-5} \exp[(17254/T) + (-9061227/T^2)] \quad (17)$$

$$k_2 = 1.068 \times 10^{-3} \exp[(10224/T) + (-6123081/T^2)] \quad (18)$$

$$k_3 = 5.7 \times 10^5 \exp[-81/RT] \quad (19)$$

where sub-indexes 1, 2, and 3 refer to three reactions shown in Figure 2, G1 and G2 refer to volatile intermediates and products, and C1 and C2 refer to char intermediates and products, respectively. T is the temperature, and R is the gas constant.

When the rates of biomass decomposition (eq 20) and char formation (eq 21) are solved, the immaterial constraints $r_{biomass}$ and r_{char} are defined. The net mass rate of the reactions can be used as a constraint, and a corresponding amount of biomass will decompose or char will be formed.

$$r_{biomass} = r_1 + r_2 \quad (20)$$

$$r_{char} = r_3 \quad (21)$$

Biomass is defined as biomass, $CH_{1.4}O_{0.63}$ (see Table 2). The intermediate biomass is composed only from carbon and hydrogen, $CH_{0.5}$. The final pyrolysis product is char, defined as pure carbon. Thermodynamic data are again obtained from HSC.[32] Two immaterial constraints are implemented in the thermodynamic system: (i) a constraint for controlling the decomposition of biomass, $r_{biomass}$, and (ii) a constraint for defining the formation of char during pyrolysis, r_{char}. Here, a positive factor is used for r_{char} because the share of char in remaining biomass is increasing.

Standard enthalpy, entropy, and heat capacity of these pseudo-compounds need to be defined for the calculation of thermodynamic equilibrium. Standard enthalpy of formation is defined according to Thornton's rule, as represented by Battley,[43] and is based on the oxycalorific equivalent, 450 kJ/mol of O_2, needed for full combustion. Entropies of formation are defined with the respective statistical method proposed by Battley.[43] This is a statistical method based on the relative small amount of available experimental data on the entropy of formation of organic substances. Battley notes that the method gives good results with larger compounds. Heat capacity is based on the average heat capacity of different wood species reported in ref 44 (eqs 22−24)

$$\Delta_f H_X = \sum \Delta_f H_{prod} - 450.0 n_{O_2,c} \quad (22)$$

dx.doi.org/10.1021/ef501343d | Energy Fuels 2014, 28, 6361−6370

Table 5. Extended Stoichiometric Matrix Used for Torrefaction Modeling

phase	constituent	C	H	O	biomass*[a]	torrefied*[a]
gas phase	water		2	1		
	CO	1				
	CO_2	1		2		
	formic acid	1	2	2		
	acetic acid	2	4	2		
	lactic acid	3	6	3		
	methanol	1	3	1		
	hydroxyacetone	3	6	2		
	furfural	5	4	2		
biomass[b]	$CH_{1.52}O_{0.72}$	1	1.52	0.72	25.04	
intermediate[b]	$CH_{1.12}O_{0.41}$	1	1.12	0.41	19.75	
torrefied[b]	$CH_{0.12}O_{0.02}$	1	0.12	0.02	12.44	12.44
constraint	$r_{biomass}$				−1	
	$r_{torrefied}$					1

[a]Immaterial constraint (biomass* and torrefied*). [b]Applied in the torrefaction case.

$$\Delta_f S_X = -0.813 \sum S^{\circ}_{X,\text{atoms}} \quad (23)$$

$$C_{p,X} = (5.304T - 299)M_X \quad (24)$$

where $\Delta_f H_X$ is the estimated standard enthalpy of formation of compound X and $\Delta_f S_X$ is the estimated standard entropy of formation of compound X. $\sum \Delta_f H_{prod}$ is the sum of the standard enthalpies of combustion products (CO_2 and H_2O). $n_{O_2,c}$ is the number of oxygen atoms needed for full combustion of reactants. $\sum S^{\circ}_{X,\text{atoms}}$ is the sum of the standard entropies of the individual atoms. $C_{p,X}$ refers to the heat capacity of compound X, and M_X refers to the molar mass of compound X. Table 4 summarizes the thermodynamic parameters of three different pseudo-biomass compounds (biomass, intermediate, and torrefied) and also those used later for torrefaction modeling.

Torrefaction of Biomass. Scheme 1 illustrates the two-stage reactions of torrefaction of biomass as proposed by Di Blasi and Lanzetta.[17] The original model includes four reaction rate constants: k_{v1} for the first stage volatilization, k_1 for the generation of first intermediate biomass, k_{v2} for the second state volatilization, and k_2 for the generation of torrefied biomass. In this study, reactions decomposing biomass and producing volatile compounds are considered (eqs 25 and 26). In addition, the formation of final torrefied biomass is included in the model (eq 27). The following equations are taken from ref 5 and define net mass production rates, r_x, and rate constants, k_x (eqs 28 and 30):

$$r_{v1} = \frac{dm_{v1}}{dt} = k_{v1} m_A \quad (25)$$

$$r_{v1} = \frac{dm_{v2}}{dt} = k_{v2} m_B \quad (26)$$

$$r_C = \frac{dm_C}{dt} = k_2 m_B \quad (27)$$

$$k_{v1} = 3.23 \times 10^7 \exp(-114214/RT) \quad (28)$$

$$k_{v2} = 1.59 \times 10^{10} \exp(-151711/RT) \quad (29)$$

$$k_2 = 1.1 \times 10^{10} \exp(-151711/RT) \quad (30)$$

where m_X is the mass of compound X, A refers to the original biomass, B refers to the intermediate biomass after first volatilization, and C refers to the final torrefied biomass. v1 and v2 refer to volatile products during torrefaction. The gas constant, R, is in J mol^{-1} K^{-1}, and T is the temperature. The biomass fractions are defined in the following way. The chemical composition of the original biomass (A) is assumed to be $CH_{1.40}O_{0.63}$. The intermediate biomass (B) is defined as $CH_{1.53}O_{0.19}$, and the final torrefied biomass (C) is $CH_{2.19}O_{0.13}$ according to Table 3 in ref 5.

The thermodynamic system is constructed as follows: nine compounds in the gaseous phase according to ref 5, water, carbon monoxide, carbon dioxide, formic acid, acetic acid, lactic acid, methanol, hydroxyacetone, and furfural. Thermodynamic data are obtained from HSC.[32] Three solid biomass phases are defined according to Table 3. Finally, two immaterial constraints are added to the thermodynamic system to control the decomposition of biomass and formation of torrefied biomass.

Constraint $r_{biomass}$ (in Table 5) is defined in such a way that the total biomass conversion to volatile species (mass loss of biomass) in mass units (grams) can be entered as a constraint (see eqs 25, 26, and 31). Constraint $r_{torrefied}$ is defined according to the generation of torrefied biomass (eqs 27 and 32).

$$r_{biomass} = r_{v1} + r_{v2} \quad (31)$$

$$r_{torrefied} = r_C \quad (32)$$

This results in a corresponding amount, $r_{biomass}$, of biomasses A, B, or C to be converted to volatile compounds, and torrefied biomass is formed according to $r_{torrefied}$. The oxygen- and hydrogen-containing species tend to be volatile first from the resulting biomass A and then converted to biomass B and finally biomass C, which corresponds to results reported in ref 5.

RESULTS

Char Gasification and Related Char Chemical Affinity To Remain in the Solid Phase. Birch char gasification was used as a first case. According to ref 11, a model was constructed where 5 mg of birch char was gasified with steam as a gasification agent. The volume of the gasification chamber was assumed as 4 mL, and steam was purged continuously with steam. The temperature is 850 °C, and local equilibrium can be assumed in the gaseous phase. The kinetic model is described in eqs 7−9. Figure 2 illustrates that the model predicts slightly

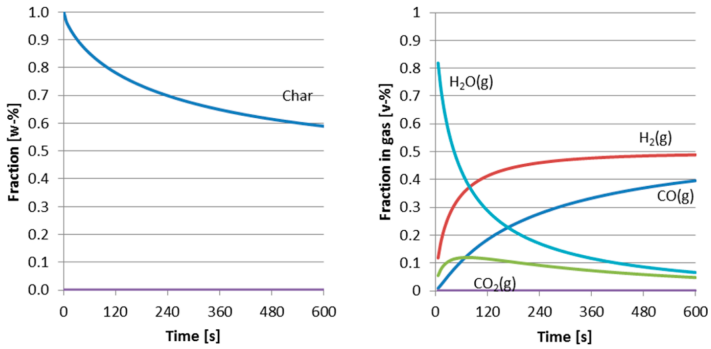

Figure 3. Batch gasification of birch char. T = 850 °C. Char conversion is on the left and composition of the gaseous phase is on the right.

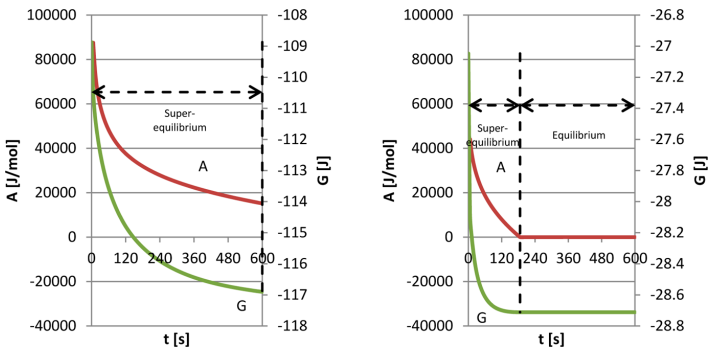

Figure 4. Chemical affinity and Gibbs free energy of the system for batch gasification of birch char. A larger amount of steam is on the left (20 mL) and a smaller amount of steam is on the right (4 mL).

faster decomposition of char at the beginning of the gasification (from 100 to 300 s) and slower decomposition thereafter. The same figure shows the composition of the gaseous phase during the char gasification process. The volatilization of hydrogen and carbon monoxide is high at the very beginning of the experiment, where the carbon conversion is fastest. Here, a local equilibrium is assumed in the gaseous phase; e.g., a water−gas shift reaction takes place after the carbon is gasified because the temperature is high (850 °C).

The proposed model is also used here to illustrate the gasification in the "batch" reaction, where gases are not purged to and from the reactor. The amount of gas in the reactor at the beginning is assumed to be 5 times larger than in the previous example (20 mL). Steam is used as a gasification agent. The temperature is 850 °C. The full char conversion cannot be achieved, because the amount of steam is limited. This can be seen in Figure 3. In addition, the composition of the gaseous phase differs here from the previous example of continuous gasification. The amount of steam is decreasing, and thus, the speed of char volatilization is decreasing as the gasification proceeds. Hydrogen and carbon dioxide are the main species in the gas phase at the end. Again, the local equilibrium in the gaseous phase is assumed, and thus, the gas-phase reactions, such as water−gas shift, will take place. This example illustrates the benefits of CFE methodology, because the local thermodynamic equilibrium can be solved simultaneously with restricted kinetic reactions.

Finally, the char affinity to remain in the solid phase is evaluated. As presented in the previous chapter, the Lagrange multipliers of immaterial constraints can be used for evaluating the reaction affinities. The affinity char gasification reaction is observed during the gasification process. This reaction does not reach chemical equilibrium. Again, the batch type of reactor is assumed here, because it fulfils the requirement of a closed system. Two cases are shown: one with an initial steam volume of 20 mL and the other with a smaller amount of steam (only 4 mL).

When the chemical affinity of the gasification reaction is observed for the first case, it can be seen that, during the 600 s progress of gasification, global equilibrium cannot be reached, because the Gibbs free energy of the system remains in decline (see Figure 4). Respectively, the affinity of the gasification reaction remains positive. Super-equilibrium of char can be defined for this case, because more char is present than in the global equilibrium. However, when smaller amounts of the gasification agent, steam, are introduced into the system at the beginning, a different kind of phenomenon is seen in Figure 4. The global equilibrium is reached when ∼180 s have passed. The Gibbs free energy of the system is at a minimum, and the affinity of the char gasification reaction is zero. Before that, there is a similar super-equilibrium condition present as in the previous example. After that point, global equilibrium is present. Discontinuation in the affinity chart is due to the fact that the net reaction rate is defined by eqs 7 and 8 and no

dx.doi.org/10.1021/ef501343d | Energy Fuels 2014, 28, 6361−6370

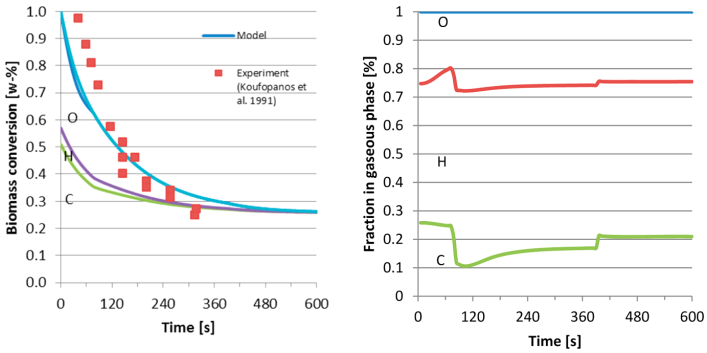

Figure 5. Biomass pyrolysis at isothermal conditions (T = 350 °C), in a continuous process, where gases are purged with nitrogen. Biomass conversion and cumulative yields of carbon, hydrogen, and oxygen during pyrolysis are on the left. Instantaneous composition of the gas phase is on the right. Validation data are from ref 14.

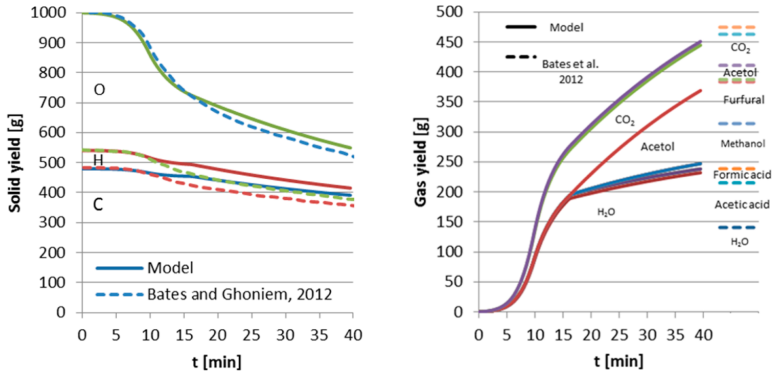

Figure 6. Biomass conversion to torrefied biomass, with the solid yield of different components (carbon, hydrogen, and oxygen in biomass). T_0 = 200 °C. ΔT = 10 °C/min. T_{max} = 300 °C. Validation data are according to ref 5.

backward reaction rate is specified. The kinetic model tries to force char from a solid phase to a gaseous phase also after global equilibrium is reached.

Biomass Conversion during Pyrolysis and Formation of Char. Biomass pyrolysis is modeled according to Scheme 1. Immaterial constraints for calculating constrained thermodynamic equilibrium are defined in eqs 14−16 and 20−21. Here, 1000 g of woody biomass (see biomass in Table 5) is pyrolyzed at an isothermal temperature of 350 °C. Nitrogen is purged to the reactor for removing the volatile species and to provide an inert atmosphere. Experimental data of biomass conversion are taken from ref 14.

Figure 5 illustrates the total biomass conversion during the pyrolysis. After 10 min, the pyrolysis is finished and ∼25% of biomass remains as char. At the beginning of pyrolysis, oxygen- and hydrogen-containing species are volatilizing and the relative ratios of these compounds in the biomass are decreasing. The intermediate biomass is formed during the beginning of gasification according to Scheme 1.

Volatility of carbon decreases after ∼70 s, and the composition of the instantaneous purged gas phase is altered: volatilization of hydrogen is high. Biomass conversion continues, and another step change can be seen when ∼400 s have passed from the beginning, when the amount of oxygen in the biomass is very small. Carbon-containing species are formed. In this case, the reaction temperature is 350 °C, and consequently, no thermodynamically driven (equilibrium) reactions will occur in the gaseous phase. For this reason, only elemental fractions of carbon, hydrogen, and oxygen are shown in Figure 5. The Gibbsian thermodynamic model is not supportive in prediction of the gas-phase composition, because no local equilibrium is formed.

The examples show that biomass conversion during pyrolysis can be modeled using CFE methodology. If additional pseudo-species for illustrating the intermediate biomass are introduced into the chemical system, the tendency of oxygen and hydrogen to volatilize first can be incorporated into the model. The respective pseudo-biomass was defined with a stoichiometric approximation ($CH_{0.5}$). However, the configuration of this pseudo-component naturally has an effect on the actual elemental composition of residual biomass during the pyrolysis and formation of volatile species.

Biomass Decomposition during Torrefaction. Biomass reacts and decomposes in the torrefaction process according to Scheme 1. The temperature at the beginning of modeling was set to 200 °C, increasing by 10 °C/min. The final temperature was 300 °C. Here, 1 kg of torrefied material was assumed. The

model is evaluated against the kinetic model developed by Bates and Ghoniem.[5]

During the torrefaction process, the ratio of hydrogen/carbon and the ratio of oxygen/carbon decrease. Figure 6 illustrates the reported solid yield for carbon, hydrogen, and oxygen during the process. The proposed model in this study succeeds in predicting the biomass conversion and elemental composition of solid biomass during the torrefaction. The immaterial constraints (one for the decomposition of biomass and the other for forming the torrefied biomass) succeed in illustrating the biomass conversion rate based on the kinetic models presented in Scheme 1. This also confirms that the proposed pseudo-components presented in Table 3 are a plausible method for modeling the decomposition of biomass, because similar results were achieved earlier with the biomass composition model during the pyrolysis process.

The proposed model indicates that mainly water and carbon dioxide are present in the gaseous phase at the beginning of torrefaction process. Bates and Ghoniem[5] report that the major volatile constituents at the first stage are water, carbon dioxide, and acetic acid. Later, during the torrefaction process, the model also predicts hydroxyacetone (acetol) as a volatile product. Bates and Ghoniem[5] report that lactic acid, methanol, acetic acid, and hydroxyacetone are the main constituents at the second stage of torrefaction. However, the thermodynamic model is not plausible in predicting the formation of gaseous components. Also, only a small subset of possible gaseous compounds is included in the calculation of the gas-phase composition. Our model mainly indicates that water, carbon dioxide, and hydroxyacetone are formed during the process (see Figure 6). However, it is possible to fully constrain the gas-phase composition with CFE methodology if this is chosen as shown by the authors in ref 26. In this case, similar gas-phase composition could be achieved as in the reference case.

CONCLUSION

This study presents three new application areas for the CFE method: (i) biomass torrefaction, (ii) biomass pyrolysis, and (iii) char gasification. The method can be successfully used for describing the biomass and char conversion and the composition of solid biomass during these processes. The proposed model succeeds in predicting local thermodynamic equilibrium in the gaseous phase when the temperature is high (>600 °C) and gas-phase equilibrium chemistry takes place. However, the proposed models fail to predict the gas-phase composition of the pyrolysis and torrefaction processes. This is due to the fact that temperatures are low (200−400 °C) and residence time is short as the gaseous phase is purged out of the reactor. Thus, it can be said that local equilibrium is not a valid assumption for low-temperature gas-phase reaction with a short residence time; in such cases, purely kinetic models give a better description of the process.

The CFE method describes the changing chemical system during each calculation as if it were a closed system. The model itself does not include terms for the mass and energy exchange between the system and its surroundings. However, with standard engineering techniques, e.g., in heat and mass transfer, it is straightforward to include such effects into the thermodynamic CFE system. In processes that are prominently governed by kinetic phenomena, such as internal transport within particles or mixing of gas film with bulk vapor, other approaches, such as diffusion or computational fluid dynamics (CFD) models, can give better estimations.

A plausible way to introduce pseudo-biomass components into the chemical system is illustrated. The method applied is based on the statistical estimate of standard enthalpy, standard entropy, and heat capacity. The technique enables rapid modeling of thermodynamic data of these biomass compounds. When incorporated into the model, these pseudo-components can be used for modeling the composition of biomass during the process and the faster volatilization of oxygen- and hydrogen-containing species at the beginning of processes.

The presented method allows for the Arrhenius type of kinetic models to be incorporated into the calculation of local constrained thermodynamic equilibrium. Thus, the kinetically constrained chemical reactions, equilibrium reactions, and reaction enthalpies can be solved simultaneously by applying CFE methodology. The CFE method appears to be most suitable in such cases where only a limited number of governing slow reactions are present, and the system can be assumed to reach local thermodynamic equilibrium otherwise. A successful example presented here is char gasification. It is possible to extend the constrained chemical system with additional constraints for compounds in the gaseous phase. In that case, a fully constrained thermodynamic system is equivalent to the kinetic description of the same system.

ASSOCIATED CONTENT

Supporting Information

Example of the CFE method for modeling mass-transfer kinetics in a closed system. This material is available free of charge via the Internet at http://pubs.acs.org.

AUTHOR INFORMATION

Corresponding Author

*Telephone: +358-20-722-4645. E-mail: petteri.kangas@vtt.fi.

Notes

The authors declare no competing financial interest.

ACKNOWLEDGMENTS

This study is partly funded by Tekes, the Finnish Funding Agency for Technology and Innovation. Support from project partners Aalto University, Process Flow, Metso, and Outotec is acknowledged.

REFERENCES

(1) Yang, H.; Yan, R.; Chen, H.; Lee, D. H.; Zheng, C. *Fuel* **2007**, *86*, 1781−1788.
(2) Aho, A. Catalytic pyrolysis of biomass in a fluidized bed reactor. Ph.D. Dissertation, Åbo Akademi University, Turku, Finland, 2008.
(3) Khazraie Shoulaifar, T.; DeMartini, N.; Willför, S.; Pranovich, A.; Smeds, A. I.; Virtanen, T. A. P.; Maunu, S.; Verhoeff, F.; Kiel, J. H. A.; Hupa, M. *Energy Fuels* **2014**, *28*, 3863−3872.
(4) Tapasvi, D.; Khalil, R.; Skreiberg, Ø.; Tran, K.-Q.; Grønli, M. *Energy Fuels* **2012**, *26*, 5232−5240.
(5) Bates, R. B.; Ghoniem, A. F. *Bioresour. Technol.* **2012**, *124*, 460−469.
(6) de Wild, P. J.; den Uil, H.; Reith, J. H.; Kiel, J. H. A.; Heeres, H. J. *J. Anal. Appl. Pyrolysis* **2009**, *85*, 124−133.
(7) Bergman, P. C. A.; Boersma, A. R. R.; Zwart, W. R.; Kiel, J. H. A. *Torrefaction for Biomass Co-firing in Existing Coal-Fired Power Stations*; Energy Research Centre of the Netherlands: Petten, Netherlands, 2005.
(8) Prins, M. J. Thermodynamic analysis of biomass gasification and torrefaction. Ph.D. Dissertation, Technische Universiteit Eindhoven, Eindhoven, Netherlands, 2005; pp 164.
(9) Di Blasi, C. *Prog. Energy Combust. Sci.* **2009**, *35*, 121−140.

(10) Barrio, M. Experimental investigation of small-scale gasification of woody biomass. Ph.D. Dissertation, Norweigian University of Science and Technology (NTNU), Trondheim, Norway, 2002; pp 222.
(11) Konttinen, J. T.; Moilanen, A.; DeMartini, N.; Hupa, M. *Biomass Convers. Biorefin.* **2012**, *2*, 265−274.
(12) Zhang, R.; Wang, Q. H.; Luo, Z. Y.; Fang, M. X.; Cen, K. F. *Energy Fuels* **2013**, 5107−5115.
(13) Zhang, R.; Wang, Q. H.; Luo, Z. Y.; Fang, M. X.; Cen, K. F. *Energy Fuels* **2014**, *28*, 832−839.
(14) Koufopanos, C. A.; Papayannakos, N.; Maschio, G.; Lucchesi, A. *Can. J. Chem. Eng.* **1991**, *69*, 907−915.
(15) Srivastava, V. K.; Jalan, R. K. *Energy Convers. Manage.* **1996**, *37*, 473−483.
(16) Babu, B. V.; Chaurasia, A. S. *Energy Convers. Manage.* **2004**, *45*, 1297−1327.
(17) Di Blasi, C.; Lanzetta, M. *J. Anal. Appl. Pyrolysis* **1997**, *40*−*41*, 287−303.
(18) Van der Stelt, M. Chemistry and reaction kinetics of biowaste torrefaction. Ph.D. Dissertation, Eindhoven University of Technology, Eindhoven, Netherlands, 2010; pp 263.
(19) Prakash, N.; Karunanithi, T. *J. Appl. Sci. Res.* **2008**, *4*, 1627−1636.
(20) Puig-Arnavat, M.; Bruno, J. C.; Coronas, A. *Renewable Sustainable Energy Rev.* **2010**, *14*, 2841−2851.
(21) Gómez-Barea, A.; Leckner, B. *Prog. Energy Combust. Sci.* **2010**, *36*, 444−509.
(22) Koukkari, P.; Pajarre, R. *CALPHAD: Comput. Coupling Phase Diagrams Thermochem.* **2006**, *30*, 18−26.
(23) Alberty, R. A. *J. Phys. Chem.* **1989**, *93*, 3299−3304.
(24) Keck, J. C. *Prog. Energy Combust. Sci.* **1990**, *16*, 125−154.
(25) Janbozorgi, M.; Ugarte, S.; Metghalchi, H.; Keck, J. C. *Combust. Flame* **2009**, *156*, 1871−1885.
(26) Kangas, P.; Hannula, I.; Koukkari, P.; Hupa, M. *Fuel* **2014**, *129*, 86−94.
(27) Kangas, P.; Koukkari, P.; Lindberg, D.; Hupa, M. *J. Sci. Technol. For. Prod. Processes* **2013**, *3*, 6−15.
(28) Pajarre, R.; Koukkari, P.; Räsänen, E. *J. Mol. Liq.* **2006**, *125*, 58−61.
(29) Kangas, P.; Pajarre, R.; Nappa, M.; Koukkari, P. *Nord. Pulp Pap. Res. J.* **2012**, *27*, 604−612.
(30) Pajarre, R.; Koukkari, P.; Tanaka, T.; Lee, J. *CALPHAD: Comput. Coupling Phase Diagrams Thermochem.* **2006**, *30*, 196−200.
(31) Blomberg, P.; Koukkari, P. *Comput. Chem. Eng.* **2011**, *35*, 1238−1250.
(32) Roine, A.; Lamberg, P.; Mansikka-aho, J.; Björklund, P.; Kentala, J.; Talonen, T.; Vartiainen, A. *HSC Chemistry 6.12*; Outotec Research Oy: Espoo, Finland, 2007.
(33) Koukkari, P.; Penttilä, K.; Hack, K.; Petersen, S. In *Microstructures, Mechanical Properties and Processes*; Bréchet, Y., Ed.; Wiley-VCH Verlag GmbH & Co. KGaA: Weinheim, Germany, 2005; pp 323−330.
(34) Smith, W. R.; Missen, R. W. *Chemical Reaction Equilibrium Analysis: Theory and Algorithms*; Krieger Publishing Company: Malabar, FL, 1991.
(35) Eriksson, G. *Acta Chem. Scand.* **1971**, *25*, 2651−2656.
(36) Eriksson, G.; Rosén, E. *Chem. Scr.* **1973**, *4*, 193−194.
(37) Koukkari, P. *Comput. Chem. Eng.* **1993**, *17*, 1157−1165.
(38) Kangas, P.; Brink, A.; Koukkari, P.; Hupa, M. *Proceedings of the 21st International Congress of Chemical and Process Engineering (CHISA 2014)*; Prague, Czech Republic, Aug 23−27, 2014.
(39) Koukkari, P. S.; Liukkonen, S. S. *Ind. Eng. Chem. Res.* **2002**, *41*, 2931−2940.
(40) Koukkari, P.; Laukkanen, I.; Liukkonen, S. *Fluid Phase Equilib.* **1997**, *136*, 345−362.
(41) Koukkari, P.; Pajarre, R. *Pure Appl. Chem.* **2011**, *83*, 1243−1254.
(42) Koukkari, P.; Pajarre, R.; Blomberg, P. *Pure Appl. Chem.* **2011**, *83*, 1063−1074.
(43) Battley, E. H. *Thermochim. Acta* **1999**, *326*, 7−15.
(44) Dupont, C.; Chiriac, R.; Gauthier, G.; Toche, F. *Fuel* **2014**, *115*, 644−651.

PUBLICATION II

Modelling super-equilibrium in biomass gasification with the constrained Gibbs energy method

Fuel 129, 86–94.

Fuel 129 (2014) 86–94

Contents lists available at ScienceDirect

Fuel

journal homepage: www.elsevier.com/locate/fuel

Modelling super-equilibrium in biomass gasification with the constrained Gibbs energy method

Petteri Kangas [a,*], Ilkka Hannula [b,1], Pertti Koukkari [a,2], Mikko Hupa [c,3]

[a] VTT Technical Research Centre of Finland, Biologinkuja 7, PO box 1000, 02044 VTT, Finland
[b] VTT Technical Research Centre of Finland, Biologinkuja 5, PO box 1000, 02044 VTT, Finland
[c] Åbo Akademi University, Processkemiska centret, Laboratoriet för oorganisk kemi, Biskopsgatan 8, 20500 Åbo, Finland

HIGHLIGHTS

- New method for modelling super-equilibrium in biomass gasification.
- Thermodynamic equilibrium is extended with immaterial constraints.
- The formation of char, tar, ammonia and light hydrocarbons is taken into account.
- The kinetically controlled phenomena are implemented into the model.
- Chemical reactions and the enthalpic effect are resolved simultaneously.

ARTICLE INFO

Article history:
Received 29 January 2014
Received in revised form 12 March 2014
Accepted 18 March 2014
Available online 3 April 2014

Keywords:
Biofuels
Computational methods
Constrained Gibbs energy
Thermodynamics

ABSTRACT

The biomass gasification process is modelled by utilising constrained thermodynamic equilibrium. The formation of char, tar, ammonia and light hydrocarbons and related syngas composition were described by extending the conventional chemical system with additional immaterial constraints and by defining process-dependent values for these constraints.

Six different model structures were evaluated from global thermodynamic equilibrium to fully constrained local equilibrium. When models were validated against gasification setups, it was not necessary to fully constrain the system, as sufficient results were obtained by implementing constraints for char, tar, ammonia, CH_4 formation as well as for the amount of carbon in light hydrocarbons. The method was shown to be versatile when it was validated against other gasification setups: by altering the models defining the constraints a new gasification conditions could be simulated.

A clear benefit of the proposed method is that the gasification process can be resolved as a restricted partial equilibrium with a single calculation step. Another benefit is that chemical reactions, gasification enthalpy and the states of the system are estimated concurrently.

1. Introduction

Biomass gasification is seen as a viable option for high-efficiency electricity generation from bio-based raw materials or as an option for the production of liquid biofuels and chemicals. Gasification is a thermochemical conversion process that takes place at elevated temperatures in reductive conditions. For such circumstances, thermodynamic equilibrium is often assumed to be a guideline (e.g. lately by Kuo et al. [1], Hejazi et al. [2] and Materazzi [3]), but is not reached in practice: during biomass gasification, light hydrocarbons (e.g. CH_4, C_2H_2, C_2H_4, C_2H_6, C_3H_8, C_6H_6), ammonia, tars and char are also formed. The phenomena leading to their formation cannot usually be modelled with equilibrium assumptions. Instead, the modelling is often based on 'grey-box' approaches or on detailed mass transfer approaches with mechanistic reaction kinetics included. A review of biomass gasification models is conducted by Gómez-Barea and Leckner [4] and by Puig-Arnavat et al. [5].

Abbreviations: CFE, constrained free energy method; Component, elementary unit; Constituent, species, compound, is composed of one or several components; EQ, thermodynamic equilibrium; Super-EQ, super-equilibrium, state, where certain constituents are super-saturated.

* Corresponding author. Tel.: +358 20 722 4645.
E-mail addresses: petteri.kangas@vtt.fi (P. Kangas), ilkka.hannula@vtt.fi (I. Hannula), pertti.koukkari@vtt.fi (P. Koukkari), mikko.hupa@abo.fi (M. Hupa).
[1] Tel.: +358 20 722 6370.
[2] Tel.: +358 20 722 6366.
[3] Tel.: +358 2 215 4454.

http://dx.doi.org/10.1016/j.fuel.2014.03.034
0016-2361/

Meticulous mass transfer models may include computational fluid dynamic (CFD) and fluidization calculations, and often give a comprehensive design basis for gasification processes occurring, for example, in fluidized bed reactors. However, the CFD models often appear too complex to be combined with for instance engineering flow sheet models, aiming at steady state simulation of energy and mass balances, including a dependable prediction of chemical conversions in the gasification reactor and related influence to mill-scale processes. For such purposes and in order to increase the accuracy of gasification models, both empirical and mechanistic models are often applied alone or combined with thermodynamic equilibrium calculations. This leads to modified equilibrium models – a 'dual' approach in which different parts of the process and their chemical reactions are modelled independently and results are merged in post-processing. As an example, Hannula and Kurkela [6,7] have extended the thermodynamic equilibrium model by introducing this dual-approach: part of the gasified material is converted to light hydrocarbons, tar, char and ammonia before the equilibrium reactor and by-passing the reactor. The remaining material is modelled using thermodynamic equilibrium. This approach gives satisfying results when the composition of syngas is considered, but includes tedious pre- and post-processing steps before and after the reactor itself. From the actual physical point of view, such an approach is also less justified, as the reactor operates as a single unit. A somewhat similar approach has been utilised by Li et al. [8]. They proposed a non-stoichiometric equilibrium model, where the amount of reactive carbon (namely carbon fed to equilibrium reactor) was limited, based on the kinetic equations. Barba et al. [9] have introduced an extended Gibbs free energy method, which includes additional parameters for the progress of steam formation and water gas shift reactions. Konttinen et al. [10] have reported a thermodynamic model with a constraint applied for the oxidation of char and utilised thermodynamic equilibrium in gaseous phase. Another option for gasification modelling is to apply the quasi-temperature model (QET) where the temperature of the reaction is lowered in order to estimate the formation of char, tars or light hydrocarbons. Temperatures can be substantially lower than the actual temperature: from 250 °C [8] to up to 500 °C [11] and need to be experimentally defined.

The aim of this study is to further develop the gasification reactor model and to present a unified solution for the simultaneous calculation of the super-equilibrium reactions of hydrocarbons, ammonia and 'tars' as well as their related reaction enthalpies in the gasification process. The proposed solution is based on the constrained free energy (CFE) method, where equilibrium computation is extended with additional immaterial constraints (or virtual constraints) for solving the local or partial constrained equilibrium, instead of the global thermodynamic equilibrium. As the conventional Gibbs energy minimisation method applies mass balance constraints for the thermodynamic system components as the necessary conditions in the Lagrange method, the analogous additional constraints have been designated 'immaterial', while a common feature for these conditions is that they are related to work factors or e.g. to extents of reaction (that is, to physical entities without material content) [12]. Differences between possible thermodynamic approaches used for the modelling of the gasification process are shown in Fig. 1: (i) equilibrium model, (ii) modified equilibrium model, (iii) quasi-temperature approach and (iv) constrained free energy-based model.

The proposed constrained free energy method has been adapted with success in several applications areas: Alberty applied the method to the conservation of 'aromaticity' in benzene combustion [13]. The chemical kinetics and related extent of the reaction were defined by Koukkari for high-temperature metallurgy processes [14], and by Keck for internal combustion problems [15]. Pajarre et al. applied the methodology to the partitioning of electrolytes in aqueous membrane systems [16] and to surface energy in multicomponent systems [17]. Reaction pathways were analysed by Blomberg and Koukkari [18] by utilising CFE methodology. Also, super-equilibrium conditions in a black liquor recovery boiler have been modelled by Kangas [19]. The methodological development of CFE has been conducted by Koukkari and Pajarre, for example by introducing virtual constituents to system [20]. Concurrently, the constrained free energy method is seen as a versatile tool for various fields of application.

In the current study, the CFE methodology is utilised for describing the super-equilibrium occurring in biomass gasification. Light hydrocarbons, ammonia, tars and char tend to decompose if thermodynamic equilibrium calculation is performed for high temperatures, and thus constraints are needed for the modelling of their presence in the super-equilibrium conditions as a local equilibrium.

2. Methods

This study focuses on the computational methodology for modelling thermal treatment of carbohydrate-containing raw material (biomass). The supporting empirical is obtained from the literature [7,21,22]. Thermodynamic standard state data is from HSC [23]. ChemSheet [24] is used as the modelling tool, as it allows extending the thermodynamic system with immaterial constraints, and thus enables the calculations of constrained free energy models. Model validation is conducted against the literature data [7,21,22].

2.1. Constrained free energy method

Thermodynamic equilibrium can be calculated by minimising the Gibbs energy of a closed isothermal system. In practice, this is done by applying the Lagrange method of undetermined multipliers (Eq. (1)) [25,26]. The minimum of the system is obtained when its partial derivatives are zero (Eqs. (2) and (3)):

$$L = G - \pi\Psi = \sum_{k=1}^{K} n_k\mu_k - \sum_{l=1}^{L}\pi_l\left(\sum_{k=1}^{K} v_{kl}n_k - b_l\right) \tag{1}$$

$$\left(\frac{\partial L}{\partial n_k}\right)_{n_{n\neq k}} = \mu_k - \sum_{l=1}^{L}\pi_l v_{kl} = 0 \tag{2}$$

$$\left(\frac{\partial L}{\partial \pi_l}\right)_{\pi_{n\neq l}} = \sum_{k=1}^{K} v_{kl}n_k - b_l = 0 \tag{3}$$

where G is the Gibbs free energy of the system; π is the Lagrange multiplier vector; Ψ is the mass balance of the different components of each constituent written in terms of the amounts of matter (mol); n is the molar amount of constituent k; μ is the chemical potential of the constituents k; k refers to each constituent in the multi-phase system; L is the number of components in the system and K the number of constituents respectively. π_l is the Lagrange multiplier of component l, and b_l is the total amount of component l in the system. The chemical potential of each component is defined in Eq. (2) as a linear combination of the Lagrange multipliers. The mass balance of the chemical system is defined in terms of the amounts of components defined by Eq. (3). A detailed description of how to compute the equilibrium can be found in [25–27]. A Gibbs energy solver such as SolGasMix and ChemSheet [24,26] can be used for practical computational work.

When the constrained thermodynamic equilibrium is calculated based on the CFE method, the stoichiometric matrix is extended with additional virtual components and constituents.

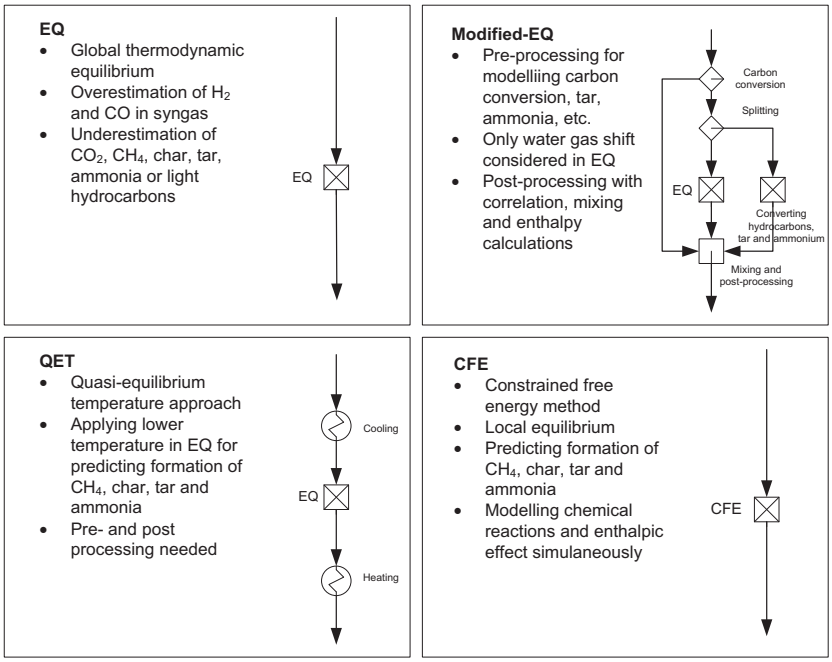

Fig. 1. Different model structures applied for thermodynamic modelling of biomass gasification.

$$N = \begin{bmatrix} \nu_{1,1} & \cdot & \nu_{1,L} & \nu_{1,L+X} \\ \cdot & \cdot & & \cdot \\ \nu_{K,1} & \cdot & \nu_{K,L} & \cdot \\ \nu_{K+X,1} & \cdot & \cdot & \nu_{K+X,L+X} \end{bmatrix} \quad (4)$$

where X is the number of immaterial constraints. The additional virtual components (columns $L+1$ to $L+X$) represent the amount of substance in a particular constituent or phase, and could be used alone for forcing particular constituents to form when calculating the local equilibrium. This approach has been used in [13–15]. When the chemical system is extended with additional virtual constituents (rows $K+1$ to $K+X$) that are connected to the respective virtual constituents (rows $K+1$ to $K+X$), it is possible to constrain either the formation or disappearance of actual constituents [20]. The forward and reverse reactions can be defined by supplying the reaction rate as a molar amount to virtual constituents.

Finally, the equilibrium and limited super-equilibrium reactions for the Gibbsian system can be deduced from Eq. (2):

$$\sum_k a_k \mu_k = 0 \quad \text{(equilibrium reactions)} \quad (5)$$

$$\sum_k a_k \mu_k = \sum_k a_k \sum_{l=1}^{L+X} \nu_{kl} \pi_l \neq 0 \quad \text{(all constrained super-equilibrium reactions)} \quad (6)$$

Here a_k is used for the stoichiometric coefficient of species k in a given reaction. As is also evident from Eq. (2), the Lagrange multipliers in the minimisation procedure represent the chemical potentials of each system component at Gibbs energy minimum [25,26]. For the equilibrium reactions, the thermodynamic affinity becomes zero by Eq. (5), when Gibbs free energy is minimised. For non-equilibrium reactions, Eq. (6), the affinity remains non-zero and can be related to the calculated 'constraint potentials' of the virtual components [12]. This feature has been utilised so as to illustrate the super-equilibrium condition in the biomass gasification.

3. Model

3.1. The thermodynamic system

The chemical system consists of 14 constituents in the gaseous phase (CO, H_2, O_2, N_2, H_2O, CH_4, C_2H_2, C_2H_4, C_2H_6, C_3H_8, C_6H_6, $C_{10}H_8$, NH_3, O_2), liquid water phase (H_2O) and two solid phases for char and ash (C and SiO_2). An additional mixed biomass phase with four elemental constituents (C, H, O and N) is introduced. The biomass phase is used only as input for the model, and is not considered in the equilibrium. The thermodynamic standard data of the system is obtained from HSC [23]. The simplified stoichiometric matrix of the gasification system is presented in Table 1.

To apply the constrained free energy method in the calculations, additional immaterial constraints are embedded into the chemical system. In total, 12 virtual constraints are introduced. Separate constraints are defined for char (R_Char), tar (R_Tar) and ammonium (R_Amm) formation. The constraints for the amount of carbon and hydrogen bound to hydrocarbons are used to control the super-equilibrium of light hydrocarbons (R_HC_C and R_HC_H). The amount of unsaturated and aromatic hydrocarbons (R_UN_C) is evaluated as one possible constraint. Finally, separate constraints are defined for each volatile hydrocarbon constituent (R_CH_4, R_C_2H_2, R_C_2H_4, R_C_2H_6, R_C_3H_8 and R_C_6H_6 respectively). The virtual constituents can be used either for the formation or disappearance of those actual constituents which have been connected with the corresponding virtual components in the stoichiometric matrix. A positive value 1 triggers the forward and a negative value −1 the reverse reaction. [12]. Different combinations of these constraints are evaluated, resulting in six different cases (cases 0–5 in Table 1).

Table 1
Sample of the extended stoichiometric matrix.

Phases	Constituents	Cases	C 0,1,2,3,4,5	O 0,1,2,3,4,5	H 0,1,2,3,4,5	N 0,1,2,3,4,5	Si 0,1,2,3,4,5	$Char^{*}_{1,2,3,4,5}$	$HC\_C^{*}_{1,2,3}$	HC_H* 2	Tar* 1,2,3,4,5	Amm* 0,1,2,3,4,5	CH_4^{*} 3,5	$C_2H_2^{*}$ 5	DB* 4	…
Gas phase	CO	0,1,2,3,4,5	1	1												
	H_2	0,1,2,3,4,5			2											
	CO_2	0,1,2,3,4,5	1	2												
	N_2	0,1,2,3,4,5				2										
	H_2O	0,1,2,3,4,5		1	2											
	CH_4	0,1,2,3,4,5	1		4				1	4			1			
	C_2H_2	0,1,2,3,4,5	2		2				2	2				1	2	
	$C_{10}H_8$	0,1,2,3,4,5	10		8						10					
	NH_3	0,1,2,3,4,5			3							1				
…	…	…														…
Char	C	0,1,2,3,4,5	1					1								
Ash	SiO_2	0,1,2,3,4,5		2			1								1	
Constraints	R_Char	1,2,3,4,5						1								
	R_HC_C	1,2,3							1							
	R_HC_H	2								1						
	R_Tar	1,2,3,4,5									1					
	R_Amm	1,2,3,4,5										1				
	R_CH_4	3,5											1			
	$R\_C_2H_2$	5												1		
	R_UN_C	4													1	
…	…															…

Immaterial constraints cannot affect the mass and energy balances of the system. Thus the extended thermodynamic database provides zero molecular mass for all virtual components. In addition, the standard chemical potentials of virtual constituents are defined as zero.

3.2. Applied constraints

In order to describe the super-equilibrium of char, tar, ammonium and light hydrocarbons in gasification, a model is needed for defining the amounts of constrained species. In general, the constraints can be defined by means of different methods, ranging from constant values based on direct measurement to multi-faceted mechanistic models. This study applies and extends the empirical model for pressurised steam/O_2-blown fluidised-bed gasification by Hannula and Kurkela [7]. Expressions for the amounts used for the twelve constraints are given in Table 2. Constant values are used for tar, ammonium and C_6H_6. Temperature-dependent expressions are used for other constraints. Some of the constrained values applied in this study appear as combinations of individual constraint factors presented in [7]. For examples, the amount of carbon in hydrocarbons is a sum of the carbon in CH_4, C_2H_2, C_2H_4, C_2H_6, C_3H_8 and C_6H_6.

3.3. Local equilibrium of H_2, CO, CO_2 and H_2O

The major syngas components H_2, CO, CO_2 and H_2O are always in local thermodynamic equilibrium. No constraints are applied for the water–gas shift reaction (Eq. (7)), which is the major chemical conversion when the composition of syngas from gasification is considered. However, the constraints applied to other constituents naturally affect the amount of hydrogen, oxygen and carbon available for the water gas shift reaction.

$$CO(g) + H_2O(g) \leftrightarrow CO_2(g) + H_2(g) \quad (7)$$

3.4. Gasification parameters

Five different gasification setups from the literature were [7] modelled for the first validation of model (Marked as A to E in Table 3). Wood chips were gasified in setups A, B and C, where the fuel properties are similar, but gasification parameters, temperature, oxygen-to-fuel ratio and steam-to-fuel ratio varied. Forest residues were used in setup D and wood chips in setup E. Most critical parameters are listed in Table 3 and explained in more detail in [7]. Two additional validation cases were studied with an air/steam-blown fluidised bed gasifier [21] and an air–blown circulating bed gasifier [22]. They also included different fuel and enriched air used in the process. Totally 40 different data points were then used for evaluating the proposed model structure based on the constrained free energy method.

4. Cases

In this study, different approaches for the modelling of global or local equilibrium of biomass gasification have been assessed. Six different cases are evaluated. Cases vary from traditional thermodynamic equilibrium to fully constrained thermodynamic equilibrium where all constituents except those appearing in water gas shift reaction, Eq. (7), are defined by empirical models. The values of introduced constraints are defined by the empirical model, see above Chapter 3.

Thermodynamic equilibrium (**EQ**) is used as the base case. No additional constraints are defined.

Table 2
Applied constraint values. The experimental model is taken from the literature [7].

Constraint	Unit	Expression	Cases
C in char	($mol/kg_{carbon\ in\ dry\ biomass}$)	71.664 + 0.012906*(T/K)	1,2,3,4,5
C in tar	($mol/kg_{dry\ biomass}$)	3.0	1,2,3,4,5
N in ammonia	($mol/kg_{dry\ biomass}$)	0.042	1,2,3,4,5
C in hydrocarbons	($mol/kg_{dry\ biomass}$)	17.642−0.009545*(T/K)	1,2,3
H in hydrocarbons	($mol/kg_{dry\ biomass}$)	50.376−0.02732*(T/K)	2
C in unsaturated and aromatic hydrocarbons	($mol/kg_{dry\ biomass}$)	3.9261−0.00208*(T/K)	4
CH_4	($mol/kg_{dry\ biomass}$)	7.074−0.003*(T/K)	3,5
C_2H_2	($mol/kg_{dry\ biomass}$)	0.06454−0.00004*(T/K)	5
C_2H_4	($mol/kg_{dry\ biomass}$)	2.987−0.002*(T/K)	5
C_2H_6	($mol/kg_{dry\ biomass}$)	1.196−0.001*(T/K)	5
C_3H_8	($mol/kg_{dry\ biomass}$)	0.150921−0.000155*(T/K)	5
C_6H_6	($mol/kg_{dry\ biomass}$)	0.27	5

Next, the super-equilibrium (**Super-EQ1**), in which carbon conversion, tar and ammonia formation are pre-defined, is studied, while the amount of carbon in volatile hydrocarbons (CH_4, C_2H_2, C_2H_4, C_2H_6, C_3H_8 and C_6H_6) is also fixed. This is then followed by a case (**Super-EQ2**) where the condition is extended by introducing an additional constraint for the amount of hydrogen in volatile hydrocarbons. **Super-EQ3** replaces the hydrogen constraint by introducing a constraint for CH_4, and **Super-EQ4** defines the amount of carbon bound to unsaturated hydrocarbons (C_2H_2 and C_2H_4) and aromatics (C_6H_6). Finally, the last super-equilibrium **(Super-EQ5)** treatment introduces a fully constrained system in which the amount of every hydrocarbon constituent is defined by empirical models. However, the water-gas shift reaction is not constrained, but local equilibrium is allowed to exist.

5. Results

The super-equilibrium composition of the gasification reactor as determined by the molar amounts of major syngas components (CO, CO_2, H_2, H_2O and CH_4) were predicted with the constrained free energy method. The accuracy of the model in terms of the added number of constraints was also defined. While the number of constraints is increased, the partial equilibrium moves further from the global equilibrium, as could be verified by calculation.

When additional constraints are introduced into the system, the Gibbs free energy at minimum is increasing, which can be seen in Fig. 2. The global minimum is found for the complete thermodynamic equilibrium and five local minima for the constrained systems. The local minimum of the fully constrained system, Super-EQ5, is furthest from the global minimum, EQ.

Differences between the thermodynamic equilibrium and constrained equilibrium can be seen in Fig. 3, while observing the amounts of components or constituents: for instance, the char formation in equilibrium situation (EQ) is non-existent. However, by implementing single temperature dependent constraint, it is possible to force a certain amount of carbon into the char. In Fig. 3, it can also be seen that formation of light hydrocarbons is very limited if equilibrium is assumed. By defining the constraint for carbon or hydrogen, the local equilibrium with light hydrocarbons is found. Finally, it can be seen that additional constraints are needed in order to form unsaturated and aromatic hydrocarbons (Super-EQ1 vs. Super-EQ2-5). Even the difference in the Gibbs free energy of the system (in Fig. 2) is rather small when comparing super-equilibrium conditions, there are significant differences in the chemical composition of the system (e.g. H in hydrocarbons in Fig. 3).

Syngas composition against temperature is shown in Fig. 4. It is obvious that thermodynamic equilibrium cannot be used to predict the composition. The equilibrium assumption does not predict the formation of CH_4 (also char, ammonia and light hydrocarbons). Thus, there is an excess amount of hydrogen available, and the water-gas shift reaction predicts false syngas composition. When additional constraints are implemented (Super-EQ3), the syngas composition is modelled in greater detail and a more usable temperature dependent model of gasification is achieved, see Fig. 4.

6. Validation

The proposed method was next validated against experimental data found in literature. Three different gasification setups were studied: (i) pressurised steam/O_2-blown fluidised-bed gasifier [7], (ii) air/steam-blown fluidised bed gasifier [21], and (iii) air–blown circulating bed gasifier [22]. In what follows, experimental data is described in more detail for the first validation case, for which also

Table 3
Experimental data from five test operations in an air–blown FBC gasifier [7].

	A	B	C	D	E
C in dry biomass (w-%)	50.7	50.7	50.7	51.3	51.1
H in dry biomass (w-%)	6.2	6.2	6.2	6.1	6.1
N in dry biomass (w-%)	0.1	0.1	0.1	0.5	0.1
O in dry biomass (w-%)	42.8	42.8	42.8	39.5	42.3
Ash in dry biomass (w-%)	0.2	0.2	0.2	2.6	0.4
Fuel moisture (%)	6.9	6.9	6.9	10.4	7.4
Gasifier temperature (C)	823	838	886	830	868
Pressure (MPa)	0.250	0.250	0.250	0.250	0.250
Oxygen-to-fuel ratio ($kg/kg_{dry\ fuel}$)	0.31	0.37	0.42	0.37	0.46
Steam-to-fuel ratio ($kg/kg_{dry\ fuel}$)	0.5	0.54	0.54	0.54	0.75
CO (v-%)	0.144	0.132	0.133	0.122	0.103
CO_2 (v-%)	0.211	0.220	0.222	0.222	0.207
H_2 (v-%)	0.167	0.154	0.156	0.167	0.149
CH_4 (v-%)	0.056	0.055	0.056	0.056	0.046
H_2O (v-%)	0.400	0.418	0.411	0.411	0.483

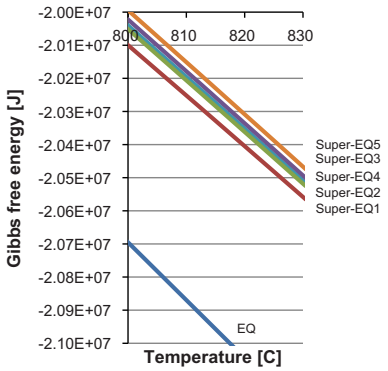

Fig. 2. Global minimum of Gibbs free energy for thermodynamic equilibrium (EQ) and five local minima for constrained thermodynamic equilibriums (Super-EQ1–Super-EQ5) as a function of temperature.

different submodels for the super-structures are evaluated. For the two other cases references to original publications are given.

6.1. Pressurised steam/O_2-blown fluidised-bed gasifier

First the developed model is validated against literature data shown in Table 3 (see details with the experimental setup in [7]). This is experimental data from pressurised steam/O_2-blown fluidised-bed gasification with power of 0.5 MW. Three different fuels were tested: two type of wood chips and forest residues. Gasification temperature ranges between 823 and 886 °C, pressure is 2.5 bar and fuel moisture from 7% to 10%. In total five different validation points are available. [7]. Six different models structures (EQ, Super-EQ1, Super-EQ2, Super-EQ3, Super-EQ4 and Super-EQ5) were evaluated against these five different gasification setups with different raw material and gasification conditions (A to E in Table 3).

Global thermodynamic equilibrium cannot satisfactorily describe the super-equilibrium conditions present in the biomass gasification process, which becomes evident from Figs. 4 and 5 when observing the amounts of major syngas species. By embedding the additional virtual constraints in the chemical system, the calculated syngas composition is much closer to measured values. The Super-EQ1 case, where the amount of char, tar, ammonia and carbon in light hydrocarbons is constrained already gives significantly better results. However, the CH_4 content is still not satisfactory. By implementing additional constraints, (Super-EQ2) amount of hydrogen in hydrocarbons, (Super-EQ3) amount of methane, (Super-EQ4) amount of carbon in unsaturated and aromatic hydrocarbons, it is possible to adjust the amount of methane. As expected, the fully constrained system (Super-EQ5) gives the best agreement, but the only partly constrained system (Super-EQ3) also gives results that are as good. It is noticeable that the amount of hydrogen is slightly off for all cases. However, the hydrogen content is the most difficult to measure in pilot-scale

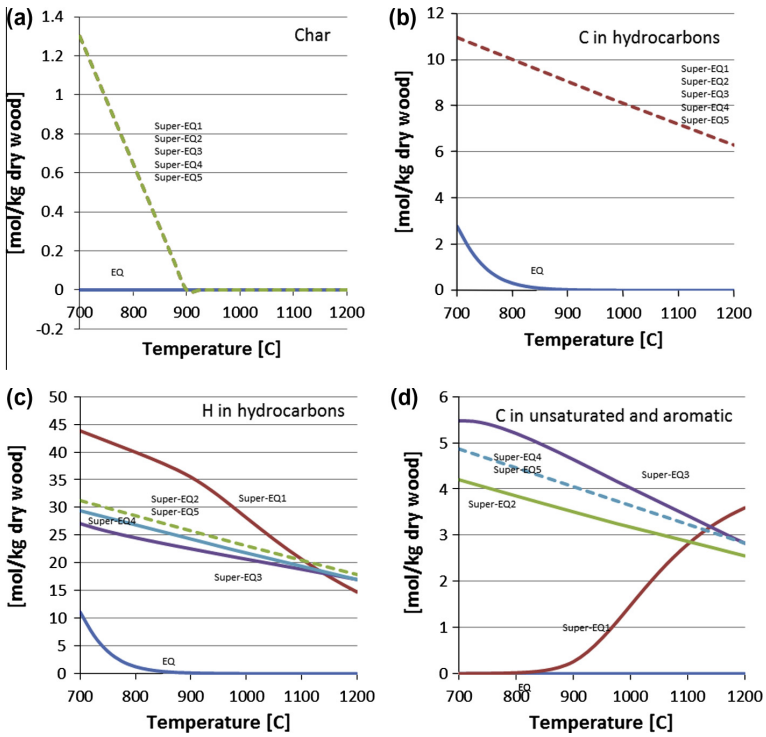

Fig. 3. Effects of constrained and global equilibrium on the carbon and hydrogen content of different constituents. The dashed line denotes the constrained value and the solid line the value in equilibrium. (a) Amount of carbon in char in constrained for Super-EQ1–Super-EQ5 by 71.664 + 0.012906°(T/K) (mol/$kg_{dry\ wood}$); (b) Amount of carbon in volatile hydrocarbons is for Super-EQ1–Super-EQ5 by 17.642−0.009545°(T/K) (mol/$kg_{dry\ wood}$), (c) amount of hydrogen in volatile hydrocarbons is constrained for Super-EQ2 and Super-EQ2 by 50.376−0.02732°(T/K) (mol/$kg_{dry\ wood}$), and (d) amount of carbon in unsaturated and aromatic species is constrained for Super-EQ4 by 3.9261−0.00208°(T/K) (mol/$kg_{dry\ wood}$).

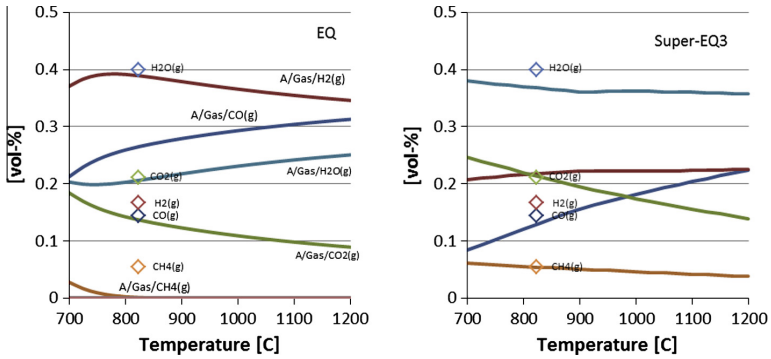

Fig. 4. Predicted composition of major syngas components (H_2, CO, CO_2, H_2O and CH_4) for thermodynamic equilibrium (EQ) and for constrained equilibrium (Super-EQ3), where the formation of char, tar, ammonia, and methane are constrained as well as the amount of carbon in light hydrocarbons. Diamonds represent validation data from [7].

situations, and measurement issues provide one explanation for the deviation.

6.2. Air/steam-blown fluidised bed gasifier

The model structure is next evaluated against the literature data from other type of gasifier. Campoy et al. [21] have studied the air/steam-blown fluidised bed system. In their process, the oxygen content varies from 21 to 40 v-% (enriched) of air and steam to biomass ratio from 0% to 63%. Operating temperature is 755–840 °C and biomass feed rate is 10–22 kg/h. Wood pellets are used as fuel. In total 20 different data sets were available in [21] (where the experimental setup is also explained in more detail).

Two constraints were defined for this validation case: (i) char yield (R_Char) and (ii) methane yield (R_CH_4). Char yield is defined based on the experimental data presented in (Table 3 and Fig. 8a. in [21]) as:

$$x_{Char} = 0.141 - 0.274 \cdot x_{O_2} \quad (21\% \leqslant OP \leqslant 40\%) \tag{8}$$

Here x_{Char} describes the fraction of carbon remaining in char out of original carbon in fuel. x_{O_2} is the oxygen content in air. Constraint of methane is defined accordingly the first validation case (see Table 2) as model fits well for the experimental results. Fig. 6 illustrates the modelled composition of syngas (CO, CO_2, H_2 and CH_4) against the measured values in [21]. The model again seems to agree reasonably with the experimental data. Yet variation here appears somewhat larger than for the first validation case. The result, however suggests that the constrained free energy method could be used for modelling various gasifiers or different gasification conditions when the kinetic models and equations describing the constraints are altered according to each new case.

6.3. Air–blown circulating bed gasifier

Third validation for the proposed modelling methodology was done against pilot scale air–blown circulating bed gasifier, as presented by Li et al. in [22]. Operating temperature was between 700 and 850 °C and pressure 1.2–1.6 bar respectively. Biomass feed rate was 16–44 kg/h. Results of six different biomass types were reported. Altogether 15 different experimental data sets were available for validation purposes. For simplicity the experimental data is not repeated here but can be found in (Tables 1 and 2 in [22]).

In this validation case three constraints were defined: (i) char formation (R_Char), (ii) methane formation (R_CH_4) and (iii) tar formation (R_Tar). Char and methane formations were according to model proposed by Li et al. in [22].

$$x_{Char} = 0.75 \cdot \exp(-\lambda/0.23) \quad (0.22 \leqslant \lambda \leqslant 0.54) \tag{9}$$

$$n_{CH_4} = 0.11(1 - \lambda) \tag{10}$$

Here x_{Char} describes the fraction of carbon remaining in char out of original amount of carbon in biomass. n_{CH_4} defines the amount of carbon bound to methane. λ is the air ratio of actual air versus stoichiometric air needed for full combustion. The constraint of tar is defined based on the experimental data in (Table 2 in [22]) and value varies between 0 and 1 mol carbon per 1 kg of dry wood. Fig. 6 illustrates predicted values against experimental values. The model now seems to predict gas composition for CO, CO_2 and CH_4 rather well, but overestimates the amount of H_2. The relatively low observed hydrogen content in the syngas is also recognised by Li et al. in their paper [27], which could indicate that there is some hydrogen remaining in coke, formation of light hydrocarbon is neglected during experiments or measurement of hydrogen content has some uncertainties. Suggestively, the largest deviation in modelled H_2 content versus measured values is observed in three cases where tar formation is largest. In the presented model tar is listed as $C_{10}H_8$ (naphthalene), but in reality other compounds with larger H:C ratios may well be bound to tar. In context with such experimental findings, the usage of a Gibbsian thermodynamic model can give additional insights for the assessment of experimental arrangement when applied concurrently with the experimental work.

7. Discussion

The current work has demonstrated that the super-equilibrium of char, tar, ammonia and light hydrocarbons in biomass gasification and related major syngas species (CO, CO_2, H_2, H_2O and CH_4) can be predicted with the constrained free energy (CFE) method. The accuracy of the model increases when additional constraints are implemented. However, it was not necessary to fully constrain the system, as is often done with the mechanistic model. By defining constraints for char, tar, ammonia, carbon in hydrocarbons and CH_4, it is possible to model the system at the same accuracy as with constraints on all light hydrocarbons.

While the adapted constraints were successful in evaluating the super-equilibrium of major species, the respective predictions for minor hydrocarbon species (C_2H_2, C_2H_4, C_2H_6, C_3H_8, C_6H_6) were not as satisfying. In practical problems this limitation could be

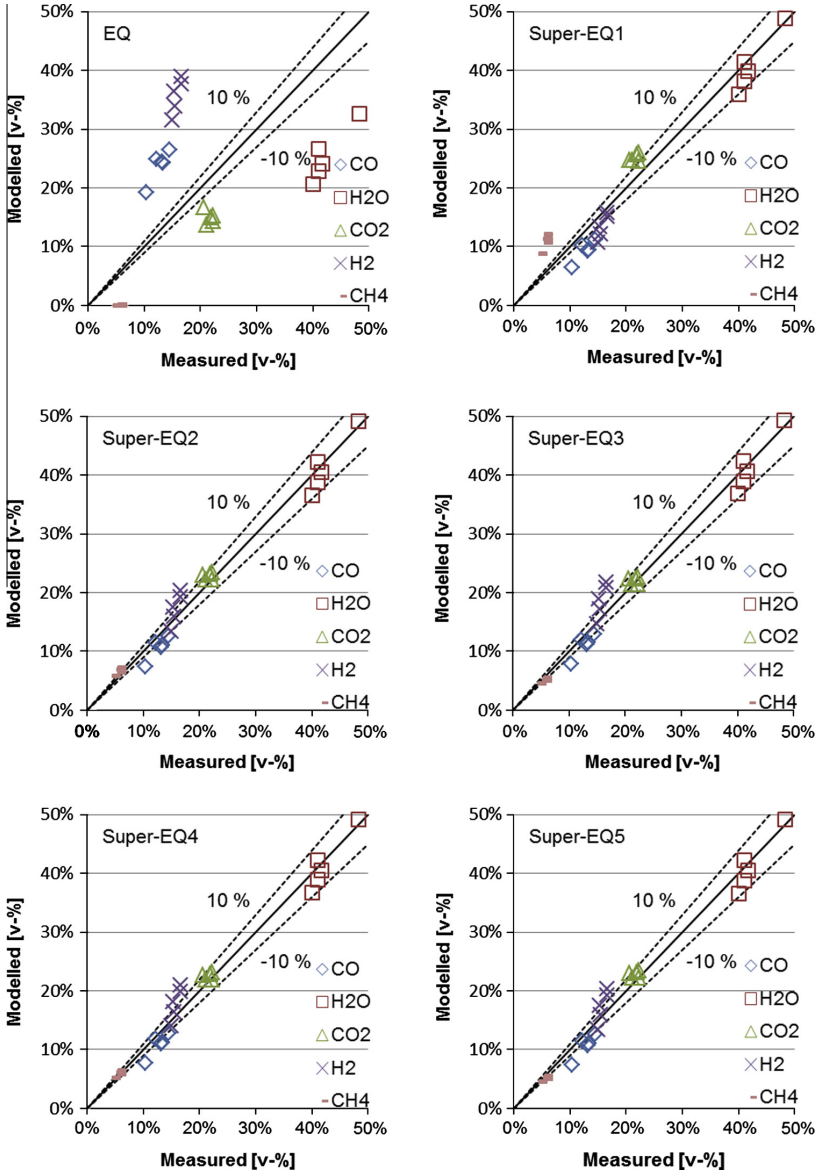

Fig. 5. Major syngas components (CO, H_2O, CO_2, H_2 and CH_4). Modelled values vs. measured values [7].

neglected, as the main interest is in major species, and minor species could be considered as surrogates for modelling several low-concentration species that might occur in the gasification process. If greater accuracy for hydrocarbon species is needed, then selection of the modelled species and respective constraints is important.

It is important to note that use of the constraints in the way shown above requires experimental information which at least partly will be process-specific, as was also indicated by the three validation cases presented above. Consequently, a model developed for one gasifier may not be directly applicable to another gasifier of different size, design or fuel and oxidant feeding system. The present study suggests that the values for constraints can be defined e.g. based on gasification temperature, air-ratio, the amount of oxygen enriching air, or based directly on experimental measurement Yet, the same model structure based on constrained free energy methodology can be re-used for different gasifiers or even for syngas reforming by re-defining the kinetic submodels and respective constraints. This allows a generic and versatile thermodynamic model structure of gasification to be developed, where different application specific descriptions and submodels could be implemented.

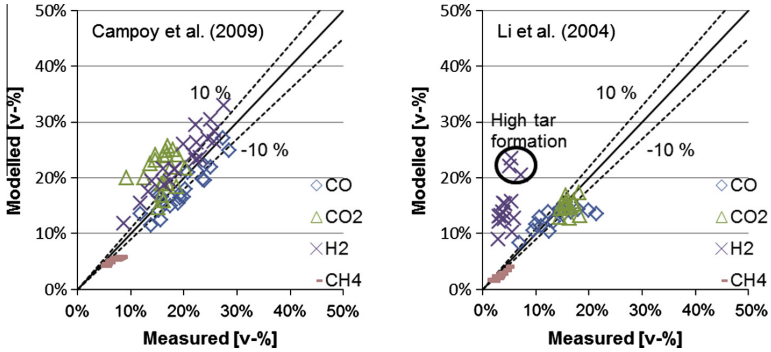

Fig. 6. Major syngas components (CO, CO_2, H_2 and CH_4) in dry gas. Modelled values vs. measured values. On the left side validation data of an air/steam-blown fluidised bed gasifier [21] and on the right hand an 6 air–blown circulating bed gasifier [22].

8. Conclusion

The biomass gasification process can be resolved as a restricted local equilibrium by applying the constrained free energy method (CFE) with a single calculation step. Thus, there is no need for post-processing corrections for, for instance, volume or enthalpy flows. For a reasonable accuracy of the simulation model, it is not necessary to define constraints for all reactions, but a set of more general constraints (e.g. carbon in hydrocarbons) remains sufficient.

The distinct benefit of the approach presented is that chemical reactions, gasification enthalpy and states of the system (such as volume) are estimated concurrently. This method is also resilient: the number of details describing constraints can vary from simpler experimental results and models as presented in this paper to complicated mechanistic models. However the models are always needed for defining the constraints.

A promising application area for the methodology presented could be as part of large-scale process simulation, where detailed thermodynamic models can be implemented and the effects on gasification chemistry could cause changes in the entire process.

Acknowledgements

This study is partly funded by Tekes – the Finnish Funding Agency for Technology and Innovation. Support from project partners Åbo Akademi University, Aalto University, Process Flow, Metso and Outotec is acknowledged.

References

[1] Kuo P-C, Wu W, Chen W-H. Gasification performances of raw and torrefied biomass in a downdraft fixed bed gasifier using thermodynamic analysis. Fuel 2014;117:1231–41.
[2] Hejazi B, Grace JR, Bi X, Mahecha-Botero A. Steam gasification of biomass coupled with lime-based CO_2 capture in a dual fluidized bed reactor: a modeling study. Fuel 2014;117:1256–66.
[3] Materazzi M, Lettieri P, Mazzei L, Taylor R, Chapman C. Thermodynamic modelling and evaluation of a two-stage thermal process for waste gasification. Fuel 2013;108:356–69.
[4] Gómez-Barea A, Leckner B. Modeling of biomass gasification in fluidized bed. Prog Energy Combust Sci 2010;36:444–509.
[5] Puig-Arnavat M, Bruno JC, Coronas A. Review and analysis of biomass gasification models. Renew Sustain Energy Rev 2010;14:2841–51.
[6] Hannula I, Kurkela E. A semi-empirical model for pressurised air–blown fluidized-bed gasification of biomass. Bioresour Technol 2010;101:4608–15.
[7] Hannula I, Kurkela E. A parametric modelling study for pressurised steam/O_2-blown fluidised-bed gasification of wood with catalytic reforming. Biomass Bioenergy 2012;38:58–67.
[8] Li X, Grace J, Watkinson A, Lim C, Ergüdenler A. Equilibrium modeling of gasification: a free energy minimization approach and its application to a circulating fluidized bed coal gasifier. Fuel 2001;80:195–207.
[9] Barba D, Prisciandaro M, Salladini a, Mazziotti di Celso G. The Gibbs free energy gradient method for RDF gasification modelling. Fuel 2011;90:1402–7.
[10] Konttinen JT, Moilanen a, DeMartini N, Hupa M. Carbon conversion predictor for fluidized bed gasification of biomass fuels—from TGA measurements to char gasification particle model. Biomass Convers Biorefinery 2012;2:265–74.
[11] Kersten S, Prins W, Van der Drift A, Van Swaaij W. Interpretation of biomass gasification by "'quasi"'-equilibrium models. Proc. Twelfth Eur. Conf. biomass energy, Ind. Clim. Prot., Amsterdam, Netherlands; 2002.
[12] Koukkari P, Pajarre R. A Gibbs energy minimization method for constrained and partial equilibria. Pure Appl Chem 2011;83:1243–54.
[13] Alberty RA. Thermodynamics of the formation of benzene series polycyclic aromatic hydrocarbons in a benzene flame. J Phys Chem 1989;93:3299–304.
[14] Koukkari P. A physico-chemical method to calculate time-dependent reaction mixtures. Comput Chem Eng 1993;17:1157–65.
[15] Keck JC. Rate-controlled constrained-equilibrium theory of chemical reactions in complex systems. Prog Energy Combust Sci 1990;16:125–54.
[16] Pajarre R, Koukkari P, Räsänen E. Inclusion of the Donnan effect in Gibbs energy minimization. J Mol Liq 2006;125:58–61.
[17] Pajarre R, Koukkari P, Tanaka T, Lee J. Computing surface tensions of binary and ternary alloy systems with the Gibbsian method. Calphad 2006;30:196–200.
[18] Blomberg P, Koukkari P. A systematic method to create reaction constraints for stoichiometric matrices. Comput Chem Eng 2011;35:1238–50.
[19] Kangas P, Koukkari P, Lindberg D, Hupa M. Modelling black liquor combustion with the constrained Gibbs energy method (accepted). J Sci Technol For Prod Process 2014.
[20] Koukkari P, Pajarre R. Calculation of constrained equilibria by Gibbs energy minimization. Calphad 2006;30:18–26.
[21] Campoy M, Gómez-Barea A, Vidal FB, Ollero P. Air–steam gasification of biomass in a fluidised bed: Process optimisation by enriched air. Fuel Process Technol 2009;90:677–85.
[22] Li XT, Grace JR, Lim CJ, Watkinson aP, Chen HP, Kim JR. Biomass gasification in a circulating fluidized bed. Biomass Bioenergy 2004;26:171–93.
[23] Roine A, Lamberg P, Mansikka-aho J, Björklund P, Kentala J, Talonen T, et al. HSC Chemistry 6.12. Outotec Research Oy; 2007.
[24] Koukkari P, Penttilä K, Hack K, Petersen S. CHEMSHEET – an efficient worksheet tool for thermodynamic process simulation. In: Bréchet Y, editor. Microstruct. mech. prop. process. Weinheim: Wiley-VCH Verlag GmbH & Co. KGaA; 2005. p. 323–30.
[25] Smith WR, Missen RW. Chemical reaction equilibrium analysis: theory and algorithms. Malabar (FL, US): Krieger Publishing Company; 1991.
[26] Eriksson G. Thermodynamic studies of high temperature equilibria. III. SOLGAS, a computer program for calculating the composition and heat condition of an equilibrium mixture. Acta Chem Scand 1971;25:2651–6.
[27] Eriksson G, Rosén E. Thermodynamic studies of high temperature equilibria. VII. General equations for calculation of equilibria in multiphase systems. Chem Scr 1973;4:193–4.

PUBLICATION III

Modelling black liquor combustion with the constrained Gibbs energy method

The Journal of Science and Technology for
Forest Products and Processes 3 (3), 6–15.

MODELLING BLACK LIQUOR COMBUSTION WITH THE CONSTRAINED GIBBS ENERGY METHOD

PETTERI KANGAS, PERTTI KOUKKARI, DANIEL LINDBERG, MIKKO HUPA*

ABSTRACT

A simulation model based on multiphase thermodynamics has been developed for the combustion of black liquor in a recovery boiler. The model provides a quantitative description of the observed super-equilibrium of excess sodium, potassium, sulphur, and chlorine in recovery-boiler fumes and the respective effects of super-equilibrium on the condensed phases. The methodology is based on the constrained free energy (CFE) technique, which is an extension of the conventional Gibbs free-energy minimization method used to estimate kinetically controlled and local equilibria of multiphase chemical systems. This work extends the Na-K-S-Cl-C-O-H-N system used for ash-chemistry studies by introducing additional constraints on the volatility of Na, K, S, and Cl. The methodology presented here enables simultaneous estimation of chemical reactions and heat of combustion in the recovery boiler.

BACKGROUND

The recovery boiler is an essential component of a Kraft pulp mill. It is primarily used for energy recovery because roughly half of all wood raw materials entering the mill are dissolved into the pulp cooking liquor during delignification. In addition, valuable cooking chemicals are salvaged during the combustion process. To ensure this dual objective, special combustion conditions are needed in the boiler furnace. The lower furnace is operated under reductive conditions for chemical recovery, while oxidative conditions are introduced in the upper furnace to ensure full combustion of the dissolved wood.

Previous experimental studies [1–5] have shown that large amounts of sulphur, sodium, potassium, and chloride become volatilized during combustion in the lower furnace and can be found in the flue gas, i.e., fumes, of the recovery boiler. Figure 1 illustrates typical industrial concentrations (in ppm) for sulphur and sodium in fumes. Volatile species can initiate corrosion as they cool in the flue-gas channel, resulting in operating problems and economic losses.

Vaporization occurs mostly during the flight of black liquor droplets as black liquor is sprayed into the boiler and droplets are dried, devolatilized, and pyrolyzed, and partly during char-bed combustion. The release of these components is due to (i) reduction of alkali carbonates (both sodium and potassium) with char to produce vaporous elemental alkali [6], (ii) direct vaporization of chlorides [6], and (iii) release of organosulphur gases [7].

Considerable work has been carried out to obtain measured volatilization data.

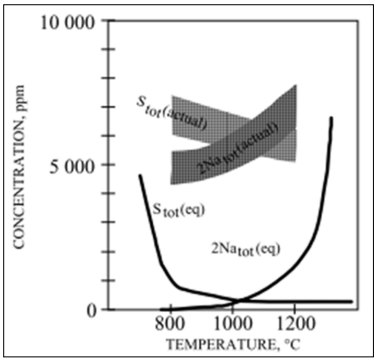

Fig. 1 - Release of sulphur and sodium in a recovery furnace as a function of temperature. Equilibrium values and typical actual boiler data [8].

Hupa *et al.* [1] measured the in-flight release of sodium from eight different black liquors under laboratory conditions; Mikkanen et al. [9] conducted industrial-scale measurements of four recovery boilers; Salmenoja *et al.* [2] performed measurements in five recovery boilers; Janka *et al.* [4] measured the release of sodium, chlorine, and potassium in a single recovery boiler under different operating conditions; and Vakkilainen [5] reported potassium and chlorine enrichment factors from 21 recovery boilers. The observations from these studies are summarized in Table 1.

PETTERI KANGAS
VTT Technical Research Centre of Finland
Finland
*Contact: petteri.kangas@vtt.fi

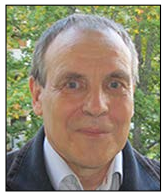

PERTTI KOUKKARI
VTT Technical Research Centre of Finland
Finland

DANIEL LINDBERG
Åbo Akademi University
Finland

MIKKO HUPA
Åbo Akademi University
Finland

TABLE 1 *Release of sulphur, sodium, potassium, and chloride to flue gases.*

	S	Na	K	Cl	Type
Hupa *et al.* [1]	54%	17%			Laboratory
Salmenoja *et al.* [2]			1.1–1.4	1.0–6.0	Industry
Mikkanen *et al.* [3]	24–36%	10–12%	1.3–1.7		Industry
Janka *et al.* [4]			1.3–1.6	3.0–4.5	Industry
Vakkilainen [5]			1.0–2.5	0.3–6.0	Industry

S: $S_{flue\ gas}/S_{black\ liquor}$ [%]
Na: $Na_{flue\ gas}/Na_{black\ liquor}$ [%]
K: $(K_{flue\ gas}/(K + Na)_{flue\ gas})/(K_{black\ liquor}/(K + Na)_{black\ liquor})$ []
Cl: $(Cl_{flue\ gas}/(K + Na)_{flue\ gas})/(Cl_{black\ liquor}/(K + Na)_{black\ liquor})$ []

Recovery-boiler modelling

In recent decades, several approaches have been used to develop models of recovery-boiler chemistry and in particular of sulphur, sodium, potassium, and chlorine volatilization.

For these purposes, comprehensive thermodynamic data for the Na-K-S-Cl-C-O-H system have been gathered and compiled in a consistent database. Assessment of these data has been recently conducted, for example by Lindberg [10], and the results are currently commercially available from FactSage [11] as the FTPULP database [12]. The latest development of this database includes bromides [13]. The database and related tools can be used to generate phase diagrams and predict sticky temperatures in the upper furnace and flue-gas channel.

Thermodynamic data and solvers have been used in recovery-boiler expert systems, for example to reduce corrosion of boiler superheaters and economizers. An early development by Pejryd and Hupa [14] as well as the work of Backman *et al.* [15] have been used to predict chemistry and deposits in the recovery boiler and to estimate the sticky temperature of fly ash. The most recent development by Enestam [16] uses multi-phase chemical models together with a large experimentally-based database of corrosion conditions. These models typically use a "dual" approach to model volatilization: release during in-flight pyrolysis is modelled experimentally and evaporation at the char bed using thermodynamic equilibrium [1] or by kinetically limited reactions [17]. By summarizing these factors, it has been possible to predict the chemistry of the upper furnace and flue-gas channel as described by Janka [4]. However, the restricted thermodynamic equilibrium in the lower furnace has not been examined in previous studies.

A similar approach has been used as part of large-scale process simulations. Uloth *et al.* [18] used thermodynamic equilibrium calculations to model the chemistry of the flue-gas channel as part of a large-scale steady-state process simulation. The lower furnace and char bed were modelled using applied temperature-dependent kinetic models. A similar approach was later used by Cardoso [19]. In their model, only 27 species were included due to the limitations of the process simulator. The model was then confined to a relatively small chemical system (e.g., when compared to that of Lindberg [10]), and the resulting predictions mainly concern the major species.

Black-liquor droplet modelling has been extensively studied because volatilization and reactions during flight strongly affect the combustion and functionality of the recovery boiler. Järvinen *et al.* [20] have developed a model that includes bubble formation during the spraying process. The model can be used to optimize splash-plate geometry and to adjust spraying parameters.

Fly-ash particle formation in the recovery boiler has been studied and modelled by Jokiniemi *et al.* and Mikkanen [3,21]. The focus of these studies has been on aerosol behaviour during combustion. The models include fume-particle formation, growth, and deposition. In addition, the chemistry of sodium, potassium, and chlorides in the fumes is considered. However, these models neglect the combustion process and chemistry of the lower furnace while again focusing on phenomena in the upper furnace and flue-gas channel.

Computational fluid dynamics have been used in recovery-boiler modelling for at least two decades. The first models, as described by Grace *et al.* [22], combined gas-phase combustion, a droplet model, and char-bed burning. The latest developments by Engblom [17] introduced a model for predicting the changing shape of the char bed. In addition, Leppänen *et al.* combined a particle-formation model with computational fluid dynamics [23].

Recovery-boiler models have been reviewed by Grace and Engblom [6,17,24], and additional details of the various approaches can be found in their papers.

However, all the recovery-boiler models referred to above either (i) neglect the lower furnace and consider the lower furnace as a fixed boundary condition for flue-gas calculations, or (ii) use a dual approach with droplet and char-bed burning treated separately. There is an apparent need for a unified solution that could be used for simultaneous estimation of chemical reactions and heat generation in the lower furnace.

Computational thermodynamics

The first computational thermodynamics software applications were developed by NASA for research into rocket-fuel combustion. Later, other Gibbs free-energy minimizing computer programs, such as SOLGAS by Eriksson [25,26], emerged and were used for high-temperature chemical equilibrium studies. These programs were further developed, for example by Weber [27], and adapted for software tools such as FactSage [11], ChemApp [28], and ChemSheet [29]. As referred to above, these early Gibbs energy programs have also been used for calculating the thermodynamic equilibrium of black liquor combustion, for example, by [1,15,16,18].

The concept of constrained thermodynamic equilibria in Gibbs energy minimization was first introduced by Alberty [30] as a method for the conservation of immaterial properties and further developed for reaction kinetics by Keck and Koukkari [31,32]. The methodology of immaterial constraints was extended by

Koukkari and Pajarre [33,34] to describe several other phenomena in the Gibbsian calculations, such as electrochemical Donnan equilibrium in aqueous pulp suspensions as well as surface-energy controlled systems. One salient application of the constraint method is the calculation of partial and local equilibria under supersaturation or kinetic conditions.

This study uses the constrained free energy (CFE) method to model the local super-equilibrium of sulphur, sodium, potassium and chlorine in flue gases in the lower part of the recovery-boiler furnace. The aim is to present a unified method for calculating chemical reactions and energy production in the lower furnace, which has been often either neglected or substantially simplified in previous models.

METHODS

The study is computational, with all measured data obtained from relevant literature. The basic black liquor properties and related data are from [1].

Thermodynamic data and the computational tool

The thermodynamic data used in this study are commercially available from FactSage [11]. The FTPULP database was adapted; its chemical system consists of seven components: sodium-potassium-chlorine-sulphur-carbon-oxygen-hydrogen (Na-K-S-Cl-C-O-H-N), and 60 phases, of which 17 are solutions or mixed phases and 43 are pure phases with a single constituent. The entire database was used with the liquid phase described by the fully optimized subsystem Na^+, $K^+//S^{2-}$, SO_4^{2-}, CO_3^{2-}, Cl^-, OH^-. The liquid components, which are alkali pyrosulphates or alkali polysulphides, were, however, not considered in the present study. A description of the database is provided in [12], and it has been reviewed in [10].

Nitrogen (N) was introduced to the system to describe the combustion air, resulting in a total of eight system components. The formation of NO_x components is kinetically driven, and thermodynamic modelling is not a suitable tool to predict NO_x chemistry. Therefore, nitrogen is assumed to form only inert N_2. Black liquor elemental composition and higher heating value were used as model parameters.

ChemSheet [29] was used as a computational tool because it enables manipulation of the multicomponent thermodynamic system by extending the stoichiometric matrix, thus making it possible to calculate constrained thermodynamic equilibria.

Thermodynamic equilibrium

The thermodynamic equilibrium of the system under study can be obtained by minimizing the Gibbs free energy [35]. Using this approach, individual reactions do not need to be specified. Instead, the multi-phase system is treated as a single assembly (if equilibrium constants are defined, each reaction must be defined accordingly). The multi-phase system and its corresponding phases and constituents are therefore defined by the stoichiometric matrix *N*:

$$\mathrm{N} = \begin{bmatrix} \nu_{11} & \nu_{12} & . & . & \nu_{1L} \\ \nu_{21} & \nu_{22} & . & . & \nu_{2L} \\ . & . & \nu_{kl} & . & . \\ . & . & . & . & . \\ \nu_{k1} & \nu_{k2} & . & . & \nu_{KL} \end{bmatrix}, \quad (1)$$

where the columns represent components *1…L*, and the rows constituents *1…K* respectively. The Gibbs free energy of the system is defined as:

$$G = \sum_{i=1}^{I} \sum_{j=1}^{J_i} n_j^i \mu_j^i = \sum_{k=1}^{K} n_k \mu_k \,, \quad (2)$$

where *i* refers to the phases and *j* refers to the constituents of each phase. Similarly, *k* refers to each constituent in the multi-phase system, *n* to the number of molar constituents, and μ to the chemical potential of the constituents. *I* is the number of phases in the system, *Ji* is the number of constituents in phase *i*, and *K* is the number of constituents in the whole system.

The Gibbs energy of this closed isothermal system can be minimized using the Lagrange method of undetermined multipliers (Eq. (3)). The minimum is obtained when its partial derivatives are zero (Eqs. (4) and (5)):

$$L = G - \pi\Psi = \sum_{k=1}^{K} n_k \mu_k - \sum_{l=1}^{L} \pi_l \left(\sum_{k=1}^{K} \nu_{kl} n_k - b_l \right) \quad (3)$$

$$\left(\frac{\partial L}{\partial n_k} \right)_{n_{m \neq k}} = \mu_k - \sum_{l=1}^{L} \pi_l \nu_{kl} = 0 \,, \quad (4)$$

$$\left(\frac{\partial L}{\partial \pi_l} \right)_{\pi_{m \neq l}} = \sum_{k=1}^{K} \nu_{kl} n_k - b_l = 0 \,, \quad (5)$$

where π is the Lagrange multiplier, Ψ is the mass balance of the different components of each constituent written in terms of the amounts of matter (mol), π_l is the Lagrange multiplier of component *l*, and b_l is the total amount of component *l* in the system as described by the matrix in Eq. (1). The chemical potential of each component is defined in Eq. (4) as a Lagrange multiplier, and the mass balance of the system in terms of the quantities of components is defined by Eq. (5).

The chemical potential of constituent k is further defined as:

$$\mu_k = \mu_{k,id} + \mu_{k,ex} \,, \quad (6)$$

where $\mu_{k,id}$ is the ideal term of the chemical potential of constituent *k* and $\mu_{k,ex}$ is the excess term of the chemical potential of constituent *k*. The ideal and excess chemical potentials were derived from the database used [12]. The set of equations, Eq. (4), is then linearized and an iterative solver is used [25]. A detailed description of the computational solution used for thermodynamic equilibrium is provided in [27,35].

Constrained thermodynamic equilibrium

As noted above, thermodynamic equilibrium is not reached in the lower part of the recovery-boiler furnace. Instead, a condition described as a "super-equilibrium" of sodium, potassium, sulphur, and chlorine is present in the gaseous phase. The term super-equilibrium refers here to "supersaturation" of the vapour phase. To model this phenomenon of partial equilibrium, in what follows the constrained free

energy (CFE) method is used.

The super-equilibrium condition can be introduced to stoichiometric matrix N (see Eq.1) by inclusion of supplementary virtual components and virtual constituents, by which additional constraints can be introduced to the Lagrangian minimization problem. The extended stoichiometric matrix then becomes:

$$N = \begin{bmatrix} \nu_{1,1} & \cdot & \nu_{1,L} & \nu_{1,L+X} \\ \cdot & \cdot & & \cdot \\ \nu_{K,1} & \cdot & \nu_{K,L} & \cdot \\ \nu_{K+X,1} & \cdot & \cdot & \nu_{K+X,L+X} \end{bmatrix}, \quad (7)$$

where X is the number of additional constraints. The virtual components (columns $L+1 \ldots L+X$) represent the amount of a substance in a particular phase or phases. These components are connected to the virtual constituents (rows $K+1$ to $K+X$). The virtual constituents can be used for either formation or destruction of these actual constituents which have been connected with the corresponding virtual components. A positive value of one is used for forward and a negative value of minus one for reverse reaction of virtual constituents [34].

To be able to use such a matrix extension in the Gibbs energy minimization program without affecting its energy or mass balances, the extended thermodynamic database provides the respective (zero) data for the virtual system components and virtual constituents. The molecular mass of each virtual component is given as zero (in practice, it is a very small number depending on the stability of the solver used), and the chemical potentials of the virtual constituents are set to zero in the extended database. This simple technique then provides a generic method by which the super-equilibrium constraints can be incorporated into the Gibbs energy minimization calculation by using the conditions derived from the observed enrichment factors of each relevant species.

From Eq. (4), the following relations can be deduced from the Gibbsian system for the equilibrium reactions and limited super-equilibrium reactions:

$$\sum_k a_k \mu_k = 0,$$

(equilibrium reactions) (8)

$$\sum_k a_k \mu_k = \sum_k a_k \sum_{l=1}^{L+X} \nu_{kl} \pi_l \neq 0.$$

(all constrained super-equilibrium reactions) (9)

In Equations (8) and (9), a_k is used for the stoichiometric coefficient of species k in a given reaction. It should be emphasized here that the Lagrange multipliers in the minimization procedure represent the chemical potentials of each system component [25,35]. As a result of the min(G) calculation, the thermodynamic affinity of all equilibrium reactions becomes zero by Equations (4) and (8). Then, although the summation of the Lagrange multipliers in Equation (9) covers all virtual components in the system, the affinity of non-equilibrium reactions is different from zero and can be related to the calculated "constraint potentials" of the virtual components [34]. In what follows, this feature has been used to illustrate the super-equilibrium conditions in the recovery boiler.

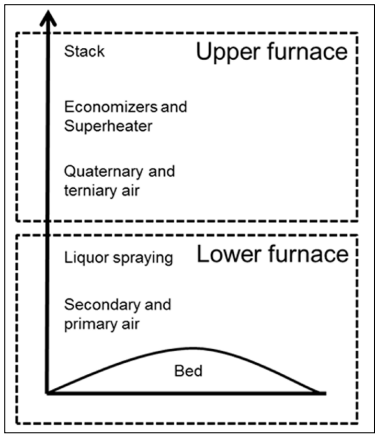

Fig. 2 - Modelling approach: the lower furnace is modelled as a super-equilibrium under conditions of excess sodium, potassium, sulphur, and chlorine in the gaseous phase. The upper furnace and flue-gas channel are modelled as a thermodynamic equilibrium.

RESULTS

In this study, the recovery boiler was modelled in two parts: the upper and lower furnace. Super-equilibrium is considered to occur in the lower furnace under conditions of excess sodium, potassium, sulphur, and chlorine in the gaseous phase. The upper furnace and flue-gas channel were considered to be in thermodynamic equilibrium (see Fig. 2).

The temperature range for the lower furnace is 500°C to 1500°C. Decreasing temperature from 1200°C to 200°C is modelled in the upper furnace, flue-gas channel, and stack. Two cases of fume composition from the lower to the upper furnace were modelled, where 900°C denotes a "cold" furnace and 1100°C a "hot" furnace. The calculation step was 25°C.

The properties of typical industrial black liquor were used [1]. The parameters used in the study are shown in Table 2. The theoretical amount of combustion air at lower temperature, $\lambda_{furnace}$, was set to 0.7. A small amount of excess air was used in the upper furnace to ensure complete combustion.

Defining super-equilibrium

The enrichment factors used are typical observed values for industrial boilers. In addition, the volatilities of sodium and sulphur have been measured in several studies. These values were used in the present study to define the super-equilibrium of sodium, potassium, sulphur, and chlorine in lower-furnace fumes. The enrichment factors used for potassium and chlorine are:

$$ER_K = \frac{\frac{K_{fg}}{K_{fg} + Na_{fg}}}{\frac{K_{bl}}{K_{bl} + Na_{bl}}}, \quad (10)$$

TABLE 2 *Black liquor composition used in this study [1].*

C [wt-%]	H [wt-%]	Na [wt-%]	K [wt-%]	S [wt-%]	Cl [wt-%]	N [wt-%]	O [wt-%]	Moisture content [wt-%]	S/2Me –ratio [%]
32.3	3.3	21.4	2.3	5.0	0.7	0.1	34.9	20.0	31.5

$$ER_K = \frac{\frac{Cl_{fg}}{K_{fg} + Na_{fg}}}{\frac{Cl_{bl}}{K_{bl} + Na_{bl}}}, \quad (11)$$

where the subscript *fg* refers to flue gas and *bl* to black liquor. The enrichment factors used were ER_K=1.4 for potassium and ER_{Cl}=2.5 for chlorine. The volatility of sodium in the lower furnace of the recovery boiler was defined as 10 wt% at 1000°C. In addition, a slight linear temperature dependence was specified according to Eq. (12):

$$Na_{vol} = \frac{10\% - 9\%}{1000C - 900C}(T - 900C) + 9\%, \quad (12)$$

where T is the temperature in the lower furnace. The volatility of sulphur is defined as a function of temperature and the total amount of volatilized alkali metals (sodium + potassium). According to the model presented by Hupa *et al.* [1], the volatility of sulphur at low temperatures is slightly greater than the expected stoichiometric amount based on volatile alkali metals, with the excess decreasing at higher temperatures. Therefore, a linear temperature-dependent description of the amount of volatile sulphur (Eq. (13)) was used in this study:

$$S_{vol} = \left[\frac{90\% - 110\%}{1100\,C - 900\,C}(T - 900\,C) + 110\%\right] Na_{vol}. \quad [13]$$

The concentrations of volatile alkali metals and sulphur can be seen in Fig. 3 and are compared to typical industrial values as presented in [8]. When Eqs. (12) and (13) are combined, a second-order description of the amount of volatile sulphur is obtained, as shown in Fig. 3. Figure 4 shows the stoichiometric ratio of alkali metals and sulphur (*S/2Me*) in the fumes and bed at thermodynamic equilibrium as well as at super-equilibrium. The ratio is almost constant at the bed for super-equilibrium conditions and decreases in the fumes. At thermodynamic equilibrium, the high volatilities of sulphur at lower temperature and of sodium at higher temperature are evident.

Use of the extended stoichiometric matrix

To describe the super-equilibrium conditions in the lower furnace, the stoichiometric matrix was extended based on the methodology presented above. Four additional virtual system components were introduced: Na^*, S^*, K^*, and Cl^*. These components denote the amount of each component in the gaseous phase and are related to the previously presented enrichment factors and volatility for each component.

The actual constituents in the gaseous phase were associated with the new virtual components based on the reaction stoichiometry. For example, the stoichiometric amount of sodium in each constituent in the gaseous phase was represented by the respective amount of Na^* component deduced from the enrichment factor. Thus, the value of the Na^* component for NaOH is 1 and for $(NaOH)_2$ is 2. Similar notation was used for S^*, K^*, and Cl^*. If the constrained constituent included several virtual components, the corresponding values were used: for example, Na^* was 1 and Cl^* was 1 for NaCl. Part of the extended stoichiometric matrix with similar examples is shown in Table 3.

Four virtual constituents were included in the stoichiometric matrix: one constituent for each virtual component. The constituents were R_Na, R_K, R_S, and R_Cl. Virtual constituents were associated with virtual components with ±1 values. Here, a positive value, +1, was used to describe the forward reaction from black liquor to constituents in the gaseous phase (e.g., Na^* for R_Na was set to 1). A similar definition was used for the virtual constituents of potassium, sulphur, and chloride. See examples in Table 3.

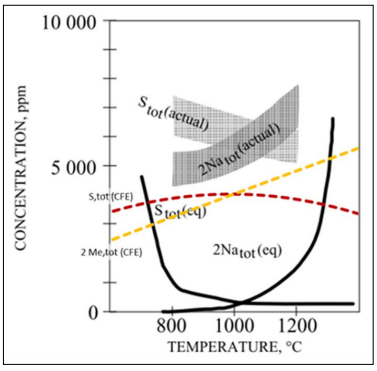

Fig. 3 - Super-equilibrium of sulphur and alkali metals as a function of temperature.

The super-equilibrium affinities in the gas phase can be deduced from Eqs. (8) and (9). To give an example, sodium volatilization from the char bed was described according to the reaction $Na_2CO_3 + 2C \rightarrow 2Na + 3CO$. This reaction was constrained in this study and the affinity defined according to Eq. (9) as:

$$\begin{aligned} Aff &= -\Delta_r G = \mu_{Na_2CO_3} + \mu_{2C} - (\mu_{2Na} + \mu_{3CO}) \\ &= 2\pi_{Na} + \pi_C + 3\pi_O + 2\pi_c - (2\pi_{Na} + 2\pi_{Na^*} + 3\pi_C + 3\pi_O). \\ &= -2\pi_{Na^*} \neq 0 \end{aligned} \quad [14]$$

On the other hand, the gas-phase reactions were allowed to reach mutual thermodynamic equilibrium, for example, the reaction of $Na + H_2O \rightarrow NaOH + H$. The affinity of the equilibrium reaction is zero and is defined as:

$$\begin{aligned} Aff &= -\Delta_r G = \mu_{NaOH} + \mu_H - (\mu_{Na} + \mu_{H_2O}) \\ &= \pi_{Na} + \pi_O + \pi_H + \pi_{Na^*} + \pi_H - (\pi_{Na} + \pi_{Na^*} + 2\pi_H + \pi_O). \\ &= 0 \end{aligned} \quad [15]$$

The calculated Lagrange multipliers for the virtual components (π_{Na^*}, π_{K^*}, π_{S^*}, and π_{Cl^*}) define the non-zero super-equilibrium affinities of the constrained

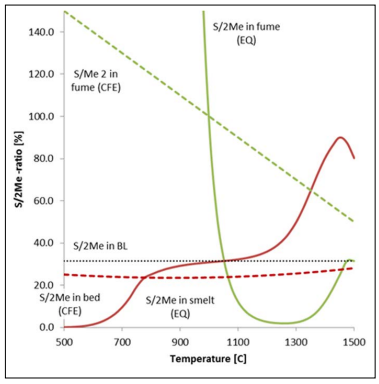

Fig. 4 - S/2Me – molar ratio of fumes, smelt and black liquor. Dashed lines refer to CFE, solid lines to EQ. $\lambda_{furnace}$ = 0.7. Volatility: x_{Na} = 10%, x_S = 30% at 1000°C. EF_K = 1.4 and EF_{Cl} = 2.5.

reactions, as shown in Eq. (14). For all equilibrium reactions, these multipliers cancel out, and the affinities are zero.

Lower furnace

The lower furnace was modelled under super-equilibrium conditions. The chosen reference state was thermodynamic equilibrium, where sulphur volatility is high at low temperature (< 900°C) and sodium volatility is high at high temperature (>1100°C). However, the equilibrium volatility of both constituents is minimal within the normal operating temperature window (900°C–1100°C) (see Fig. 5).

To compensate for this unrealistic representation, a dual approach has been used in previous studies for lower-furnace modelling, for example according to [1,15], in which thermodynamic equilibrium was assumed for the bed-burning conditions and an additional volatilization model was used for the black liquor droplets. The present study has used a unified solution where super-equilibrium is modelled as a single constrained equilibrium. From Fig. 6, it is evident that the volatilities of sodium and sulphur within this super-equilibrium temperature window (from 900°C to 1100°C) is much higher than outside it.

Figures 7 and 8 indicate the differences in char-bed composition. The distinction between thermodynamic and super-equilibrium conditions was less evident within the 900°C to 1100°C temperature window, where the calculated amounts of Na_2CO_3, Na_2S, and NaOH were fairly close to each other. The differences were greater when low or high temperatures were considered, corresponding to the observations in Figs. 4, 5, and 6.

The reaction enthalpy of the lower furnace as a function of time is shown in Fig. 9. The reaction is exothermic when the temperature is below ~1225°C when thermodynamic equilibrium is assumed and below 1250°C for super-equilibrium conditions. Clear differences in the endothermic reaction profile are evident at high temperatures > 1300°C.

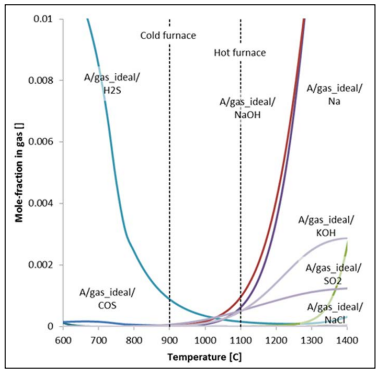

Fig. 5 - Equilibrium concentrations of S and Na in the fumes. Only major constituents including S and Na shown. $\lambda_{furnace}$ = 0.7. Volatility: x_{Na} = 10%, x_S = 30% at 1000°C. EF_K = 1.4 and EF_{Cl} = 2.5.

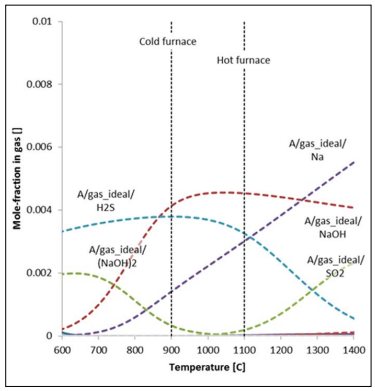

Fig. 6 - Super-equilibrium concentrations of S and Na in the fumes. Only constituents including S and Na shown. $\lambda_{furnace}$ = 0.7. Volatility: x_{Na} = 10%, x_S = 30% at 1000°C. EF_K = 1.4 and EF_{Cl} = 2.5.

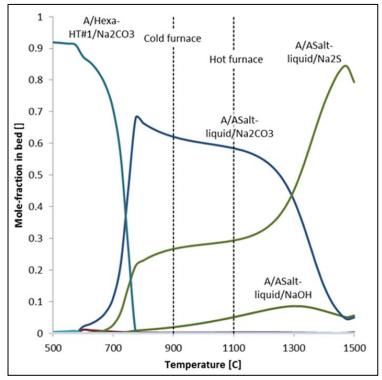

Fig. 7 - Equilibrium concentrations of S and Na in smelt. Only major constituents shown. $\lambda_{furnace}$ = 0.7. Volatility: x_{Na} = 10%, x_S = 30% at 1000°C. EF_K = 1.4 and EF_{Cl} = 2.5.

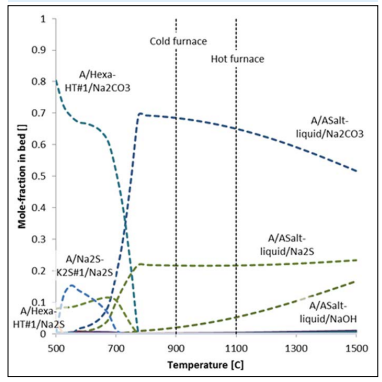

Fig. 8 - Super-equilibrium concentrations of S and Na in smelt. Only major constituents shown. $\lambda_{furnace}$ = 0.7. Volatility: x_{Na} = 10%, x_S = 30% at 1000°C. EF_K = 1.4 and EF_{Cl} = 2.5.

TABLE 3 *Sample of the extended stoichiometric matrix. Original database is from [12]. Four virtual system components (Na*, S*, K*, and Cl*) and four virtual constituents (R_Na, R_K, R_S, and R_Cl) are introduced to calculate super-equilibrium.*

Phase	Constituent	K	Cl	S	Na	O	N	C	H	Na*	K*	S*	Cl*
Gas phase	H								1				
	Na				1					1			
	NaOH				1	1			1	1			
	H_2O					1			2				
	CO					1		1					
	NaCl		1		1					1			1
	KCl	1	1								1		1
	SO_2			1		2						1	
	…												
Salt-liquid	Na_2CO_3				2	3		1					
C	C							1					
…	…												
R_Na	R_Na									+1			
R_K	R_K										+1		
R_S	R_S											+1	
R_Cl	R_Cl												+1

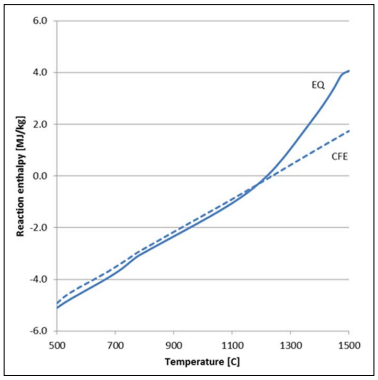

Fig. 9 - Reaction enthalpy vs. temperature. Dashed line denotes CFE and solid line EQ. $\lambda_{furnace}$ = 0.7. Volatility: x_{Na} = 10%, x_S = 30% at 1000°C. EF_K = 1.4 and EF_{Cl} = 2.5.

Upper furnace and flue-gas channel

The super-equilibrium in the lower furnace was further used to define the composition of the released fumes. Two temperatures were used for the lower furnace: 900°C corresponding to a "cold" furnace and 1100°C to a "hot" furnace. Thermodynamic equilibrium was postulated in the upper furnace based on the work of previous authors. A comparison was then conducted against the respective values from the lower furnace under global thermodynamic equilibrium assumptions.

The major condensed components, including sodium and sulphur from the fumes, are shown in Fig. 10 for the "cold" furnace and in Fig. 11 for the "hot" furnace. Because of the constraints used on super-equilibrium in the lower furnace, the ratios of Na_2SO_4 and Na_2CO_3 appear different when comparing the full thermodynamic and super-equilibria. The phenomenon is more distinct under hot furnace conditions. Distinct differences are visible for the constituents with potassium, Fig. 12, and with chlorine, Fig. 13.

There is an evident difference in the sticky temperature (of the condensed phases from the fumes) when thermodynamic equilibrium and super-equilibrium conditions are considered. The difference appears larger for T_{15} temperature (where 15% of condensed phases are in liquid form) than for T_{70} (where 70% are in liquid form), as shown in Fig. 14. When the amount of volatile sodium is increased, the sticky temperature window extends even further, as shown in Fig. 15.

DISCUSSION

The difference in fume composition is evident when comparing the results for thermodynamic equilibrium and super-equilibrium. This observation is in line with previous studies which used a dual approach to lower-furnace modelling to compensate for the limitations of assuming thermodynamic equilibrium alone.

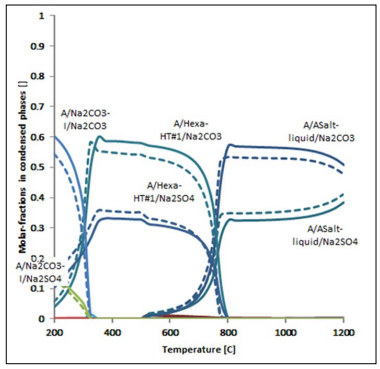

Fig. 10 - Condensed phases from the fumes. Only major constituents shown. Dashed lines refer to Super-EQ, solid lines to EQ. $T_{furnace}$ = 900°C. $\lambda_{furnace}$ = 0.7. Volatility: x_{Na} = 10%, x_S = 30% at 1000°C. EF_K = 1.4 and EF_{Cl} = 2.5.

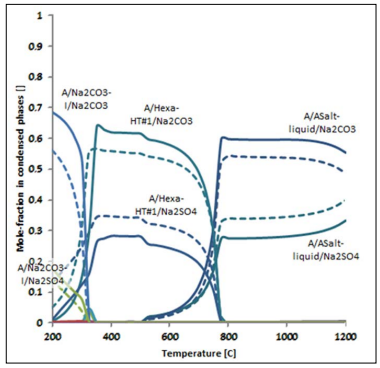

Fig. 11 - Condensed phases from the fumes. Only major constituents shown. Dashed lines refer to Super-EQ, solid lines to EQ. $T_{furnace}$ = 1100°C. $\lambda_{furnace}$ = 0.7. Volatility: x_{Na} = 10%, x_S = 30% at 1000°C. EF_K = 1.4 and EF_{Cl} = 2.5.

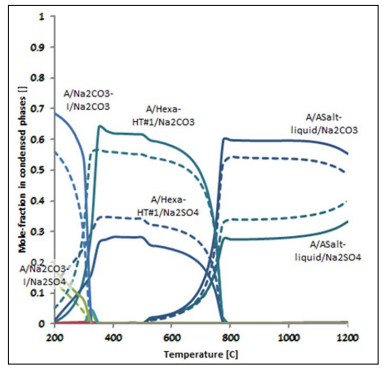

Fig. 12 - Condensed phases from the fumes. Major constituents with potassium shown. Dashed lines refer to Super-EQ, solid lines to EQ. $T_{furnace}$ = 900°C. $\lambda_{furnace}$ = 0.7. Volatility: x_{Na} = 10%, x_S = 30% at 1000°C. EF_K = 1.4 and EF_{Cl} = 2.5.

The super-equilibrium approach can be used successfully to limit the volatility of sulphur in a "cold" furnace as well as the volatility of sodium (and potassium) in a "hot" furnace. In addition, the volatility of these species is much higher in reality than the global equilibrium would predict in the normal temperature range (from 900°C to 1100°C). This phenomenon can also be modelled using the super-equilibrium method. In addition, the enrichment of potassium and chlorine can be described.

The model presented here shows smaller differences in char-bed and smelt

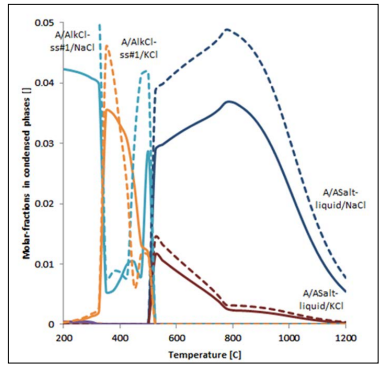

Fig. 13 - Condensed phases from the fumes. Major constituents with chlorine shown. Dashed lines refer to Super-EQ, solid lines to EQ. $T_{furnace}$ = 900°C. $\lambda_{furnace}$ = 0.7. Volatility: x_{Na} = 10%, x_S = 30% at 1000°C. EF_K = 1.4 and EF_{Cl} = 2.5.

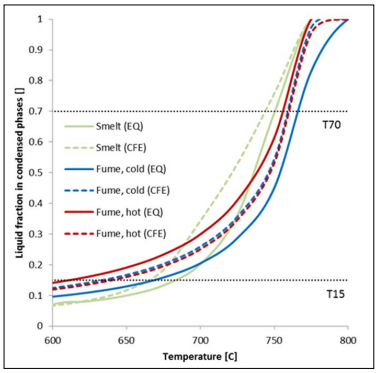

Fig. 14 - Liquid fraction in condensed phases. Dashed lines refer to Super-EQ, solid lines to EQ. T_{15} and T_{70} marked as horizontal lines. $\lambda_{furnace}$ = 0.7. Volatility: x_{Na} = 10%, x_S = 30% at 1000°C. EF_K = 1.4 and EF_{Cl} = 2.5.

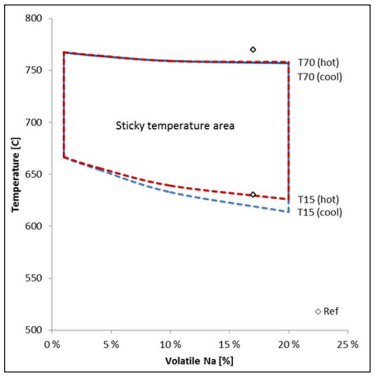

Fig. 15 - Sticky temperature between T_{15} and T_{70} as a function of sodium volatility, x_{Na}, at fume super-equilibrium. Super-EQ assumption. $\lambda_{furnace}$ = 0.7. Volatility: x_S = 30% at 1000°C. EF_K = 1.4 and EF_{Cl} = 2.5. Reference data from Hupa *et al.* (2001).

composition when comparing thermodynamic equilibrium and super-equilibrium, at least under normal operating temperatures. With cold and hot furnaces, similar differences can be seen as in fume composition.

Noticeable differences between equilibrium and super-equilibrium conditions are evident for the condensing phases of the fumes. The ratio of sulphur vs. carbonate increases with the super-equilibrium assumption. Sticky temperature decreases as the amount of fume sodium increases. T_{15} declines by 40°C–50°C and T_{70} by ~10°C when the percentage of sodium is changed from 1% to 20% (when the super-equilibrium assumption is used). It is possible to extend the super-equilibrium system, for example by constraining the sulphidity of the char bed to a fixed value. This would naturally lead also to larger differences in char-bed composition. However, each additional constraint removes a degree of freedom from the system, and therefore the partial equilibrium condition obtained moves further from the global equilibrium.

Only the contents of the fumes were considered in this study because the amount of carry-over particles in the flue gas is typically small. Carry-over and fumes are usually regarded as two separate flows in the flue gas. If needed, carry-over particles could be added to the model, either by considering them as a completely separate flow without any interactions with the fumes, or by calculating the equilibrium between the fumes and the carry-over particles. It should be emphasized that the present results have so far been validated with published literature data. Future studies coupled with experimental results either on laboratory or industrial scale will make it possible to evaluate the further applicability of the model.

CONCLUSIONS

The constrained free energy method was successfully used to model the super-equilibrium behaviour of volatile sodium, potassium, sulphur, and chlorine in black liquor combustion. The model as developed consists of temperature-dependent parameters for the amount of volatile sodium and sulphur and fixed enrichment factors for potassium and chlorine. These parameters are used as virtual constraints to describe the affinity of these species to form constituents and remain in the fumes.

The super-equilibrium model determines fume and smelt properties based on super-equilibrium in the lower furnace and predicts the effects of higher volatility and enrichment of species on the composition of condensed phases in the fumes in the upper furnace and the flue-gas channel. When compared to global equilibrium conditions, considerable differences in the sticky temperatures for the condensed phases in the fumes are observed.

The method as developed does not describe the actual volatilization phenomena during droplet flight or char-bed burning, but in these respects draws on previous studies. The principle of volatility can nevertheless be implemented into the CFE approach, for example, by using appropriate mechanistic models for the enriching species and deducing the constraints from these data. Alternatively, the CFE model can be based simply on "forced" amounts of fume constituents. The accuracy of the solution would then depend on the implemented sub-models or constants.

The evident advantage of the CFE approach is that super-equilibrium, or constrained partial equilibrium, can be determined in a single calculation step while obtaining the chemical composition and interdependent enthalpic effects simultaneously. The defined super-equilibrium can be used as a boundary condition for upper-furnace and flue-gas modelling, and in a second calculation step, to predict condensed phases, sticky temperatures, and corrosion risks.

A promising application for the approach presented is to implement the CFE model as part of a large-scale process simulator. The new model can be parameterized with a few widely used factors (black liquor properties, enrichment factors, etc.). Despite simple parameterization, a high-fidelity thermochemical calculation can then be conducted as part of a more extensive process simulation. Another possible application area for the proposed concept is corrosion-related studies for designing new boilers as well as trouble-shooting old ones. In addition, this type of knowledge could be implemented in a soft sensor for on-line monitoring of the recovery-boiler process.

It is anticipated that a similar super-equilibrium approach can be applied to other high-temperature processes where chemical equilibrium is not reached due to chemical kinetics or limited mass and

energy transfer. The major advantage of this approach is its thermodynamic base, which enables the determination of heat of reaction and chemical composition simultaneously and interdependently.

ACKNOWLEDGEMENTS

This study was funded by the Finnish Funding Agency for Technology and Innovation (Tekes) and VTT Technical Research Centre of Finland.

REFERENCES

1. Hupa, M., Backman, R., Skrifvars, B., and Forssén, M., "Liquor-to-Liquor Differences in Combustion and Gasification Processes : Dust Composition and Melting Properties", Journal of Pulp and Paper Science, 27(12):416–422 (2001).
2. Salmenoja, K., Veli-Antti, K., Hupa, M., and Backman, R., "Chemical Balance of Non-Process Elements in Five Finnish Pulp Mills", Proceedings, International Chemical Recovery Conference, Charleston, SC, USA (2004).
3. Mikkanen, P., Fly-Ash Particle Formation In Kraft Recovery Boilers, Dissertation, Helsinki University of Technology (2000).
4. Janka, K., Wall, J., and Backman, R., "Prediction of Dust Content and Properties in Kraft Recovery Boilers: Comparison of Theory and Experimental Results", Pulp and Paper Canada, 105(1): 46–50 (2004).
5. Vakkilainen, E.K., "Predicting Ash Properties in Recovery Boilers", Proceedings, International Chemical Recovery Conference, Williamsburg, VA, USA (2010).
6. Grace, T.M., "A Review of Char Bed Combustion", Proceedings, International Chemical Recovery Conference, Whistler, BC, Canada, 215–220 (2001).
7. Sricharoenchaikul, C., Frederick, W.J., and Grace, T.M., "Sulphur Species Transformations during Pyrolysis of Kraft Black Liquor", Journal of Pulp and Paper Science, 23(8):J394–J400 (1997).
8. Hupa, M., "Recovery Boiler Chemical Principles", Proceedings, TAPPI Kraft Recovery Short Course, St. Petersburg, FL, USA (2008).
9. Mikkanen, P., Kauppinen, E.I., Pyykönen, J., Jokiniemi, J.K., Aurela, M., Vakkilainen, E.K., et al., "Alkali Salt Ash Formation in Four Finnish Industrial Recovery Boilers", Energy & Fuels, 13(4):778–795 (1999).
10. Lindberg, D., Thermochemistry and Melting Properties of Alkali Salt Mixtures in Black Liquor Conversion Processes, Dissertation, Åbo Akademi (2007).
11. Bale, C.W., Chartrand, P., Decterov, S.A., Eriksson, G., Hack, K., Ben Mahfoud, R., et al., "FactSage Thermochemical Software and Databases", Calphad, 26(2):189–228 (2002).
12. Bale, C.W., Bélisle, E., Chartrand, P., Decterov, S.A., Eriksson, G., Hack, K., et al., FactSage Thermochemical Software and Databases—Recent Developments, Calphad, 33(2):295–311 (2009).
13. Bankiewicz, D., Vainikka, P., Lindberg, D., Frantsi, A., Silvennoinen, J., Yrjas, P., et al., "High-Temperature Corrosion of Boiler Waterwalls Induced by Chlorides and Bromides, Part 2: Lab-Scale Corrosion Tests and Thermodynamic Equilibrium Modeling of Ash and Gaseous Species", Fuel 94:240–250 (2012).
14. Pejryd, L. and Hupa, M., "Bed and Furnace Gas Composition in Recovery Boilers—Advanced Equilibrium Calculations", Proceedings, TAPPI Pulping Conference, San Francisco, CA, USA (1984).
15. Backman, R., Eriksson, G., and Sundström, K., "The Recovery Boiler Advisor: A Combination of Practical Experience and Advanced Thermodynamic Modeling", Proceedings, 3rd Colloquium on Process Simulation, Espoo, Finland (1996).
16. Enestam, S., Corrosivity of Hot Flue Gases in the Fluidized Bed Combustion of Recovered Waste Wood, Dissertation, Åbo Akademi (2011).
17. Engblom, M., Modeling and Field Observations of Char Bed Processes in Black Liquor Recovery Boilers, Dissertation, Åbo Akademi (2010).
18. Uloth, V., Richardson, B., Hogikyan, R., and Haynes, J., "Using a Recovery Boiler Computer Simulation to Evaluate Process Alternatives for Obtaining Incremental Recovery Capacity", TAPPI Journal, 75(11):137–147 (1992).
19. Cardoso, M., Análise da unidade de recuperação do licor negro de eucalipto •no processo "kraft", avaliando alternativas de processamento, Dissertation, Universidade Estadual de Campinas (1998).
20. Järvinen, M.P., Kankkunen, A.P., Miikkulainen, P.H., and Heikkilä, V.P., "A One-Dimensional Flow Model of a Flashing Black Liquor Gun: Study of Vapor Generation Sub-Models", Proceedings, Swedish-Finnish Flame Days 2011, Piteå, Sweden, 1–14 (2011).
21. Jokiniemi, J.K., Pyykönen, J., Mikkanen, P., and Kauppinen, E.I., "Modeling Fume Formation and Deposition in Kraft Recovery Boilers", TAPPI Journal, 79(7):171–181 (1996).
22. Grace, T., Walsh, A., Jones, A., Sumnicht, D., and Farrington, T., "Three-Dimensional Mathematical Model of the Kraft Recovery Furnace", Proceedings, International Chemical Recovery Conference, Ottawa, ON, CA (1989).
23. Leppänen, A., Välimäki, E., and Oksanen, A., "Modeling Fine Particles and Alkali Metal Compound Behavior in a Kraft Recovery Boiler", TAPPI Journal, 11(7):9–14 (2012).
24. Grace, T.M., "A Critical Review of Computer Modeling of Kraft Recovery Boilers", TAPPI Journal, 79(7):182–190 (1996).
25. Eriksson, G., "Thermodynamic Studies of High Temperature Equilibria, III. SOLGAS, a Computer Program for Calculating the Composition and Heat Condition of an Equilibrium Mixture", Acta Chemica Scandinavica, 25(7):2651–2656 (1971).
26. Eriksson, G. and Rosén, E., "Thermodynamic Studies of High-Temperature Equilibria, VII. General Equations for Calculation of Equilibria in Multiphase Systems", Chemica Scripta, 4(5):193–194 (1973).
27. Weber, C.F., "Convergence of the Equilibrium Code SOLGASMIX",

Journal of Computational Physics, 145(2):655–670 (1998).
28. Petersen, S. and Hack, K., "The Thermochemistry Library ChemApp and its Applications", International Journal of Materials Research, 98(10):935–945 (2007).
29. Koukkari, P., Penttilä, K., Hack, K., and Petersen, S., "CHEMSHEET—An Efficient Worksheet Tool for Thermodynamic Process Simulation", In: Microstructures, Mechanical Properties, and Processes, Y. Bréchet (ed.), Wiley-VCH, Weinheim (2005).
30. Alberty, R.A., "Thermodynamics of the Formation of Benzene Series Polycyclic Aromatic Hydrocarbons in a Benzene Flame", Journal of Physical Chemistry, 93(8):3299–3304 (1989).
31. Keck, J.C., "Rate-Controlled Constrained-Equilibrium Theory of Chemical Reactions in Complex Systems", Progress in Energy and Combustion Science, 16(2):125–154 (1990).
32. Koukkari, P., "A Physico-Chemical Method to Calculate Time-Dependent Reaction Mixtures", Computers & Chemical Engineering, 17(12): 1157–1165 (1993).
33. Koukkari, P. and Pajarre, R., "Calculation of Constrained Equilibria by Gibbs Energy Minimization", Calphad, 30(1):18–26 (2006).
34. Koukkari, P. and Pajarre, R., "A Gibbs Energy Minimization Method for Constrained and Partial Equilibria", Pure and Applied Chemistry, 83(6): 1243–1254 (2011).
35. Smith, W.R. and Missen, R.W., Chemical Reaction Equilibrium Analysis: Theory and Algorithms, Krieger, Malabar, FL, USA (1991).

PUBLICATION IV

Feasibility of constrained free energy method for modeling the NO formation in combustion

Chemical Engineering & Technology, in press.

Chemical Engineering & Technology Research Article 1

Petteri Kangas[1]
Pertti Koukkari[1]
Anders Brink[2]
Mikko Hupa[2]

[1]Process Chemistry and Environmental Engineering, VTT Technical Research Centre of Finland, Espoo, Finland.

[2]Process Chemistry Centre, Åbo Akademi University, Turku, Finland.

Feasibility of the Constrained Free Energy Method for Modeling NO Formation in Combustion

Emissions of nitrogen oxide (NO) from combustion are modeled based on the constrained free energy method (CFE). The CFE method is an extension of the Gibbs' free energy minimization technique, using additional immaterial constraints which allow for the calculation of local thermodynamic equilibria. Chemical reactions, enthalpic effect, and thermochemical state variables are calculated concurrently. Various kinetic constraints were applied in this study for modeling thermal and fuel-based NO emissions for a number of combustion problems. The results were validated against data obtained from detailed kinetic models. The results indicate that the CFE method can be used for modeling post-flame thermal and fuel-based NO emissions. Where more specific estimation of radical buildup, radical overshoot, and ignition delay is needed, however, the accuracy of the applied CFE method was deemed insufficient.

Keywords: Gibbs' free energy, Global reaction rate, Local thermodynamic equilibrium, NO emission, Reduced kinetic model

Received: October 28, 2014; *revised:* January 21, 2015; *accepted:* February 12, 2015

DOI: 10.1002/ceat.201400633

1 Introduction and Background

Nitrogen oxide emissions (NO_X = NO + NO_2) are regulated in most parts of the world due to their role in acid rain formation and their detrimental contribution to tropospheric ozone. A rough estimate of annual anthropogenic NO_X emissions is $\sim 30\ Tg_N\ a^{-1}$, whereas emissions from the soil are $\sim 10\ Tg_N\ a^{-1}$. The contribution of biomass combustion to anthropogenic emission is $6\ Tg_N\ a^{-1}$. [1]

In general, four different routes leading to NO_X formation in combustion have been identified [2]: (i) in the thermal process, atmospheric nitrogen is oxidized under high temperatures and thermal NO_X is formed; (ii) prompt NO_X is generated during combustion in a fuel-rich environment when hydrocarbons are reacting with atmospheric nitrogen; (iii) N_2O is either volatilized from fuel or formed when NO is reacting with radical derived from HCN and NH_3; (iv) nitrogen bound to the fuel becomes released during the devolatilization stage and is oxidized to fuel NO_X. NO_X emissions can be controlled by introducing additional fuel in the upper level of boilers, by staging air in combustion, or by flue gas recirculation [3, 4].

The mechanism of NO_X formation can be studied based on three different kinds of approaches: (i) Detailed kinetic models (DKMs) are based on the large set of elementary reactions and relates experimentally defined kinetic parameters. Examples of DKMs are the Gri-Mech 3.0 mechanism [5] and the ÅA mechanism [6]. The latter reaction mechanisms include five elements, 60 species and 371 reactions in total. These mechanisms describe the combustion of small hydrocarbons and formation of NO_X emissions. (ii) Reduced kinetic models which consist solely of a smaller subset of kinetic reactions defined in DKMs. (iii) Global reaction rate models, which are simplified empirical presentations of NO_X formation mechanisms. Often these surrogate models are based on fitting of the parameters based on experimental results or on data derived from DKMs. Examples of global models are presented by de Soete [7], Mitchell and Tarbell [8], and Brink et al. [9]. These models describe the formation of fuel-based NO emissions from intermediates NH_3 or HCN and destruction of NO emission. Global models are also often used for describing the oxidation of hydrocarbons [10].

If detailed description of the chemical reactions behind NO_X formation and on the factors and conditions influencing these reactions are of interest, DKM models are often employed. The mixing of fuels and air is simplified by some ideal reactor assumptions, such as perfectly stirred tank reactors or plug-flow reactors. Hydrocarbon oxidation and NO_X formation are calculated simultaneously, and thus the effect of free radicals, e.g., is easier to include in the model. Software tools such as ChemKin are applied for solving the large number of stiff chemical reactions simultaneously.

When details of the flow and mixing patterns in a combustion chamber or furnace are of interest, computational fluid

Correspondence: Petteri Kangas (petteri.kangas@vtt.fi), VTT Technical Research Centre of Finland, P. O. Box 1000, 02044 VTT, Finland.

dynamics (CFD) simulations are utilized. Typically, reduced kinetic models or global reaction rate mechanisms are applied. The mixing is described in some simplified way, either by a network of ideal reactors of some kind, or by description of the turbulent fluctuations. Often NO_X emissions are calculated by appending a post-processing step to large CFD models as the effect of NO emission is minimal to hydrocarbon combustion. Detailed information on NO_X emission modeling is given among others in the review papers by Vanderlans et al. [11], Hill and Smoot [2], and Glarborg [12].

This study proposes an alternative thermochemical approach for modeling NO_X emission. The new approach is based on the constrained free energy (CFE) method, which allows calculation of a non-mechanistic local thermodynamic equilibrium while the chemical system is constrained with dominating kinetic reaction rates. This methodology is an extension of the traditional Gibbs' free energy method, where the chemical system is extended with immaterial constraints. These constraints are used for controlling the extent of selected reactions, while the rest of the system is allowed to reach local chemical equilibrium. Thus, the number of species can be the same as in more detailed mechanistic models, while the number of defined kinetic reactions can be substantially reduced.

The authors have had previous success in applying the CFE method to other combustion problems: (i) formation of methane, tars, and char during biomass gasification [13], (ii) gasification of char with steam and carbon dioxide [14], and (iii) the superequilibrium of sodium, potassium, chlorine, and sulfur in the flue gas of a kraft pulp mill recovery boiler. A similar approach had earlier been used in combustion of benzene [15], hydrogen [16, 17], methane [16, 18, 19], methanol [19], formaldehyde [19], and ethanol [18]. Certain studies have been conducted on CO and NO [20, 21] emissions from internal combustion engines. Some of the previously mentioned models still contain hundreds of reactions and tens of constraints, and thus, can be considered as only slightly reduced detailed kinetic models.

Formulated by Koukkari and Pajarre [22], the CFE method is considered a generic method for inclusion of different kinds of work-related constraints in the calculation of a thermodynamic equilibrium. CFE thus allows for a quantifiable solution of complex chemical problems in systems affected by either internal or external forces, due to, e.g., surface tension, charge, and electric-magnetic factors. The same principle can also be applied to nonequilibrium processes, and enables the user to implement constraints related to the chemical reaction rate in the thermodynamic multiphase analysis. Successful modeling examples thus range from chemical kinetics [23, 24] to partitioning of electrolytes in an aqueous membrane [25, 26], and from reaction pathways [27] to surface energy in a multicomponent system [28] and para-equilibria in steelmaking [29]. The thermochemical software ChemSheet [30] is often used as a modeling tool, as it allows extension of the chemical system with immaterial constraints. Nevertheless, the CFE method can be applied in other solvers as well, such as FactSage [29] and NASA equilibrium code [17].

2 Methods

This study develops the computational methodology by means of a CFE approach for selected combustion problems, with particular focus on evaluating the feasibility of the method in the modeling of NO_X emissions. ChemSheet [30] is used as the modeling tool. The results are compared against results from DKM using ChemKin. The ÅA mechanism is employed in these calculations [6], where all elementary reactions, respective Arrhenius-type kinetic data and thermodynamic properties, are obtained. A laminar plug-flow reactor is assumed in this study. NO_2 emissions are neglected here as NO_X formation is dominated by NO emissions. Thus, NO_X emissions are hereafter referred to as NO emissions.

2.1 Constrained Free Energy Method

Global thermodynamic equilibrium is often solved by minimizing the Gibbs' free energy of a system. In practice, the Lagrange method for undetermined multipliers is applied, see Eq. (1). The partial derivatives with respect to the amount of constituents and the Lagrange multipliers are set to zero according to Eqs. (2) and (3). In practice, Eq. (2) defines the chemical potential of the constituents and Eq. (3) the mass balance of the system. Additional information on Gibb's energy minimization is given in, e.g., [31–33].

$$L = G - \pi\Psi = \sum_{k=1}^{K} n_k\mu_k - \sum_{l=1}^{L} \pi_l \left(\sum_{k=1}^{K} \nu_{kl} n_k - b_l \right) \tag{1}$$

$$\left(\frac{\partial L}{\partial n_k}\right)_{n_{n\neq k}} = \mu_k - \sum_{l=1}^{L} \pi_l \nu_{kl} = 0 \tag{2}$$

$$\left(\frac{\partial L}{\partial \pi_l}\right)_{\pi_{n\neq l}} = \sum_{k=1}^{K} \nu_{kl} n_k - b_l = 0 \tag{3}$$

In the equations, G[1)] is the Gibbs' free energy of the system; π is the Lagrange multiplier vector; Ψ is the mass balance of the different components of each constituent, written in terms of the amount of matter (mol); n is the molar amount of the constituent k; μ is the chemical potential of the constituent k; k refers to each constituent in the multiphase system; L is the number of components in the system, and K denotes the number of constituents, respectively. π_l is the Lagrange multiplier of component l, b_l is the total amount of component l in the system, and ν_{kl} is stoichiometric coefficient of component l in the constituent k.

When applying kinetic constraining, the chemical system is extended with X number of additional net reaction rate constraints, r_x in Eq. (4). The implemented as X amount of immaterial constituents is connected to Y number of immaterial components based on the reaction stoichiometry. The net reaction rate is defined based on forward and backward reaction rates, as in Eq. (4). If irreversible reaction is considered, only a

1) List of symbols at the end of the paper.

one-way reaction rate is applied. This study employs Arrhenius-type reaction kinetics, Eqs. (5) and (6).

$$r_x = r_{xf} - r_{xr} \tag{4}$$

$$r = k \prod_b [j]^{a_b} \tag{5}$$

$$k = AT^B \exp^{(-E/RT)} \tag{6}$$

Here r_x refers to the net reaction rate of reaction x, the subscript f denotes the forward reaction and r the reverse reaction. k is the rate constant, j is the constituent in the reaction matrix, a is the stoichiometric coefficient of the constituent, and b refers to all constituents involved in the reaction. A is the frequency factor, B is the temperature exponent, E means the activation energy, R is the gas constant, and T is the temperature.

The stoichiometric matrix N of the extended chemical system is given in Eq. (7). In practice, constituent k is linked to the immaterial component y with a positive value of ν_{ky}. The net reaction rate r_x is connected to the corresponding immaterial components by applying a positive value for ν_{xy}. Values are set according to the reaction stoichiometry. Practical examples are presented in the next chapter, when the CFE methodology is applied for various models.

$$N = \begin{bmatrix} \nu_{1,1} & \cdot & \nu_{1,L} & \cdot & \nu_{1,L+Y} & & \\ \cdot & \cdot & \cdot & & \cdot & \cdot & \cdot \\ \nu_{K,1} & \cdot & \nu_{K,L} & & \cdot & \cdot & \cdot \\ \nu_{K+1,1} & \cdot & \cdot & & \nu_{K+1,L+1} & \cdot & \cdot \\ \cdot & \cdot & \cdot & & \cdot & \cdot & \cdot \\ \nu_{K+X,1} & \cdot & \cdot & & \cdot & \cdot & \nu_{K+X,L+Y} \end{bmatrix} \tag{7}$$

2.2 Detailed Kinetic Model

The CFE model is validated against results obtained with a detailed kinetic model. The DKM is based on the ÅA mechanism [6], with calculations assuming isothermal plug-flow conditions. The composition Y in the plug-flow reactor as a function of residence time can be obtained from the following set of s ordinary differential equations, Eq. (8):

$$\rho u a \frac{dY_s}{dx} = M_k \dot{\omega}_k a \tag{8}$$

where a is the cross-sectional area, Y is the mass fraction, M means the molecular weight, $\dot{\omega}$ denotes the molar rate of production by the gas phase reactions, and ρ is the density. In the DKM, these equations are solved with the software package ChemKin.

3 Calculations

The feasibility of the CFE method for modeling NO formation is evaluated by several cases with increasing complexity: (i) heating in pure air, (ii) combustion of CO in dry and moist air, and (iii) combustion of biomass where methane and ammonia serve as model components for the volatiles. Different model structures are presented next. All applied reactions are summarized in Tab. 1 and referred here according to the running number from R1 to R20. The extended stoichiometric matrix for all model configurations is given in Tab. 2.

3.1 Thermal NO Formation with Pure Air (Model 1)

The Zeldovich mechanism [34] (N_2+O ⇌ N+NO and N+O_2 ⇌ NO+O) is widely applied for modeling thermal NO emissions. Here, nitrogen is reacting with an oxygen radical, forming NO and a nitrogen radical which directly reacts with oxygen, generating a second NO molecule; see reactions R1 and R2 in Tab. 1. The chemical system is extended with two immaterial constraints, one for NO* and the other for N*. All other species and radicals are considered to reach local thermodynamic equilibrium.

3.2 Thermal NO Formation during CO Oxidation (Model 2)

CO combustion is modeled according to two reactions with oxygen and the oxygen radical; see R3 and R4 in Tab. 1. Three immaterial components, NO*, CO*, and O*, are used; see Tab. 2. A simplified Zeldovich mechanism is applied here: R1 creates two molecules of NO instantaneously (R2 is omitted here).

In addition, the steady-state approach is applied for the oxygen radical as a second option: $d[O]/dt = 0$ and thus $[O] = k_{3f} k_{4f}^{-1} [O_2][M]^{-1}$. This assumption is made in order to improve the numerical stability of simulation.

3.3 Thermal NO Formation during CO Oxidation with Additional Constraints for Radicals (Model 3)

New reactions become active when water or hydrogen exists in the system: besides the O radicals, OH and H radicals are also present. The third model applies two different approaches for modeling the radical formation: (i) individual constraints O*, OH*, and H* are applied for the radicals or (ii) combined constraint Rad* is used for the sum of all radicals; see Tab. 2. In both cases, R4 and R5 are taken to describe the CO oxidation rate. Reactions R6–R13 define the radical formation and R1 the thermal NO formation; see Tab. 1.

3.4 Oxidation of CH_4 and NH_3 with Global Reaction Rate Constraints (Model 4)

The fourth model applies global reaction rates for the combustion of methane to CO and further to CO_2, as well as for the formation of fuel NO emissions. The hydrocarbon oxidation model, reactions R14–R18 in Tab. 1, is the Jones and Lindstedt model modified by Andersen [10]. The NO formation model, reactions R19 and R20 in Tab. 1, is from Brink et al. [9]. All these reactions, except R18, are irreversible. Immaterial components CH_4*, CO*, NH_3*, H_2*, are NO implemented; see Tab. 2.

Table 1. Applied reactions for NO emission modeling ($k = AT^B\exp^{(-E/RT)}$; units s, K, J, mol, cm^3).

Reaction		Type	Model	A	B	E	Exponents forward	Exponents reverse	Ref. [b]
R1	$N+NO \rightleftharpoons N_2+O$	Elementary	1,2,3,4	3.3×10^{12}	0.3	0	$[N][NO]$	$[N_2][O]$	ÅA
R2	$N+O_2 \rightleftharpoons NO+O$	Elementary	1	6.4×10^{9}	1	26 276	$[N][O_2]$	$[NO][O]$	ÅA
R3	$CO+O_2 \rightleftharpoons CO_2+O$	Elementary	2	2.5×10^{12}	0	199 577	$[CO][O_2]$	$[CO_2][O]$	ÅA
R4[a]	$CO+O+M \rightleftharpoons CO_2+M$	Elementary	2,3	6.2×10^{14}	0	12 552	$[CO][O][M]$	$[CO_2][M]$	ÅA
R5	$CO+OH \rightleftharpoons CO_2+H$	Elementary	3	1.4×10^{5}	1.9	−5636	$[CO][OH]$	$[CO_2][H]$	ÅA
R6	$O+OH \rightleftharpoons H+O_2$	Elementary	3	2.0×10^{14}	−0.4	0	$[O][OH]$	$[H][O_2]$	ÅA
R7	$O+H_2 \rightleftharpoons OH+H$	Elementary	3	5.1×10^{4}	2.7	26 317	$[O][H_2]$	$[OH][H]$	ÅA
R8	$OH+H_2 \rightleftharpoons H_2O+H$	Elementary	3	2.1×10^{8}	1.5	14 435	$[OH][H_2]$	$[H_2O][H]$	ÅA
R9	$OH+OH \rightleftharpoons H_2O+O$	Elementary	3	4.3×10^{3}	2.7	−10 401	$[OH]^2$	$[H_2O][O]$	ÅA
R10 [a]	$H+OH+M \rightleftharpoons H_2O+M$	Elementary	3	8.4×10^{21}	−2	0	$[H][OH][M]$	$[H_2O][M]$	ÅA
R11 [a]	$O+O+M \rightleftharpoons O_2+M$	Elementary	3	1.9×10^{13}	0	−7481	$[O]^2[M]$	$[O_2][M]$	ÅA
R12 [a]	$H+H+M \rightleftharpoons H_2+M$	Elementary	3	1.0×10^{18}	−1	0	$[H]^2[M]$	$[H_2][M]$	ÅA
R13 [a]	$H+O+M \rightleftharpoons OH+M$	Elementary	3	6.2×10^{16}	−0.6	0	$[H][O][M]$	$[OH][M]$	ÅA
R14	$CH_4+{}^1/_2O_2 \rightarrow CO+2H_2$	Global	4	7.82×10^{13}	0	125 520	$[CH_4]^{0.25}[O_2]^{1.25}$		JL
R15	$CH_4+H_2O \rightarrow CO+3H_2$	Global	4	3×10^{11}	0	125 520	$[CH_4][H_2O]$		JL
R16	$H_2+{}^1/_2O_2 \rightarrow H_2O$	Global	4	1.21×10^{18}	−1	167 360	$[H_2]^{0.25}[O_2]^{1.5}$		JL
R17	$H_2O \rightarrow H_2+{}^1/_2O_2$	Global	4	7.1×10^{17}	−0.88	409 614	$[H_2]^{-0.75}[O_2][H_2O]$		JL
R18	$CO+H_2O \rightleftharpoons CO_2+H_2$	Global	4	2.75×10^{12}	0	83 680	$[CO][H_2O]$	$[CO_2][H_2]$	JL
R19	$NH_3+O_2 \rightarrow NO+H_2O+{}^1/_2H_2$	Global	4	1.21×10^{8}	2	66 516	$[NH_3][O_2]^{0.5}[H_2]^{0.5}$		B
R20	$NH_3+NO \rightarrow N_2+H_2O+{}^1/_2H_2$	Global	4	8.73×10^{17}	−1	66 516	$[NH_3][NO]$		B

a) Enhancing factors of three body reactions. R4: N_2: 1.5×10^{0}, O_2: 1.5×10^{0}, H_2O: 1.6×10^{1}; R10: N_2: 4.04×10^{1}, H_2O: 1.65×10^{1}; R11: N_2: 1.5×10^{0}; R12: H_2O: 0.0×10^{0}, H2: 0.0×10^{0}; R13: N_2: 1.5×10^{0}. b) ÅA mechanism [6]; JLA: Jones-Lindstedt-Andersen mechanism [10]; B: Brink mechanism [9].

4 Results

The first case evaluated in this study was heating of pure dry air from 1200 °C to 2200 °C. Fig. 1 shows the equilibrium value, reference results from DKM after 1 and 1000 s, and the results of the CFE model after 1 s. Model 1 with the Zeldovich mechanism is applied here. The results obtained from the CFE model agree well with the reference. It can be noticed that at low temperature, below 1400 °C, DKM results vary from the equilibrium value due to the very low reaction rates.

Next is a study of the combustion of CO. Model 1 with the Zeldovich mechanism is again applied. Here, two different temperatures are investigated, 1500 °C and 1900 °C, using both dry and moist combustion air. Fig. 2 summarizes the results: In the 1900 °C case, the level of final NO emission is similar with the CFE and DKM models and also for the equilibrium model. For short residence times, the CFE model slightly underpredicts the NO level, although the level predicted by the CFE model is in much better agreement than the pure equilibrium model. In the 1500 °C case, the CFE model cannot predict the development of NO emissions. The level of NO is much lower,

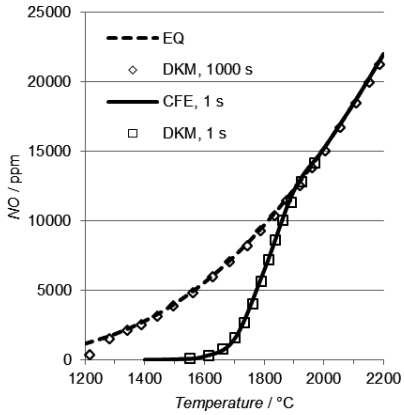

Figure 1. NO emission during the heating of dry air (21 vol % O_2 and 79 vol % N_2). Model 1 applied for constrained free energy (CFE). Detailed kinetic model (DKM) after 1 and 1000 s and equilibrium (EQ) value are shown.

Table 2. Outline of extended stoichiometric matrix for modeling NO emissions. The full matrix includes five elements and 60 constituents. The chemical system is extended with ten immaterial components and with 14 immaterial constituents.

Constituents	Model	Components				Immaterial components									
		C	H	O	N	NO*	N*	O*	CO*	OH*	H*	Rad*	CH_4*	NH_3*	H_2*
Constituents															
O_2	All			2											
N_2	All				2										
CO_2	All	1		2											
H_2	All		2												1
H_2O	All		2	1											
NO	All			1	1	1									
N	All				1		1								
O	All			1				1				1			
CO	All	1		1					1						
OH	All		1	1						1		1			
H	All		1								1	1			
CH_4	All	1	4										1		
NH_3	All		3		1									1	
(47 other constituents)	All														
Immaterial constituents															
r_1: $N+NO \rightleftharpoons N_2+O$	1,2,3,4					−1	−1								
r_2: $N+O_2 \rightleftharpoons NO+O$	1					1	−1								
r_3: $CO+O_2 \rightleftharpoons CO_2+O$	2							1	−1						
r_4: $CO+O+M \rightleftharpoons CO_2+M$	2,3							−1	−1						
r_5: $CO+OH \rightleftharpoons CO_2+H$	3								−1						
$\Sigma r_O = r_1+r_2+r_3-r_6-r_7+r_9-2r_{11}-r_{13}$	2,3							1							
$\Sigma r_{OH} = -r_5-r_6+r_7-r_8-2r_9-r_{10}+r_{13}$	3									1					
$\Sigma r_H = r_5+r_6+r_7+r_8-r_{10}-2r_{12}-r_{13}$	3										1				
$\Sigma r_{radicals} = r_3-r_4-r_6+r_7-r_9-2r_{10}-2r_{11}-2r_{12}-r_{13}$	3											1			
$\Sigma r_{CH4} = -r_{15}-r_{16}$	4												−1		
$\Sigma r_{CO} = r_{15}+r_{16}-r_{18}$	4								1						
$\Sigma r_{NH3} = -r_{19}-r_{20}$	4													−1	
$\Sigma r_{NO} = -2r_1+r_{19}-r_{20}$	4					1									
$\Sigma r_{H2} = 2r_{14}+3r_{15}-r_{16}+r_{17}+r_{18}+{}^1/_2 r_{19}+{}^1/_2 r_{20}$	4														1

* Immaterial components used for controlling the extent of chemical reactions.

and the rapid increase in NO, especially when moist combustion air is applied, is not seen.

It is generally accepted that the Zeldovich mechanism is best for modeling the high-temperature post-flame thermal NO emissions. Following this inference, an evaluation was made of the applicability of the CFE model 1 with Zeldovich mechanism for post-flame NO formation. Here, the initial level of NO after the flame is taken as the boundary condition for the CFE mod-

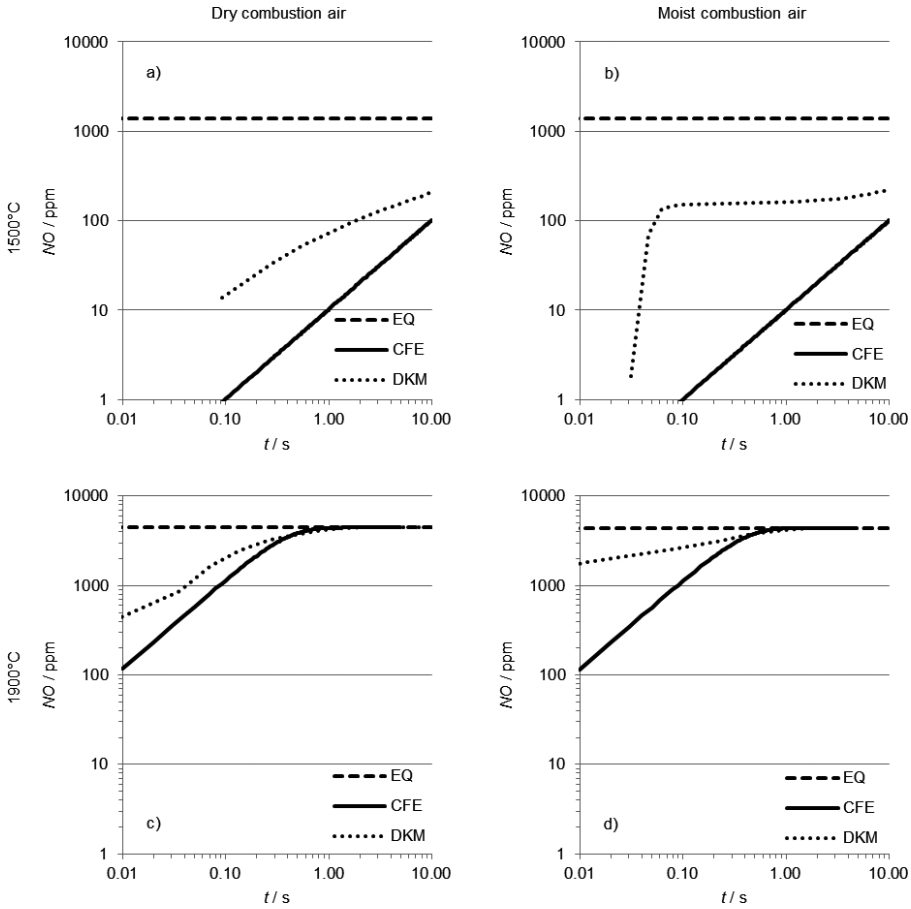

Figure 2. NO emissions in CO oxidation. Model 1 is applied for the CFE model. Results are compared to the DKM and EQ. λ = 1.2. (a) Temperature 1500 °C, dry air (21 vol % O_2 and 79 vol % N_2). (b) Temperature 1500 °C, moist air (21 vol % O_2, 78 vol % N_2, 1 vol % H_2O). (c) Temperature 1900 °C, dry air. (d) Temperature 1900 °C, moist air.

el. In this case, the CFE model can predict the NO level correctly in both dry and moist air; see Fig. 3.

In the beginning of combustion, there is radical overshoot due to a multitude of nonequilibrium processes. This superequilibrium of the free radical is causing a rapid increase in NO emission levels, which cannot be described with the Zeldovich mechanism and the proposed CFE model 1. Thus, additional elementary reactions for the oxidation of CO and formation of the oxygen radical must be included. Fig. 4 illustrates the results for CFE model 2. The development of NO emissions can also be well modeled during the first moments of combustion for dry combustion air; see Fig. 4 a. If a steady-state assumption is applied for the oxygen radical, there is small deviation in O and NO levels at the end of the simulation as indicated in Fig. 4 b. On the other hand, this assumption improves the numerical stability of the model.

The chemical system is more complex when combustion of CO in moist air is considered. The hydrogen radicals and hydroxyl radicals involved are also implemented in CFE model 3. The overshoot of radicals becomes reasonably well quantified, with additional constraints set for O, H, and OH radicals; see Fig. 5 a. For robust calculation over the whole reaction time, however, where the applied algorithm needs to be made more stable, numerical issues occurred due to the stiff chemical system applied here. An alternative approach was also tried, combining the sum of all radicals (O + H + OH) into a single constraint, and allowing the system itself to find proper local thermodynamic equilibrium between the radicals; see Fig. 5 b. With the latter approach, the time set shape of radicals formation becomes qualitatively similar to that of the DKM solution, but deviates significantly in the level of concentrations. The sole benefit of the combined constraining was that no numerical issues occurred.

The last case to be evaluated is the oxidation of CH_4 and NH_3 and the formation of fuel-based NO emissions. CH_4 and

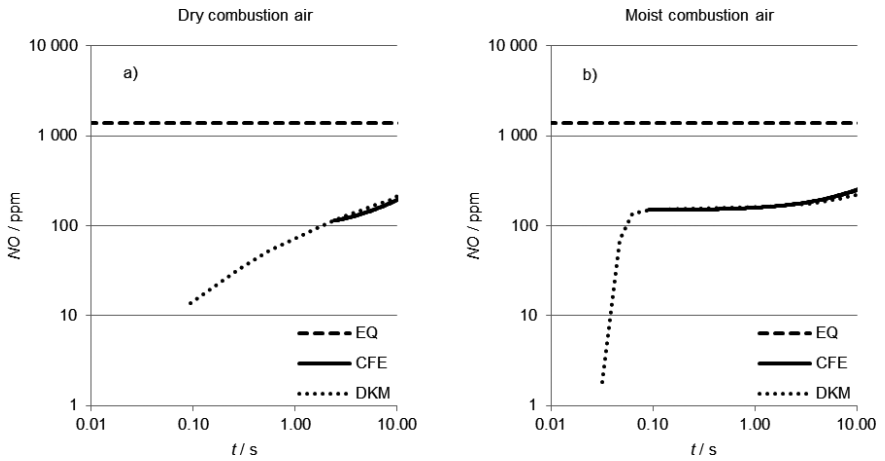

Figure 3. NO emissions in post-flame CO combustion. Model 1 is applied for the CFE model. Results are compared to the DKM and EQ. λ = 1.2. (a) Temperature 1500 °C, dry air (21 vol % O_2 and 79 vol % N_2). (b) Temperature 1500 °C, moist air (21 vol % O_2, 78 vol % N_2, 1 vol % H_2O).

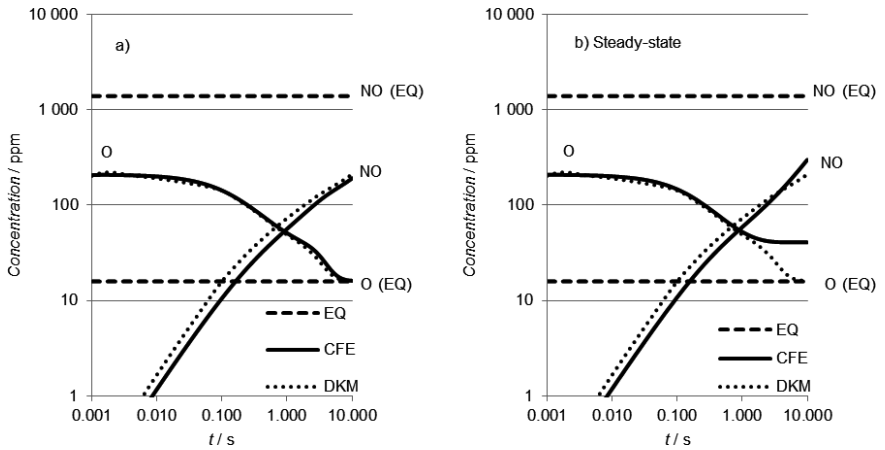

Figure 4. NO emissions in combustion of CO in dry air. Model 2 applied for the CFE model. Temperature 1500 °C, λ = 1.2, and dry air (21 vol % O_2 and 79 vol % N_2). Results are compared to the DKM and EQ. (a) Oxygen radical formation and destruction based on the CO combustion and nitric oxide formation reactions. (b) Steady-state assumption for the generation and destruction of the oxygen radical due to the CO combustion.

NH_3 represent the volatile compounds, e.g., from biomass combustion. Here, global reaction kinetics was applied for constraining instead of elementary reaction rates. Model 4 was used for the CFE method. Fig. 6 a presents the results of oxidation of CH_4 and CO. Oxidation of CH_4 in the CFE model is faster than shown by results from the DKM, which can be seen on the logarithmic scale in Fig. 6 a. The timing of CO oxidation is, however, slightly better. Fig. 6 b illustrates the formation of fuel and thermal NO emissions. The level of thermal NO is right; however, the timing here is again too fast. The additional thermal NO formation is predicted well.

5 Discussion

The aim of this study was to evaluate the feasibility of the CFE method for modeling NO emissions in combustion. CFE modeling proved to be applicable when considering the high-temperature situation and post-flame combustion. The Zeldovich mechanism can be used, and its inclusion in CFE models is straightforward. Results are comparable to those received with DKM.

When considering combustion of CO, it was found that the CFE method is a plausible way of modeling the NO emissions.

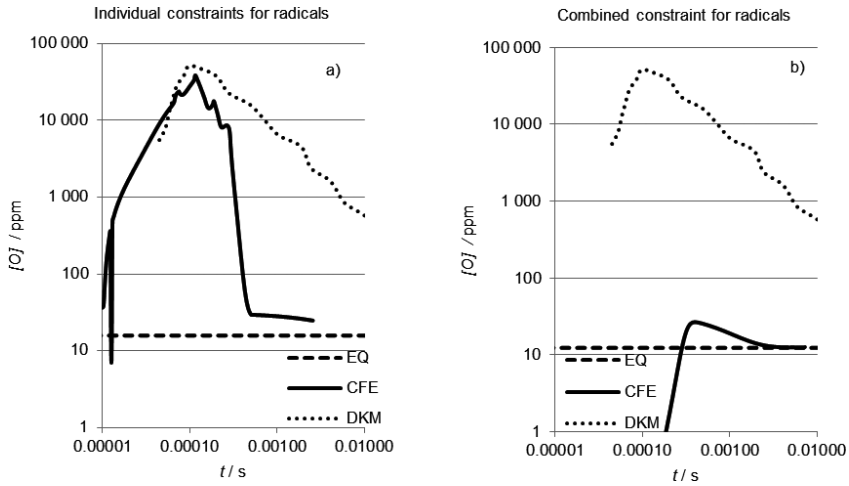

Figure 5. Oxygen radical concentration in combustion of CO in moist air (21 vol % O_2, 78 vol % N_2, 1 vol % H_2O). Temperature 1500 °C and $\lambda = 1.2$; CFE model 3 is compared to the DKM and EQ. (a) Separate constraints defined for radicals. (b) Total sum of radicals (O + H + OH) used as constraint.

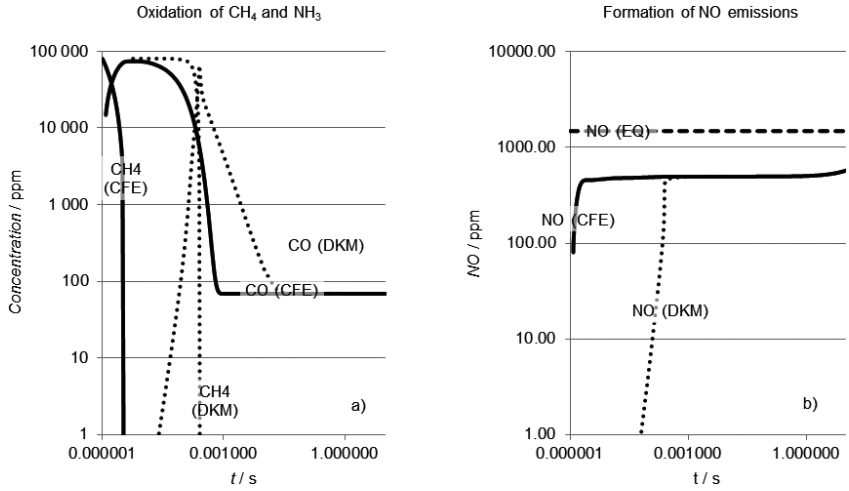

Figure 6. Formation of fuel-based NO emissions. Biomass is modeled as methane, nitrogen in biomass as ammonia. CFE model 4 is compared with the DKM and EQ. Temperature 1500 °C and $\lambda = 1.2$. (a) Oxidation of CH_4 and CO. (b) Formation of fuel and thermal NO emission.

In the case of somewhat superficial dry combustion air, the CFE model can predict the oxygen radical overshoot and the development of NO emissions. Problems arose with moist combustion air, as hydrogen and hydroxyl radicals are also formed. The thermochemical approach seems less well-suited for the prediction of early radical buildup during the overshoot period. The meticulous processes occurring in the ignition stage are difficult to interpret with reduced or global models, including CFE. For these conditions, DKMs are the most suitable.

It was also seen that stiff chemical systems are causing numerical problems with the CFE method. When several competing reactions with different time scales are applied in the model, there is a risk that the model diverges. A steady-state assumption for radicals can usually improve the stability of the calculation system. Another option for achieving improved robustness is to combine the ordinary differential equations with the Gibbs energy minimization, as proposed by [17]. In such cases, the stiff ODE solvers like DASSL could be applied.

When a suitable reduced mechanism or global reaction rate model can be found, it seems straightforward to implement it as part of CFE calculations. This study showed that reduced mechanism or global rate equations can easily be implemented in the CFE method and, thus, be used to predict the carbohydrate combustion and NO formation at process unit level. In the future, it might be possible to estimate and control NO emission levels of different biofuels by combining CFE methodology to emission-considered diesel blending optimization [35].

6 Conclusions

The CFE method was found to be apt for modeling thermal and fuel-based NO emissions. The Arrhenius-type of reaction kinetics applicable for reduced reaction mechanisms, such as the Zeldovich mechanism, or global reaction rate models can be incorporated in the calculation of restricted local thermodynamic equilibrium. Post-flame thermal emissions and fuel-derived emissions were successfully modeled in this way. However, when considering the precise estimation of ignition delay, radical overshoot and related NO formation (thermal and prompt), the best choice is the DKM model.

Numerical issues may occur when incorporating a large amount of stiff chemical reactions in the CFE method. Alternative approaches are thus needed, such as steady-state assumptions or lumping the species together. The other option is to improve the numerical solvers to cope with these large reaction sets.

The distinct benefit of the CFE method can be seen when evaluating the effects of chemical changes in unit processes. At the unit level, the calculation of local restricted thermodynamic equilibrium can be used for estimating chemical reactions, reaction enthalpy, and state variables concurrently. An interesting application area might also be large-scale process simulation where detailed chemistry is needed for boiler units.

Acknowledgment

This study is partly funded by Tekes, the Finnish Funding Agency for Technology and Innovation. Support from project partners Aalto University, Process Flow, Metso, and Outotec is acknowledged.

The authors have declared no conflict of interest.

Symbols used

A	[J mol^{-1}]	frequency factor
a	[m^2]	cross-sectional area
B	[–]	exponent of temperature in Arrhenius equation
b	[mol]	mass balance of component
E	[J]	activation energy
G	[J mol^{-1}]	Gibbs' free energy of the system
j	[–]	constituent in reaction matrix
k	[–]	rate constant
L	[–]	Lagrange expression
M	[g mol^{-1}]	molecular weight
N	[–]	stoichiometric matrix
n	[mol]	molar amount
R	[J K^{-1}mol^{-1}]	gas constant
r	[mol s^{-1}]	reaction rate
T	[°C or °K]	temperature
t	[s]	time
Y	[–]	mass fraction

Greek letters

λ	[–]	lambda ratio; combustion air equivalence ratio
μ	[J mol^{-1}]	chemical potential
ν	[–]	stoichiometric coefficient
π	[J mol^{-1}]	Lagrange multiplier
ρ	[kg m^{-3}]	density
Ψ	[mol]	mass balance of the different components of each constituent in the chemical system
$\dot{\omega}$	[mol s^{-1}]	molar rate of production

Sub- and Superscripts

a	stoichiometric coefficient in reaction matrix
b	constituent involved in reaction
f	forward reaction
K	number of constituents in the chemical system
k	constituent
L	number of components in the chemical system
l	component
r	reverse reaction
X	number of immaterial constituents/reactions
x	immaterial constituent/reaction
Y	number of immaterial components
y	immaterial component

Abbreviations

CFE	constrained free energy method
DKM	detailed kinetic model
NO_X	nitrogen oxide emissions (NO + NO_2)
ODE	ordinary differential equation

References

[1] L. Jaeglé, L. Steinberger, R. V. Martin, K. Chance, *Faraday Discuss.* **2005**, *130*, 407–423. DOI: 10.1039/b502128f

[2] S. Hill, L. D. Smoot, *Prog. Energy Combust. Sci.* **2000**, *26 (4–6)*, 417–458. DOI: 10.1016/S0360-1285(00)00011-3

[3] D. Stapf, K. Ehrhardt, W. Leuckel, *Chem. Eng. Technol.* **1998**, *21 (5)*, 412–415. DOI: 3.0.CO;2-4">10.1002/(SICI)1521-4125(199805)21:5<412::AID-CEAT412>3.0.CO;2-4

[4] F. Qian, C. Chyan, C. Yeh, J. Tso, *Chem. Eng. Technol.* **2013**, *36 (2)*, 268–276. DOI: 10.1002/ceat.201200146

[5] G. P. Smith, D. M. Golden, M. Frenklach, N. W. Moriarty, B. Eiteneer, M. Goldenberg, C. T. Bowman, R. K. Hanson, S. Song, G. J. William C., V. V. Lissianski, Z. Qin, http://www.me.berkeley.edu/gri_mech/

[6] E. Coda Zabetta, M. Hupa, *Combust. Flame* **2008**, *152 (1–2)*, 14–27. DOI: 10.1016/j.combustflame.2007.06.022

[7] G. G. De Soete, *Symp. Combust.* **1975**, *15 (1)*, 1093–1102. DOI: 10.1016/S0082-0784(75)80374-2

[8] J. W. Mitchell, J. M. Tarbell, *AIChE J.* **1982**, *28 (2)*, 302–311. DOI: 10.1002/aic.690280220

[9] A. Brink, P. Kilpinen, M. Hupa, *Energy Fuels* **2001**, *15 (5)*, 1094–1099. DOI: 10.1021/ef0002748

[10] J. Andersen, *Dissertation*, Technical University of Denmark, Lyngby **2009**.

[11] R. Vanderlans, P. Glarborg, K. Dam-Johansen, *Prog. Energy Combust. Sci.* **1997**, *23 (4)*, 349–377. DOI: 10.1016/S0360-1285(97)00012-9

[12] P. Glarborg, *Prog. Energy Combust. Sci.* **2003**, *29 (2)*, 89–113. DOI: 10.1016/S0360-1285(02)00031-X

[13] P. Kangas, I. Hannula, P. Koukkari, M. Hupa, *Fuel* **2014**, *129*, 86–94. DOI: 10.1016/j.fuel.2014.03.034

[14] P. Kangas, P. Koukkari, M. Hupa, *Energy Fuels* **2014**, *28 (10)*, 6361–6370. DOI: 10.1021/ef501343d

[15] R. A. Alberty, *J. Phys. Chem.* **1989**, *93 (8)*, 3299–3304. DOI: 10.1021/j100345a081

[16] J. C. Keck, *Prog. Energy Combust. Sci.* **1990**, *16 (2)*, 125–154. DOI: 10.1016/0360-1285(90)90046-6

[17] D. Hamiroune, P. Bishnu, M. Metghalchi, J. C. Keck, *Combust. Theory Model.* **1998**, *2 (1)*, 81–94. DOI: 10.1080/713665370

[18] G. J. Nicolas, *Dissertation*, Northeastern University, Boston, MA 2012.

[19] M. Janbozorgi, S. Ugarte, H. Metghalchi, J. C. Keck, *Combust. Flame* **2009**, *156 (10)*, 1871–1885. DOI: 10.1016/j.combustflame.2009.05.013

[20] J. C. Keck, D. Gillespie, *Combust. Flame* **1971**, *17 (2)*, 237–241. DOI: 10.1016/S0010-2180(71)80166-9

[21] M. Delichatsios, J. Keck, *ACS Symp. Prepr.* **1975**.

[22] P. Koukkari, R. Pajarre, *Calphad* **2006**, *30 (1)*, 18–26. DOI: 10.1016/j.calphad.2005.11.007

[23] P. Koukkari, *Comput. Chem. Eng.* **1993**, *17 (12)*, 1157–1165. DOI: 10.1016/0098-1354(93)80096-6

[24] P. Koukkari, I. Laukkanen, S. Liukkonen, *Fluid Phase Equilib.* **1997**, *136 (1–2)*, 345–362. DOI: 10.1016/S0378-3812(97)00123-4

[25] R. Pajarre, P. Koukkari, E. Räsänen, *J. Mol. Liq.* **2006**, *125 (1)*, 58–61. DOI: 10.1016/j.molliq.2005.11.016

[26] P. Kangas, R. Pajarre, M. Nappa, P. Koukkari, *Nord. Pulp Pap. Res. J.* **2012**, *27 (3)*, 604–612. DOI: 10.3183/NPPRJ-2012-27-03-p604-612

[27] P. Blomberg, P. Koukkari, *Comput. Chem. Eng.* **2011**, *35 (7)*, 1238–1250. DOI: 10.1016/j.compchemeng.2010.07.024

[28] R. Pajarre, P. Koukkari, T. Tanaka, J. Lee, *Calphad* **2006**, *30 (2)*, 196–200. DOI: 10.1016/j.calphad.2005.08.003

[29] A. D. Pelton, P. Koukkari, R. Pajarre, G. Eriksson, *J. Chem. Thermodyn.* **2014**, *72*, 16–22. DOI: 10.1016/j.jct.2013.12.023

[30] P. Koukkari, K. Penttilä, K. Hack, S. Petersen, in *Microstructures, Mechanical Properties and Processes* (Ed: Y. Bréchet), Wiley-VCH Verlag GmbH & Co. KGaA, Weinheim **2005**.

[31] G. Eriksson, E. Rosén, *Chem. Scr.* **1973**, *4 (5)*, 193–194.

[32] G. Eriksson, *Acta Chem. Scand.* **1971**, *25 (7)*, 2651–2656.

[33] W. R. Smith, R. W. Missen, *Chemical Reaction Equilibrium Analysis: Theory and Algorithms*, Krieger Publishing Company, Malabar, FL **1991**.

[34] J. Zeldovich, *Acta Physicochem. USSR* **1946**, *21*, 577–628.

[35] V. Mittal, T. Cai, K. Krishnadevarajan, Q. Xu, *Chem. Eng. Technol.* **2014**, *37 (2)*, 293–300. DOI: 10.1002/ceat.201300267

Research Article: An alternative thermochemical approach for modeling NO_X emissions is proposed. NO emissions in combustion are modeled with the constrained free energy (CFE) method which allows calculations of local restricted thermodynamic equilibrium by implementing reaction kinetic rates as constraints. Thermal and fuel NO emissions were successfully estimated with the CFE approach.

Feasibility of the Constrained Free Energy Method for Modeling NO Formation in Combustion

P. Kangas*, P. Koukkari, A. Brink, M. Hupa

Chem. Eng. Technol. **2015**, *38 (4)*,
XXX … XXX

DOI: 10.1002/ceat.201400633

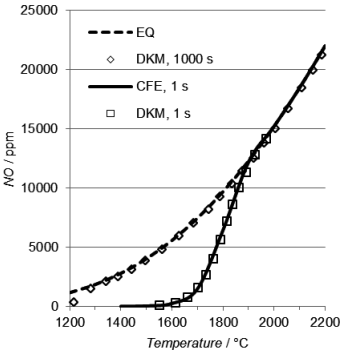

PUBLICATION V

Multi-phase thermodynamic modelling of pulp suspensions: Review of the methodology

Nordic Pulp & Paper Research Journal 27 (3), 604–612.

Series title and number

VTT Science 92

Title	**Modelling the super-equilibria in thermal biomass conversion** Applications and limitations of the constrained free energy method
Author(s)	Petteri Kangas
Abstract	In various thermal biomass conversion processes, super-equilibrium concentrations of chemical species are observed. In such cases, the super-equilibrium is consid-ered as a local equilibrium state where an excess amount of certain species or phases exists. Solid biomass conversion in torrefaction and pyrolysis, as well as char conversion in gasification, are kinetically constrained phenomena in which conditions of super-equilibria can be observed. The formation of methane, tar, ammonia and char in biomass gasification can be further described using the super-equilibrium concept. A respective example is the enrichment of sodium, potassium, sulfur and chlorine into flue gas in a kraft pulp recovery boiler. Free radical over-shoot and the related non-equilibrium phenomena during high-temperature combustion result in elevated NO emission levels and may also be contemplated using the super-equilibrium hypothesis. The feasibility of modelling these super-equilibria with a constrained free energy method was evaluated in this study. The applied method is an extension of Gibbs free energy minimisation technique, accompanied by an extension of the thermo-chemical system with additional immaterial constraints. In this study, these additional constraints are defined based on the extent of the reactions. The presented method is an applicable modelling practice in high temperature processes, where local super-equilibrium state is a valid assumption. Suitable processes include biomass gasification, black liquor combustion and NO emission estimation. When low temperature processes are considered, the gas phase composition originates largely from the wood structure and fully kinetic models tend to give a better estimation than the constrained Gibbs'ian method. Kinetic constraints were successfully defined based on empirical constant values, on temperature dependent experimental reaction rate models and on global kinetic models. When models based on elementary kinetic reactions were considered, heavily reduced models were shown to be suitable for incorporation into the constrained free energy method. However, implementing a large number of kinetic reactions in the constrained free energy model was impractical. If a precise estimation of the super-equilibrium concentrations of free radicals is needed, detailed kinetic models should be used. Based on the results, this thesis endorses the use of the constrained free energy method for modelling the super-equilibria in thermal biomass conversion. Such a method concurrently provides a unified solution including chemical reactions, and the enthalpic effect and state variables of the system. Thus, it can be considered an alternative to the commonly used global equilibrium models or reduced kinetic models applied when modelling the thermal conversion of biomass.
ISBN, ISSN	ISBN 978-951-38-8297-6 (Soft back ed.) ISBN 978-951-38-8298-3 (URL: http://www.vtt.fi/publications/index.jsp) ISSN-L 2242-119X ISSN 2242-119X (Print) ISSN 2242-1203 (Online)
Date	May 2015
Language	English; Finnish and Swedish abstracts
Pages	60 p. + app. 61 p.
Name of the project	
Commissioned by	
Keywords	biomass, gasification, pyrolysis, torrefaction, recovery boiler, NO emissions, Gibbs free energy
Publisher	VTT Technical Research Centre of Finland Ltd P.O. Box 1000, FI-02044 VTT, Finland, Tel. 020 722 111

Julkaisun sarja ja numero

VTT Science 92

Nimeke	**Malleja supertasapainotiloista puun termisessä konversiossa** Rajoitetun vapaaenergiatekniikan sovellukset ja rajoitukset
Tekijä(t)	Petteri Kangas
Tiivistelmä	Puun termisessä konversiossa kemialliset supertasapainotilat ovat usein läsnä. Supertasapainotilalla tarkoitetaan tässä työssä laajasti tilannetta, jossa ylimäärä tiettyjä yhdisteitä on havaittavissa. Kiinteän biomassan kaasuuntumista torrefiointi- ja pyrolyysiprosesseissa ja koksin kaasutusta voidaan pitää esimerkkeinä rajoitetuista supertasapainotiloista. Samoin metaania, ammoniakkia, tervoja ja koksia muodostuu ylimäärin biomassan kaasutusprosessissa, ja niiden syntymistä voidaan niin ikään kuvata supertasapainotilana. Vastaava esimerkki on natriumin, kaliumin, rikin ja kloorin rikastuminen savukaasuihin sellutehtaan soodakattilassa. Myös osa typpioksidipäästöistä syntyy vapaiden radikaalien hetkellisen supertasapainotilan seurauksena korkealämpöisissä polttoprosesseissa. Tässä työssä tutkitaan edellä mainittujen supertasapainotilojen mallintamista rajoitetun vapaaenergiatekniikan avulla. Tekniikka perustuu Gibbsin vapaaenergian minimointiin ja laajentaa käsiteltyä kemiallista systeemiä aineettomilla rajoittimilla. Reaktion etenemisastetta on käytetty tässä työssä rajoittimien määrittelemiseen. Esitetty tekniikka toimii hyvin korkealämpöprosessien laskennassa. Biomassan kaasutuksen, mustalipeän polton ja typpioksidipäästöjen tapauksessa päästiin hyviin tuloksiin, kun korkealämpöprosesseissa voidaan olettaa paikallinen tasapainotila kaasufaasissa. Sen sijaan matalammalla lämpötila-alueella toimittaessa, kuten torrefioinnissa ja pyrolyysissä, kaasufaasi ei saavuta paikallista tasapainotilaa. Täysin rajoitetut kineettiset mallit antavat paremman tuloksen näissä sovelluksissa kuin rajoitettu vapaaenergiatekniikka. Käytetyt rajoittimet voidaan määritellä monin tavoin: mittauksiin perustuvia vakioarvoja käyttäen, empiirisiin malleihin pohjautuen ja globaalien kinetiikkamallien avulla. Mikäli halutaan käyttää malleja, jotka perustuvat alkeisreaktioihin, on syytä valita vain kriittiset reaktiot mukaan tarkasteluun. Täyden kineettisen mallin avulla voidaan kuitenkin ennustaa tiettyjä ilmiöitä, kuten radikaalien määrää palamisen alussa, paremmin kuin rajoitetulla vapaaenergiatekniikalla. Tulosten pohjalta suositellaan rajoitettua vapaaenergiatekniikkaa vaihtoehdoksi perinteisille tasapainomalleille ja kineettisille malleille tarkasteltaessa puun termistä konversiota. Tekniikan avulla voidaan laskea kemialliset reaktiot, reaktiolämmöt ja tilasuureet samanaikaisesti, mikä on käytännöllistä monen ongelman ratkaisemisessa.
ISBN, ISSN	ISBN 978-951-38-8297-6 (nid.) ISBN 978-951-38-8298-3 (URL: http://www.vtt.fi/publications/index.jsp) ISSN-L 2242-119X ISSN 2242-119X (Painettu) ISSN 2242-1203 (Verkkojulkaisu)
Julkaisuaika	Toukokuu 2015
Kieli	Englanti; suomenkielinen ja ruotsinkielinen tiivistelmä
Sivumäärä	60 s. + liitt. 61 s.
Projektin nimi	
Rahoittajat	
Avainsanat	biomassa, kaasutus, pyrolyysi, torrefiointi, soodakattila, NO-päästöt, Gibbsin vapaaenergia
Julkaisija	Teknologian tutkimuskeskus VTT Oy PL 1000, 02044 VTT, puh. 020 722 111

Series namn och nummer
VTT Science 92

Titel	**Modeller av super-jämvikter i termisk konversion av biomassa – Tillämpningar och begränsningar av frienergimetod med bivillkor**
Författare	**Petteri Kangas**
Referat	Super-jämviktskoncentrationer observeras i olika termiska konversionsprocesser av biomassan. I det här arbetet har super-jämviktsbegreppet generaliserats och utvärderats för system, där någon eller några bivillkor får systemet att avvika från jämvikt. Exempel på processer som modellerats på det här sättet är torrifiering och avgasning av biomassa samt förgasning. I förgasning har t.ex. bildningen av metan, tjäror, ammoniak och träkol kunnat beskrivas med super-jämviktskonceptet. Andra exempel är anrikningen av natrium, kalium, svavel och klor i sodapannans rökgaser samt bildning av kväveoxid vid förbränning av gasformiga bränslen. Metoden som tillämpas baserar sig på minimering av Gibbs fria energi för ett system utökat med immateriella bivillkor. De immateriella bivillkoren definieras utgående från reaktionens omsättningsgrad. Studien visar att metoden lämpar sig väl för att beskriva högtemperaturprocesser, där lokala jämviktstillstånd förekommer. Exempel på sådana processer är förgasning av biomassa, förbränning av svartlut och bildning av kväveoxider. För lågtemperaturprocesser, så som torrifiering och avgasning, verkar förutsätta en beskrivning helt baserad på reaktionshastigheten. De bivillkor som beskriver de processer som förhindrar systemet att nå jämviktstillstånd kan definieras m.h.a. empiriska konstanter, empiriska hastighetsuttryck eller reaktionsmekanismer. Det visade sig att användandet av en detaljerad reaktionsmekanism för att definiera de immateriella bivillkoren gav upphov till numeriska svårigheter, medan användning av förenklade mekanismer fungerade bra. Slutsatsen av detta är att ifall en noggrann uppskattning av super-jämviktsnivåer är det primära målet, bör beräkningarna basera sig på detaljerade reaktionsmekanismer. Arbetet visar att en modellering baserad på minimering av Gibbs fria energi för ett system utökat med immateriella bivillkor fungerar för att beskriva termisk konversion av biomassa. Metoden beskriver effekten av reaktionskinetiska begränsningar och effekten av reaktionsentalpi. Vidare innehåller lösningen samtidigt information om systemets tillståndsvariabler. Sammanfattningsvis kan metoden anses vara ett alternativ till globala jämviktsmodeller eller till modeller som enbart bygger på användning av reaktionskinetik i modellering av termisk omvandling av biomassa.
ISBN, ISSN	ISBN 978-951-38-8297-6 (hft.) ISBN 978-951-38-8298-3 (PDF) ISSN-L 2242-119X ISSN 2242-119X (hft.) ISSN 2242-1203 (PDF)
Datum	Maj 2015
Språk	Engelska, referat på svenska och finska
Sidor	60 s. + bil. 61 s.
Projektets namn	
Uppdragsgivare	
Nyckelord	biomassa, förgasning, avgasning, torrifiering, sodapanna, NO-emissioner, Gibbs fria energi
Utgivare	Teknologiska forskningscentralen VTT Ab PB 1000, 02044 VTT, tfn. +358 20 722 111

Modelling the super-equilibria in thermal biomass conversion

Applications and limitations of the constrained free energy method

Thermal bioenergy processing covers over a fifth of domestic energy consumption in Finland. The technologies include combustion, gasification and pyrolysis, which yet seldom operate flawlessly and thus different kinds of emissions, particulates and tars are observed. Also precipitates and corrosion products are eroding process equipment. These problems are often caused by non-equilibrium phenomena: certain compounds are accumulating into the process and thus a thermochemical super-equilibrium state is formed. In the present study a new computational method has been developed to describe such super-equilibrium states. The new technique allows concurrent and interdependent calculation of dominant chemical reactions, heat generation and relevant state properties in the system. The work applies the novel constrained free energy technique (CFE) and presents a new application area in energy production for this generic method. The approach was found well applicable for the high temperature processes such as combustion of black liquor and wood, biomass gasification, and formation of nitric oxide emissions. The necessary constraints can be defined based on the industrial measurements or on experimental and reaction rate models. Limitations were found in low temperature processes such as torrefaction and pyrolysis, or if the number of constraints were too large for efficient numerical calculation. Use of CFE provides a technique for future in-depth studies of biomass or biofuel combustion and gasification as well as for process engineering and optimisation in the field. The method can be seen as a viable alternative for traditional mechanistic and phenomenological approaches by combining the benefits of both in a single elegant solution.

ISBN 978-951-38-8297-6 (Soft back ed.)
ISBN 978-951-38-8298-3 (URL: http://www.vtt.fi/publications/index.jsp)
ISSN-L 2242-119X
ISSN 2242-119X (Print)
ISSN 2242-1203 (Online)

VTT

Åbo Akademi